

## **INFORMATION TO USERS**

This manuscript has been reproduced from the microfilm master. UMI films the text directly from the original or copy submitted. Thus, some thesis and dissertation copies are in typewriter face, while others may be from any type of computer printer.

**The quality of this reproduction is dependent upon the quality of the copy submitted.** Broken or indistinct print, colored or poor quality illustrations and photographs, print bleedthrough, substandard margins, and improper alignment can adversely affect reproduction.

In the unlikely event that the author did not send UMI a complete manuscript and there are missing pages, these will be noted. Also, if unauthorized copyright material had to be removed, a note will indicate the deletion.

Oversize materials (e.g., maps, drawings, charts) are reproduced by sectioning the original, beginning at the upper left-hand corner and continuing from left to right in equal sections with small overlaps.

Photographs included in the original manuscript have been reproduced xerographically in this copy. Higher quality 6" x 9" black and white photographic prints are available for any photographs or illustrations appearing in this copy for an additional charge. Contact UMI directly to order.

ProQuest Information and Learning  
300 North Zeeb Road, Ann Arbor, MI 48106-1346 USA  
800-521-0600

**UMI<sup>®</sup>**



**NOVEL UNCONDITIONALLY STABLE  
FINITE-DIFFERENCE TIME-DOMAIN METHOD FOR  
ELECTROMAGNETIC AND MICROWAVE MODELING**

by

Fenghua Zheng

Submitted  
in partial fulfilment of the requirements  
for the degree of

**DOCTOR OF PHILOSOPHY**

Major Subject: Electrical and Computer Engineering

at

**DALHOUSIE UNIVERSITY**

Halifax, Nova Scotia

April, 2001

© Copyright by Fenghua Zheng, 2001



**National Library  
of Canada**

**Acquisitions and  
Bibliographic Services**

395 Wellington Street  
Ottawa ON K1A 0N4  
Canada

**Bibliothèque nationale  
du Canada**

**Acquisitions et  
services bibliographiques**

395, rue Wellington  
Ottawa ON K1A 0N4  
Canada

*Your file Votre référence*

*Our file Notre référence*

**The author has granted a non-exclusive licence allowing the National Library of Canada to reproduce, loan, distribute or sell copies of this thesis in microform, paper or electronic formats.**

**The author retains ownership of the copyright in this thesis. Neither the thesis nor substantial extracts from it may be printed or otherwise reproduced without the author's permission.**

**L'auteur a accordé une licence non exclusive permettant à la Bibliothèque nationale du Canada de reproduire, prêter, distribuer ou vendre des copies de cette thèse sous la forme de microfiche/film, de reproduction sur papier ou sur format électronique.**

**L'auteur conserve la propriété du droit d'auteur qui protège cette thèse. Ni la thèse ni des extraits substantiels de celle-ci ne doivent être imprimés ou autrement reproduits sans son autorisation.**

0-612-63485-X

**Canada**

**Dalhousie University**  
**Faculty of Engineering**

The undersigned hereby certify that they have examined, and recommend to the Faculty of Graduate Studies for acceptance, the thesis entitled "Novel Unconditionally Stable Finite-Difference Time-Domain Method for Electromagnetic and Microwave Modeling" by Fenghua Zheng in partial fulfillment of the requirements for the degree of Doctor of Philosophy.

Dated: April 9, 2001

Supervisor:

\_\_\_\_\_

Dr. Zhizhang (David) Chen

External Examiner:

\_\_\_\_\_

Dr. Ke Wu

Ecole Polytechnique

Examiners:

\_\_\_\_\_

Dr. Sherwin Nugent

\_\_\_\_\_

Dr. William Phillips

**Dalhousie University**  
**Faculty of Engineering**

DATE: Apr 11, 2001

**AUTHOR:** Fenghua Zheng  
**TITLE:** Novel Unconditionally Stable Finite-Difference Time-Domain Method for Electromagnetic and Microwave Modeling  
**MAJOR SUBJECT:** Electrical and Computer Engineering  
**DEGREE:** Doctor of Philosophy  
**CONVOCATION:** April, 2001

Permission is herewith granted to Dalhousie University to circulate and to have copied for non-commercial purposes, at its discretion, the above thesis upon the request of individuals or institutions.

  
Signature of Author

The author reserves other publication rights, and neither the thesis nor extensive extracts from it may be printed or otherwise reproduced without the author's written permission.

The author attests that permission has been obtained for the use of any copyrighted material appearing in this thesis (other than brief excerpts requiring only proper acknowledgement in scholarly writing), and that all such use is clearly acknowledged.

## Table of Contents

<b>TABLE OF CONTENTS</b> .....	<b>IV</b>
<b>LIST OF FIGURES</b> .....	<b>VI</b>
<b>LIST OF TABLE</b> .....	<b>VIII</b>
<b>LIST OF ABBREVIATIONS</b> .....	<b>IX</b>
<b>DEDICATION</b> .....	<b>X</b>
<b>ACKNOWLEDGEMENTS</b> .....	<b>XI</b>
<b>ABSTRACT</b> .....	<b>XII</b>
<b>CHAPTER 1 INTRODUCTION</b> .....	<b>1</b>
1.1 LITERATURE REVIEW: THE STATE OF THE ART FOR SOLVING MAXWELL'S EQUATIONS .....	1
1.1.1 <i>Frequency Domain Methods</i> .....	3
1.1.2 <i>Time Domain Methods in Electromagnetics: Advantages and Restrictions</i> .....	11
1.1.3 <i>Other Computational Efficiency Improved Techniques</i> .....	16
1.2 MOTIVATION OF THE THESIS .....	24
1.3 SCOPE AND ORGANIZATION OF THE THESIS.....	24
<b>CHAPTER 2 DEVELOPMENT OF THE ADI-FDTD METHOD FOR ELECTROMAGNETIC PROBLEMS</b> .....	<b>26</b>
2.1 INTRODUCTION.....	26
2.2 FDTD FUNDAMENTALS .....	27
2.2.1 <i>Yee's Grid and FDTD Scheme</i> .....	27
2.2.2 <i>Selections of Grid Size and Time Step Size</i> .....	33
2.2.3 <i>Numerical Dispersion</i> .....	33
2.2.4 <i>Numerical Stability</i> .....	35
2.3 ADI BASICS .....	37
2.4 DEVELOPMENT OF ADI BASED FDTD ALGORITHM .....	39
2.4.1 <i>Derivation of ADI-FDTD scheme</i> .....	39
2.4.2 <i>Advantages of modified ADI technique</i> .....	45
2.4.3 <i>Efficient Computation Approach</i> .....	46
2.5 TWO-DIMENSIONAL ADI-FDTD FORMULATION .....	53
2.6 SIMULATIONS AND RESULTS .....	57
2.7 DISCUSSION AND CONCLUSIONS .....	60
<b>CHAPTER 3 NUMERICAL STABILITY ANALYSIS: PROOF OF UNCONDITIONAL STABILITY</b> .....	<b>61</b>

3.1	INTRODUCTION.....	61
3.2	UNCONDITIONAL STABILITY OF THREE-DIMENSIONAL ADI-FDTD ALGORITHM .....	62
3.3	STABILITY ANALYSIS OF THE TWO-DIMENSIONAL ADI-FDTD FORMULATIONS.....	71
3.4	NUMERICAL EXPERIMENT AND RESULT.....	75
3.4.1	<i>Numerical Verification of the Stability</i> .....	75
3.4.2	<i>Numerical Accuracy Versus Time Step</i> .....	78
3.5	DISCUSSION AND CONCLUSION .....	80
<b>CHAPTER 4 NUMERICAL DISPERSION ANALYSIS .....</b>		<b>82</b>
4.1	INTRODUCTION.....	82
4.2	NUMERICAL DISPERSION OF THREE-DIMENSIONAL ADI-FDTD ALGORITHM .....	83
4.3	CONVERGENCE OF ADI-FDTD SOLUTIONS .....	87
4.4	NUMERICAL DISPERSION OF TWO-DIMENSIONAL TE AND TM CASE .....	88
4.5	DISPERSION CHARACTERISTICS OF THE ADI-FDTD SCHEME -NUMERICAL RESULT .....	90
4.5.1	<i>Effects of the propagation direction on the dispersion</i> .....	90
4.5.2	<i>Effects of the large time step on the numerical dispersion</i> .....	92
4.5.3	<i>The three dimensional view of the numerical dispersion</i> .....	95
4.5.4	<i>Dispersion on the <math>k_x</math>-<math>k_y</math> plane</i> .....	98
4.6	AN IMPORTANT COROLLARY .....	101
4.7	DISCUSSION AND CONCLUSION .....	105
<b>CHAPTER 5 A HIGH ORDER ADI-FDTD METHOD FOR REDUCING DISPERSION .....</b>		<b>107</b>
5.1	INTRODUCTION.....	107
5.2	FOURTH ORDER ADI-FDTD FORMULATION .....	108
5.3	NUMERICAL STABILITY AND DISPERSION ANALYSIS .....	109
5.4	COMPARISONS BETWEEN THE FOURTH ORDER ADI-FDTD AND THE SECOND ORDER ADI-FDTD .....	113
5.5	DISCUSSIONS AND CONCLUSIONS.....	115
<b>CHAPTER 6 CONCLUSION AND SUGGESTIONS FOR FUTURE DIRECTIONS .....</b>		<b>116</b>
6.1	SUMMARY .....	116
6.2	FUTURE DIRECTIONS.....	117
6.2.1	<i>Absorbing boundary condition (ABC)</i> .....	117
6.2.2	<i>Application of nonlinear materials</i> .....	118
6.2.3	<i>Combination of MRTD and ADI-FDTD for high accuracy</i> .....	118
6.2.4	<i>Temporal High-order ADI-FDTD schemes</i> .....	118
<b>REFERENCES.....</b>		<b>120</b>



## List of Figures

Figure 1.1	Finite difference grid .....	7
Figure 2.1	Position of electric and magnetic field components in Yee's grid. ....	30
Figure 2.2	The block diagram of the difference equation. ....	36
Figure 2.3	The cavity half filled with air and the other half filled with dielectric material. ....	58
Figure 3.1	Time-domain electric fields with the conventional FDTD and the proposed FDTD. (a) The conventional FDTD solutions that becomes unstable with $\Delta t_j = 1.2 ps$ ; (b) The proposed FDTD solution with $\Delta t_i = 120 ps$ . ....	76
Figure 3.2	Time-domain electric fields at the center of the cavity recorded with the conventional FDTD and the proposed ADI-FDTD. The conventional FDTD solutions that become unstable with $\Delta t_j = 2 \times 10^{-10} s$ ; The proposed ADI-FDTD solution with $\Delta t_i = 200 \times 10^{-10} s$ .....	77
Figure 3.3	Relative errors of the conventional FDTD and the proposed FDTD as the function of relative time step $\Delta t / \Delta t_{FDTDMAX}$ . Dash line represents the unstable point of the conventional FDTD scheme. ....	80
Figure 4.1	Numerical wave phase velocity versus wave propagation angle in the ADI-FDTD grid with $\delta = \lambda / 20$ and $\Delta t = \delta / c / 5$ . ....	91
Figure 4.2	Numerical wave phase velocity with wave propagation angle in the grid for the conventional FDTD grid with at $\delta = \lambda / 20$ and $\Delta t = \delta / c / 5$ .....	91
Figure 4.3	Numerical wave phase velocity versus wave propagation angle in the ADI-FDTD grid with at $\delta = \lambda / 20$ and $\Delta t = \delta / c / \sqrt{3}$ (CFL limit) .....	93
Figure 4.4	Numerical wave phase velocity versus wave propagation angle in the ADI-FDTD grid with $\delta = \lambda / 20$ and $\Delta t = \delta / c$ (1.73 times of CFL limit). ....	93
Figure 4.5	Numerical wave phase velocity with wave propagation angle in the unconditionally stable FDTD grid with at $\delta = \lambda / 20$ and $\Delta t = 1.5 \delta / c$ (2.6 times of CFL limit).....	94
Figure 4.6	Dispersion characteristics with grid size $\delta = \lambda / 20$ and $\Delta t = \delta / c$ (1.73 times of CFL limit). ....	96
Figure 4.7	Dispersion characteristics with grid size $\delta = \lambda / 20$ and $\Delta t = 2 \delta / c$ (3.46 times of CFL limit). ....	97
Figure 4.8	Dispersion characteristics of different mash sizes at time step $\Delta t = \delta / c / 5$ .....	98
Figure 4.9	Dispersion characteristics of different mash sizes at time step $\Delta t = \delta / c / 5$ for FDTD. ....	99

Figure 4.10	Dispersion characteristics of different mesh sizes at time step $\Delta t = \delta / c / \sqrt{3}$ (CFL limit) .....	99
Figure 4.11	Dispersion characteristics of different mesh sizes at time step $\Delta t = \delta / c$ (1.73 times of CFL limit).....	100
Figure 4.12	Dispersion characteristics of different mesh sizes at time step $\Delta t = 1.5\delta / c$ (2.6 times of CFL limit).....	100
Figure 4.13	Multigridding meshes.....	102
Figure 4.14	Dispersion characteristics of different $r$ at time step $\Delta t = \delta_a / c / \sqrt{3}$ (CFL limit). 103	
Figure 4.15	Dispersion characteristics of different $r$ at time step $\Delta t = \delta_a / c$ (1.73 times of the CFL limit) .....	104
Figure 4.16	Dispersion characteristics of different $s$ at time step $\Delta t = 1.5\delta_a / c$ (2.6 times of CFL limit) .....	104
Figure 5.1	Numerical phase velocity versus wave propagation angle in the fourth order ADI-FDTD grid with $\delta = \lambda / 20$ and $\Delta t = \delta / c / 3$ .....	113
Figure 5.2	Numerical phase velocity versus wave propagation angle in the second order ADI-FDTD grid with $\delta = \lambda / 20$ and $\Delta t = \delta / c / 3$ .....	114
Figure 5.3	Numerical phase velocity versus wave propagation angle in the fourth order ADI-FDTD grid with $\delta = \lambda / 10$ and $\Delta t = \delta / c / 3$ .....	114
Figure 5.4	The numerical phase velocity error versus time step for the fourth order and the second order scheme .....	115

## List of Table

Table 1.1: Comparisons of results with the conventional FDTD and ADI-FDTD .....	57
Table 1.2: Comparisons of results with the conventional FDTD and ADI-FDTD .....	59
Table 3.1: The Proposed ADI-FDTD simulation results with different $\Delta t$ .....	78

## List of Abbreviations

ABCs	Absorbing boundary conditions
ADI	Alternating direction implicit
CFL	Courant-Friedrich-Levy
EM	Electromagnetic
EMP	Electromagnetic pulse
FD	Frequency domain
FDM	Finite difference method
FDTD	Finite-difference time-domain
FEM	Finite element method
FFT	Fast Fourier transform
MoL	Method of lines
MoM	Method of moments
MRTD	Multiresolution time-domain
PML	Perfectly matched layers
PSTD	Pseudospectral time-domain
RF	Radio frequency
SDA	Spectral domain approach
TD	Time domain
TDDE	Time-domain differential equation
TDFEM	Time domain finite element method
TE	Transverse electric
TM	Transverse magnetic
TLM	Transmission line method

## **Dedication**

This work is dedicated to my wife Jin Sun, whose postgraduate study was coincident with mine, making our joint endeavor that much more fun.

## **Acknowledgements**

First and foremost, my thanks go to my supervisor Dr. Zhizhang (David) Chen for his most valuable guidance throughout this thesis work. Thanks also go to Killam Scholarship from Dalhousie University and financial support from the National Science and Engineering Research Council of Canada. Thanks to the Electromagnetic Laboratory and the Department of Electrical and Computer Engineering in DalTech, Dalhousie University, for sponsoring my use of the computing and network facilities, which enabled me to undertake this research.

Thanks to Dr. W. Phillips for the helpful discussions especially on solving high order equations. Thanks to Dr. S. Nugent for the suggestions on my thesis proposal presentation. Thanks to Dr. J. Zhang for his helpful discussions.

Special thanks to Mrs. S. Pace and Mrs. C. Twai for their kindly help during the period of my study.

Thanks to my parents for making all this possible.

## **ABSTRACT**

Computational electromagnetics has been an important research area because its capability and flexibility to accurately model and simulate what is really occurring in an actual electrical and electronic circuit and system. In particular, the demands for efficient analysis of the high-frequency broadband structures have driven the research into the application of time domain techniques. As a result, the finite-difference time-domain (FDTD) method, one of the most popular time domain techniques, has been widely studied and applied in solving electromagnetic problems. Its capability of handling electrically large or high-Q structure problems is, however, limited by the requirements of large computation memory and time. Such requirements are due to the numerical dispersion errors and the Courant-Friedrich-Lewy (CFL) stability condition. Consequently, a way to improve the computational efficiency would be to remove or alleviate the two constraints. Most of the recent research efforts so far have been focused on developing low-dispersion schemes such as multiresolution time-domain (MRTD) method and pseudospectral time-domain (PSTD) method to lower computation memory requirement.

In this thesis a new direction is opened in improving the FDTD computation efficiency; i.e. the removal of the CFL stability condition. The principle of alternating direction implicit (ADI) technique that has been used to solve parabolic differential equations is applied. However, unlike the conventional ADI algorithms, a modified ADI technique is developed. The alternation is performed in the mixed coordinates each time step rather than in each coordinate each time step. Consequently, in the three-dimensional case, only two alternations in solution marching are required. Therefore, the CFL stability constraint is completely removed in a FDTD method based on the modified ADI technique. The FDTD time step is no longer restricted by the CFL stability condition but by the modeling accuracy of the FDTD algorithm because of the mixed ADI and the FDTD. The new scheme is named ADI-FDTD.

Theoretical proof of the unconditional stability of ADI-FDTD scheme is given and numerical results are presented to demonstrate the effectiveness and efficiency of the proposed method. It is found that the number of iterations with the proposed ADI-FDTD can be at least four times less than that with the conventional FDTD at the same numerical accuracy. As a result, FDTD iteration number and CPU time are reduced.

Furthermore, a comprehensive analysis of the numerical anisotropy and dispersion of the ADI-FDTD is presented. The dispersion relation is derived analytically and the effects of spatial and time steps on the numerical dispersion are investigated. From the dispersion analysis, it is found that the ADI-FDTD method has advantages over the conventional FDTD of Yee's scheme in modeling structures with fine geometry where a fine local mesh is required. The ADI-FDTD allows the use of a much larger time step while numerical dispersion errors remain acceptable. Finally, a high-order ADI-FDTD is proposed and its unconditional stability is shown as well. Numerical dispersion analysis shows that the dispersion in high-order ADI-FDTD scheme is reduced significantly compared to the second-order ADI-FDTD scheme.

In conclusion, the ADI-FDTD is expected to become a very efficient tool in simulating electromagnetic behaviors in RF/microwave circuits and devices, although many other issues such as interfacing multigrid regions still need to be investigated further.



# **Chapter 1 Introduction**

## **1.1 Literature Review: The State of the Art for Solving Maxwell's Equations**

Maxwell's partial differential equations of electrodynamics represent a fundamental unification of electric and magnetic fields. They provide the starting point for the study of electromagnetic problems, together with certain principles and theorems such as superposition, reciprocity, equivalence, induction, duality, linearity, and uniqueness. The solutions of these equations are widely investigated for the purpose of analyzing electromagnetic wave guiding, radiation and scattering. Applications based on solving Maxwell's equations can be found in various areas since Maxwell's equations were firstly formulated in 1870. These applications include atom smashes, cathode-ray oscilloscopes, radar, satellite communication, television reception, remote sensing, radio astronomy, microwave electronics, optical fiber communication, transients in transmission lines, electromagnetic compatibility, aircraft-landing systems, electromechanical energy conversion, and wireless communication.

Generally there are three ways to predict electromagnetic effects. They are experiment, analytical analysis and numerical computation. Among these three methods, numerical computation is the newest and fastest growing approach, inspired by two major factors: its flexibility and ability to solve complex real-world electromagnetic field problems, and the dramatic advance in computer hardware that allows the handling of numerical problems with heavy requirements in computation time and memory [1]-[100].

Electromagnetic computation encompasses the modeling, simulation, and analysis of electromagnetic responses of a complex electrical system to various electromagnetic stimuli. It may be defined as the branch of electromagnetics that intrinsically and routinely involves using a digital computer to obtain numerical

results. Electromagnetic computation results provide a better understanding of the system response that allows for more optimized design or modification of the system.

Accurate electromagnetic computation has become a significant part of a design process as the demand for CAD tools for circuits and devices operating with high-frequency broadband signals is increasing. Advanced processing technique in fabrication has enabled large-scale circuit integration, with the incorporation of hundreds or even thousands of components into a single package or circuit board. While such integration leads to the development of high speed, compact devices such as ultra high speed transceiver for internet backbone and personal communication systems (pagers, cellular phones, broad band wireless modems, etc.), various electromagnetic interactions such as cross-talk among different circuits parts become more and more predominant in determining the circuit performance. Consequently, the analysis of the electromagnetic computation is essential to the design of today's high-frequency systems, and it can reduce the need for difficult and time-consuming measurement of the system or a trial-and-error design procedure.

Based on the solution domain of the problem, there are two major types of methods in computational electromagnetics: frequency domain (FD) [1-37] methods (where the phase and frequency responses of a system are considered) and time domain (TD) methods [38-110] (where the time evolution of a signal or system is considered).

Naturally, frequency domain methods can be computationally more efficient since only a narrow range of frequency is of interest. However, they cannot easily deal with nonlinear elements. Time domain methods can provide solutions of wideband frequency spectrum and can easily handle nonlinear elements but require a large number of iterations if high frequency is of interest. Conversion

between time and frequency domain results may be achieved by Fourier transform.

Both frequency domain methods and time domain methods are reviewed in following sections. Their advantages and disadvantages are discussed.

### **1.1.1 Frequency Domain Methods**

#### **A Method of Moments (MoM)**

The method of moments is a general form of weighted residuals techniques. In the theory of mathematics the method of moments is an interior weighted residual method in which the power series are chosen as the weighting function. In electromagnetic field theory, method of moments, originally used by Harrington [1], extends the use of weighting functions to non-power series. It is shown that such method of moments is ideally suitable for solving electromagnetic radiation and scattering problems [2-7].

The method of moments can be summarized as follows. Suppose that the equation to be solved is

$$Lu = f . \tag{1.1}$$

where  $L$  can be either differential or integral operators.  $f$  is known force function and  $u$  is the solution to be found.

Assume the solution can be approximated with

$$u = \sum_{i=1}^n \alpha_i \psi_i \tag{1.2}$$

where  $\alpha_i$  are unknown parameters of the approximate solution and  $\psi_i$  are the basis functions.

By selecting a set of test functions  $w_i$  ( $i = 1, 2, \dots, n$ ), which are linearly independent functions, and setting the residual to zero, a set of algebraic equations are generated:

$$\sum_{i=1}^n \alpha_i \langle L\psi_i, w_i \rangle = \langle f, w_m \rangle \quad m = 1, 2, \dots, n. \quad (1.3)$$

In a matrix form, they become

$$A\{\alpha\} = B \quad (1.4)$$

where  $\{\alpha\}$  is a column vector which consists of the unknown parameters of the approximate solution; and

$$A = \begin{bmatrix} \langle L\psi_1, w_1 \rangle & \langle L\psi_2, w_1 \rangle & \cdots & \langle L\psi_n, w_1 \rangle \\ \langle L\psi_1, w_2 \rangle & \langle L\psi_2, w_2 \rangle & \cdots & \langle L\psi_n, w_2 \rangle \\ \vdots & \vdots & \vdots & \vdots \\ \langle L\psi_1, w_n \rangle & \langle L\psi_2, w_n \rangle & \cdots & \langle L\psi_n, w_n \rangle \end{bmatrix}$$

$$B = \begin{bmatrix} \langle f, w_1 \rangle \\ \langle f, w_2 \rangle \\ \vdots \\ \langle f, w_n \rangle \end{bmatrix}$$

By solving the matrix (1.4), we can obtain an approximate solution (1.2).

Due to the flexible choice of the basis functions  $\psi_i$  and the weighting functions  $w_i$ , the method of moments can be used to solve static, quasi-static and dynamic problems expressed by differential or integral equations [8-11]. Some commercial EM (electromagnetic) simulators such as HP Momentum are based on this technique.

## B Finite Element Method

Finite element method (FEM) [12] is one of most popular frequency domain computational methods for solving electromagnetic problems [13][14]. The FEM is based on energy functional which represents the total energy associated with a particular system. Solutions of Maxwell's equations always require that the energy within a structure is minimized, i.e. that the functional is minimized. In FEM, a solution space is first discretized into many discrete elements. The discrete elements are usually triangles (in 2D) and tetrahedra (in 3D). Each discrete element can be of different size and shape. Any field quantity can be expanded in terms of user-defined basis functions. The basis functions are usually linear function over the surface or volume of the finite element. By minimizing the functional, a system of equation is obtained for the expansion coefficients. Solved for the expansion coefficients, the FEM solutions are obtained. In general, electromagnetic properties can differ from cell to cell, hence inhomogeneous structures can be modeled [12].

The energy functional can be obtained by integrating the field over a structure volume and may be different for various problems [15][16]. For example, to solve a three-dimensional time-harmonic problem is equivalent to minimizing the integral

$$F = \int_v \left( \frac{\mu |H|^2}{2} + \frac{\epsilon |E|^2}{2} - \frac{J \cdot E}{2j\omega} \right). \quad (1.5)$$

This integral is referred to as a functional. We can calculate the integral by expanding the unknown field as a sum of known basis functions with unknown coefficients: we thus obtain a functional based on these coefficients. Minimizing the functional by setting its first derivatives with respect to all coefficients equal to zero leads to a matrix equation with all the unknown coefficients. By solving the equations for the coefficients, we can obtain the FEM solutions in terms of the

expansion. As a result, instead of solving field quantities directly, we solve a system of linear equations for expansion coefficients.

In general, the node-based elements will cause spurious modes when modeling problems such as cavities [17]. Consequently, edge-based finite elements have been developed for free of this shortcoming. These types of edge-based elements were described in reference [18] by Whitney and have been revived in reference [19] by Nedelec. In recent years, the edge-based elements were applied to model full three-dimensional vector problems [20][21].

An important advantage of FEM is the flexibility in its discretization of the structure. Tetrahedral elements are used in FEM rather than the simple cubic cells used in finite difference method (which will be introduced in the following section). Such tetrahedral elements can conform well with boundaries for easy handling of non-rectangular structures. Nevertheless, pre and post-data processing of FEM are more complex than that of the finite difference method. In addition, because the whole region has to be discretized, a tremendous number of nodes and elements are required.

### C Finite Difference Method

The finite difference method (FDM) [22] is an approximate method for solving partial differential equations. It has been used in solving a wide range of problems [22][23]. The method can be applied to EM problems with different boundary shapes, different kinds of boundary conditions, and regions containing a number of different materials. The application of FDM is simple and straightforward as it involves only simple arithmetic in the derivation of discretized equations and in writing the corresponding computer codes. During 1950-1970, FDM was the most important numerical method used to solve practical EM problems [24][25]. With the development of high-speed computers with large scale storage capability, and the ease of application of the finite

differential method, it becomes increasingly popular in solving electromagnetic problems [26][27]. Its time domain version, FDTD, has become one of the most widely used schemes which will be discussed later on.

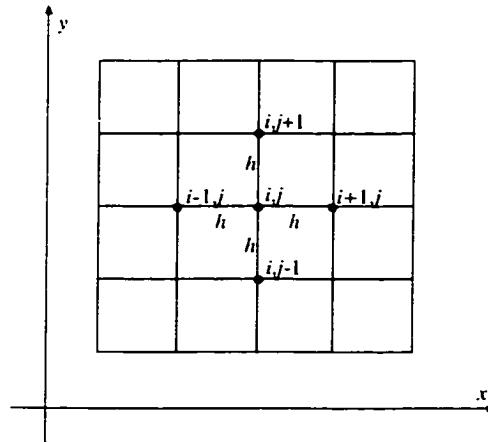


Figure 1.1 Finite difference grid

The basic idea of FDM is to replace the derivatives of an unknown function by the difference quotients of the unknown functions. The procedure can be viewed in three steps:

- 1) Discretize the solution domain of interest.
- 2) Replace the derivatives of the unknown function by the difference quotient of the function related to several adjacent nodes and form a system of linear equations with the field quantities at the grid nodes to be found. For example,

$$\nabla^2 u = \frac{\partial^2 u}{\partial x^2} + \frac{\partial^2 u}{\partial y^2} \approx \frac{u_{i+1,j} + u_{i-1,j} - 2u_{i,j}}{h^2} + \frac{u_{i,j+1} + u_{i,j-1} - 2u_{i,j}}{h^2} \quad (1.6)$$

where  $\nabla^2 u$  at node  $(i,j)$  is replaced by an algebraic finite-difference operation of the function at five adjacent nodes which are shown in Figure 1.1.

3) Solve the system of linear equations with certain boundary conditions.

It was reported that FDM is more efficient than the FEM by a factor of 2 in computer storage for calculating the propagation constants and fields of a dielectric wave guide [27]. For solving 3-D problems within a cubic volume, the FDM is still considered to be an efficient method. If a region contains different materials and complex shapes, the programs become more complicated. If the field contains rapid changes of gradient, the accuracy declines. In these cases, the finite element method is preferred.

#### D Spectral Domain Approach (SDA)

The spectral domain approach (SDA) is a Fourier-transformed version of integral equation method applied to planar structures. SDA is also referred as spectral domain method or spectral domain analysis in some references. It was presented by Itoh and Mittra to calculate the dispersion characteristics of microstrip lines [28]. It has been widely used in investigating planar structures including the microstrip line, finline, slotline and coplanar waveguide [28-30].

The formulation of this method involves a coupled set of two algebraic equations that are actually Fourier transforms of coupled integral equations derived in the spatial domain. Determining a Green's function is one of the most important and indispensable steps in SDA to obtain those two algebraic equations. The derivation of these Green's functions can be done readily by the use of immittance approach [31]. These equations are then solved for the Fourier transformed unknown current distribution for a strip by means of Galerkin's method. The unknown currents are expanded in terms of known basis functions. Note that the basis functions need to be Fourier transformed analytically.

The major advantage of the SDA is its numerical efficiency. The price is, however, the required significant amount of analytical pre-processing before numerical calculation. In addition, the range of its application is limited. For



example, the application is usually restricted to well shaped structures. Another limitation is that it requires infinitesimally thin conductors. It is not easy to treat a strip with finite conductivity [31].

### E Method of Lines (MoL)

The method of lines (MoL) was developed in order to solve partial difference equations [33]. Schulz and Pregla applied the principle of MoL to the calculation of planar microwave structure [34].

The concept of MoL is that all but one of independent variables of partial differential equations are discretized to obtain an order-reduced system of ordinary differential equations. For instance, for the analysis of waveguides with constant cross-section, it could be done with respect to one coordinate direction. The electromagnetic fields can be described by the independent field components  $E_z$  and  $H_z$ , which have to satisfy the Helmholtz equation

$$\frac{\partial^2 \psi}{\partial x^2} + \frac{\partial^2 \psi}{\partial y^2} + (k^2 - k_z^2) \psi = 0, \quad (1.7)$$

where  $\psi$  can be either  $E_z$  or  $H_z$ .

The  $x$  direction is discretized by a set of  $N$  straight lines parallel to the  $y$ -axis. Assume the distance between adjacent lines is  $h$ , the potential can be replaced by a set  $(\psi_1, \psi_2, \dots, \psi_N)$  at the lines at  $x_i = x_0 + ih$   $i = 1, 2, \dots, N$ .

By replacing the partial derivative with respect to the  $x$  coordinate with the difference approximation, equation (1.7) yields a system of  $N$  coupled ordinary differential equations in respect to the non-discretized coordinate,  $y$ .

$$\frac{\partial^2 \psi_i}{\partial y^2} + \frac{1}{h^2} (\psi_{i+1}(y) - 2\psi_i(y) + \psi_{i-1}(y)) + (k^2 - \beta^2) \psi_i(y) = 0 \quad i = 1, 2, \dots, N \quad (1.8)$$

or in matrix form

$$h^2 \frac{\partial^2 \Psi}{\partial y^2} + (\mathbf{P} - h^2(k^2 - \beta^2)\mathbf{I})\Psi = 0 \quad (1.9)$$

where  $\mathbf{I}$  is the identity matrix and  $\mathbf{P}$  is a tridiagonal matrix determined by the lateral boundary condition at  $x=0$  and  $x=a/2$ .  $\Psi$  is the column vector  $(\Psi_1, \Psi_2, \dots, \Psi_N)$ . Note that the discretization lines for  $E_z$  and  $H_z$  are shifted by  $h/2$ , which makes it easy to implement the lateral boundary condition.

Because  $\mathbf{P}$  is a real symmetric matrix, there is a orthogonal matrix  $\mathbf{T}$  such that

$$\mathbf{T}'\mathbf{P}\mathbf{T} = \text{diag}(\lambda). \quad (1.10)$$

where  $\mathbf{T}'$  denotes the transpose of  $\mathbf{T}$  and the elements of the diagonal matrix  $\text{diag}(\lambda)$  are eigenvalues of  $\mathbf{P}$ .

By introducing

$$\mathbf{T}'\Psi = \mathbf{U}, \quad (1.11)$$

the system of  $N$  coupled ordinary equations (1.9) can be uncoupled:

$$h^2 \frac{\partial^2 U_i}{\partial y^2} + (\lambda_i - h^2(k^2 - \beta^2))U_i = 0 \quad i = 1, 2, \dots, N \quad (1.12)$$

which can be solved analytically for each homogeneous region.

The method of lines has been extensively used for a number of practical problems such as microstrip resonator [35], stripline coupler [36], and via hole in multilayer packaging [37]. However, in most cases MoL is restricted to the analysis of planar and quasiplanar wave guide structures.

### **1.1.2 Time Domain Methods in Electromagnetics: Advantages and Restrictions**

Although the Maxwell curl equations are usually presented in the time domain (TD), i.e., with time as an explicit, independent variable, until relatively recently most electromagnetic instruction and research has taken place in the frequency domain where time-harmonic behavior is assumed. A major reason for favoring the FD over the TD in the precomputer era had been that a FD approach was generally more tractable analytically. Furthermore, the experimental hardware available for making measurements in the past years was largely confined to the frequency domain. The inferior position of time domain methods began to change with the arrival of the cheap powerful digital computer. In recent times, there have been increased interest in the direct time domain methods to calculate electromagnetic scattering/interaction phenomenon. This may be due to the surge in activities in such areas as:

- 1) electromagnetic pulse (EMP) application and short-pulse radar [38][39] that involve strong transient effects.
- 2) high speed digital circuit packaging and interconnects which include the propagation, crosstalk and radiation of electronic digital pulses.
- 3) broad band signal transmission, where signals are mostly interpreted in time domain.

Direct transient analysis is preferred in these applications. Thus, the time domain method is natural choice because they have several advantages over conventional frequency domain methods:

- 1) they work better for wideband signature studies, are better suited for parallel processing, and can provide better visual representations for understanding the field interactions;

- 2) they need to be run only once to obtain the information over a wide range of frequencies, and the frequency domain information may be extracted from the time domain data via Fourier transform.
- 3) they can handle very short pulse excitations such as electromagnetic pulse and lightning which are not very suitable for frequency domain method.

Representative examples of the growing variety of TD research include the original time-domain differential equation (TDDE) approach by Yee [40], which forms the basis of the widely used finite difference time domain (FDTD) model [41]. An alternate implementation of TDDE models was shortly thereafter developed as the transmission line method (TLM) by John and Beurle [42]. To extend TD method to a nonorthogonal grid, the method of point-matched finite elements was developed by A. C. Cangellaris et al. [43] who proposed the use of finite-element interpolation for the development of a time-domain integration scheme. It is so called time domain finite element method (TDFEM). Recently, TD versions of the method of lines (TDML) and geometrical theory of diffraction (TDGTD) were presented by Nam et al. [44] and Veruttipong [45], respectively.

The following sections review the published work that has been conducted in several popular time domain electromagnetic modeling.

#### A The Finite-Difference Time Domain Method (FDTD)

FDTD approaches are widely used because of their simplicity for numerical implementation and relatively low requirements in respect with CPU time. It is a computationally efficient means of directly solving Maxwell's time-dependent curl equations or their equivalent integral equations using the finite difference approximations. In general, FDTD is simple and flexible. It can be used to solve various types of electromagnetic problems [46], such as anisotropic and nonlinear problems. Since it is a time-domain method, one single run of

simulation can provide information over a large bandwidth when the excitation is chosen to be of large bandwidth.

Despite its simplicity and flexibility, the FDTD applications have been limited to solving electrically small structure problems. The main reason is that the FDTD is not yet computationally efficient. For an electrically large problem, it requires large memory and CPU time to obtain accurate solutions. As a result, computation efficiency becomes the bottleneck for the further applications of the FDTD method.

Theoretical studies on the FDTD show that the intensive memory and CPU time requirements mainly come from the following two modeling constraints [46][47]. Firstly, the spatial increment step must be small enough in comparison with the wavelength (usually 10-20 steps per smallest wavelength) in order to obtain accurate field component values. Secondly, the time step must be small enough to meet the Courant-Friedrich-Levy (CFL) stability condition. If the time step is not within the CFL bound, the FDTD scheme will become numerically unstable, leading to a spurious increase of the field values without limit as a FDTD solution marches.

Since the thesis work is based on FDTD, more details and discussions of FDTD will be given in Chapter 2.

## B The Transmission Line Method (TLM)

TLM is another popular time domain method developed by Johns and Beurle [42], who took a conceptually different approach from that of the straightforward differencing of the Maxwell equations. The work is then extended to inhomogeneous material [48], lossy media [49], and the three-dimension case [50]. It employs the analogy between transmission line and plane wave propagation. The field space is discretized into a 2D or 3D grid or mesh of transmission lines interconnected at nodes. The discrete mesh elements are

usually rectangles (in 2D) and cuboids (in 3D). TLM can be viewed as a three-dimensional transmission-line discrete-model of Maxwell equations. The method, though, can also be interpreted as an implementation of Huygen's principle, in which fields spreading in space can develop and form as a series of secondary sources. The equivalence between the TLM and a modified FDTD approach was shown by Chen et al. [51]. They showed this equivalence by using a mesh in which the field components are all defined at the same cell-centered node and decomposed the field components into components traveling toward and away from nodes.

Similar to FDTD, TLM models involve space and time discretization. As a result, they are also subject to problems of mesh dispersion and anisotropy [52][53][54]. Nevertheless, there are several major differences between TLM and FDTD. Firstly, the partial fields of oppositely propagating waves are separately represented in TLM, whereas in FDTD the summed fields are computed. Secondly, because the electric and magnetic fields are determined at common points, defining a surface in TLM is less ambiguous than in the FDTD. Thirdly, that knowledge of wave propagation in opposite directions along each leg of a transmission line of known impedance makes it possible to solve directly for the electrical properties required to provide a reflectionless boundary [55]. However, TLM is not as widely used as FDTD because it is less intuitively structured and sometimes more difficult to understand than FDTD. In addition, TLM seems to possess more set of spurious modes than FDTD.

### C The Time Domain Finite Element Method (TDFEM)

Unlike the FDTD and TLM described in previous sections, the TDFEM can be used with unstructured grids which improves the modeling capabilities of arbitrary geometries. The FEM introduced before was originally applied for approximate solutions of boundary value problems. It was a natural step in developing similar methods for initial value problems. The recently developed TDFEM [43][56-58] is

base on solving the wave equation for electric or magnetic field. The functional corresponding to the equation:

$$\nabla^2 u - \mu\epsilon \frac{\partial^2 u}{\partial t^2} = 0 \quad (1.13)$$

is

$$F(u) = \int_v \left( 0.5 |\nabla u|^2 + \mu\epsilon u \frac{\partial u}{\partial t} \right) dv. \quad (1.14)$$

where  $u$  is electric or magnetic field.  $\epsilon$  is the medium permittivity and  $\mu$  is the medium permeability.

By following the FEM procedure for space discretization and field expansions, and minimizing the functional, a system of ordinary differential equations may be obtained

$$\mu\epsilon A \frac{\partial^2 u}{\partial t^2} + B u = C, \quad (1.15)$$

where  $A$  and  $B$  are known matrices related to discretization steps and geometry. The vector  $C$  consists of known elements related to the excitation functions and boundary conditions. The above equation can be discretized in time domain and then can be solved by updating the electromagnetic field distribution in a leapfrog fashion.

In comparison with FDTD, the TDFEM techniques have the remarkable stability and the flexibility of modeling complex structures with curved boundaries. Much research [59-62] has been carried out on the improvement of the TDDEM. However, TDFEM techniques have not been used widely. The reasons are that: (A) it requires unstructured 3-D mesh generation, which takes a significant amount of effort to develop; (B) it needs large pre and post-data processing,

which adds more computation loads; and (C) it is more time consuming than the FDTD on every time step advancing. Therefore, some research [63-67] has been conducted on a hybrid method that combines finite-difference and finite element time domain techniques.

### **1.1.3 Other Computational Efficiency Improved Techniques**

As mentioned in the previous section, FDTD requires large memory and CPU consumption due to small spatial discretization and CFL constraint. To circumvent or relax the above constraints, various time-domain techniques have been developed [68-73], resulting in the improvement of the computation efficiency. Along the line of relaxing the first constraint, multiresolution time-domain (MRTD) method was proposed by Krumpholz and Katehi [68]. Through the applications of orthonormal wavelet spatial expansions to Maxwell's equations, MRTD scheme can reduce numerical dispersion significantly. The spatial discretization resolution can be made as low as two grid points per wavelength, leading to a large saving in computation memory. Similarly, another technique, the pseudospectral time-domain (PSTD) method, was also developed recently [69]. By applying the Fourier transform to spatial derivatives, the PSTD method can also achieve a spatial grid of two points per wavelength while maintaining a high accuracy. Nevertheless, in both cases, the second constraint still remains. For MRTD, the stability condition becomes even more stringent. The time to spatial step ratio becomes five times less than that with the conventional FDTD.

A few attempts were made to relax or even remove the stability constraint. Early work [70] was reported in 1984 where the alternating-direction-implicit (ADI) technique [74] was first applied to the Yee's grid in order to formulate an implicit FDTD scheme. In that paper, the finite-difference operator for a 3D solution of Maxwell's equations was factored into three operators with each operator being



performed in one of the coordinate direction (namely,  $x$ ,  $y$ , or  $z$ ). The scheme required three implicit sub-step computations for each FDTD recursive cycle and it was never found to be completely stable without adding significant dielectric loss. In 1990, a specially designed two-dimensional FDTD algorithm, which employs time steps larger than those allowed by methods with explicit time advancement, was presented in references [71][72]. Nevertheless, it is based on a new staggered grid different from Yee's and the grid points and field components are twice that of the Yee's on a body surface. Consequently, the method consumes more computer memory and computation resources. In addition, only two-dimensional problems were solved and presented in reference [71]. Very recently, a two-dimensional FDTD algorithm free of the CFL stability conditions was proposed for a 2D-TE case [73].

In the following sections, a more detailed review of these new developed techniques are presented.

#### A The Pseudospectral Time-Domain (PSTD)

The pseudospectral method in time-domain was introduced by Q. H. Liu [69] [75]. The method is called pseudospectral time-domain (PSTD) method. It uses the Fast Fourier Transform (FFT) instead of finite difference to compute spatial derivatives in the spatial spectral domain. According to Nyquist sampling theorem, only two grids per wavelength are necessary, compared to 10 grid per spatial wavelength needed by the FDTD method. Therefore, the memory requirement of PSTD is much less than the FDTD method. PSTD has been extended to dispersive and lossy media [76] [77].

To be more explicit, the following paragraphs explain the main difference between PSTD and FDTD in the representation of spatial derivatives. In the Yee's FDTD algorithm, central difference approximation for space derivatives is used:

$$\frac{\frac{\partial f(n\Delta x, m\Delta y, l\Delta z, k\Delta t)}{\partial x}}{\frac{f(n\Delta x + \frac{\Delta x}{2}, m\Delta y, l\Delta z, k\Delta t) - f(n\Delta x - \frac{\Delta x}{2}, m\Delta y, l\Delta z, k\Delta t)}{\Delta x}} = \quad (1.16)$$

In the PSTD method, the space derivative is computed through the Fourier transform [69]

$$\frac{\partial f(n\Delta x, m\Delta y, l\Delta z, k\Delta t)}{\partial x} = -F^{-1}[ik_x F\{f(n\Delta x, m\Delta y, l\Delta z, k\Delta t)\}], \quad (1.17)$$

where  $F$  and  $F^{-1}$  denote the forward and inverse Fourier transform, and  $k_x$  is Fourier transform variable, or spatial frequency along the  $x$  direction.

To eliminate the wraparound effect introduced by FFT, it is necessary to implement perfectly matched layers [78] (PML) (an efficient absorbing boundary condition originally developed for FDTD) at the outside edge.

In the PML layers, Maxwell equations are split and derived with a coordinate-stretching variable  $e_\eta = a_\eta + i\frac{\omega_\eta}{\omega}$  ( $\eta = x, y, z$ ) [79]:

$$a_\eta \mu \frac{\partial \mathbf{H}^{(\eta)}}{\partial t} + \mu \omega_\eta \mathbf{H}^{(\eta)} = -\frac{\partial}{\partial \eta} (\hat{\eta} \times \mathbf{E}) - \mathbf{M}^{(\eta)}, \quad (1.18a)$$

$$a_\eta \varepsilon \frac{\partial \mathbf{E}^{(\eta)}}{\partial t} + (a_\eta \sigma + \omega \varepsilon_\eta) \mathbf{E}^{(\eta)} + \omega_\eta \sigma \int_{-\infty}^t \mathbf{E}^{(\eta)} dt = -\frac{\partial}{\partial \eta} (\hat{\eta} \times \mathbf{H}) - \mathbf{J}^{(\eta)}, \quad (1.18b)$$

where  $\mathbf{E} = \sum_{\eta=x,y,z} \mathbf{E}^{(\eta)}$ , and  $\mathbf{H} = \sum_{\eta=x,y,z} \mathbf{H}^{(\eta)}$ .

By using FFT algorithm stated in equation (1.17), equation (1.18) can be rewritten as

$$a_\eta \mu \frac{\partial \mathbf{H}^{(\eta)}}{\partial t} + \mu \omega_\eta \mathbf{H}^{(\eta)} = \hat{\eta} \times \mathbf{F}_\eta^{-1} \{ i k_\eta \mathbf{F}_\eta [\mathbf{E}] \} - \mathbf{M}^{(\eta)}, \quad (1.19a)$$

$$a_\eta \varepsilon \frac{\partial \mathbf{E}^{(\eta)}}{\partial t} + (a_\eta \sigma + \omega \varepsilon_\eta \mathbf{E}^{(\eta)} + \omega_\eta \sigma \int_{-\infty}^t \mathbf{E}^{(\eta)} dt) = \hat{\eta} \times \mathbf{F}_\eta^{-1} \{ i k_\eta \mathbf{F}_\eta [\mathbf{H}] \} - \mathbf{J}^{(\eta)}. \quad (1.19b)$$

Equation (1.19) consists twelve scale equations, since both  $\mathbf{E}^{(\eta)}$  and  $\mathbf{H}^{(\eta)}$  have two scalar components perpendicular to  $\hat{\eta}$ . Because the PSTD method does not use the spatial staggered grid, all field components are co-located at the same point or condensed nodes are used. This advantage makes the programming simpler.

Compared to FDTD, PSTD method use only  $(1/8)^D - (1/4)^D$  [75] ( $D$  is the dimensionality) memory that required by FDTD, and it is simple to implement because the nodes are condensed.

The dispersion relation of PSTD is given as [69]

$$k = \frac{2}{c\Delta t} \sin \frac{\omega\Delta t}{2}. \quad (1.20)$$

In comparison with the dispersion relation of FDTD [47]

$$k = \frac{\Delta x}{c\Delta t} \sin \frac{\omega\Delta t}{2}, \quad (1.21)$$

the dispersion error of PSTD is smaller.

Because spatial Fourier transform requires the field to be continuous within the whole spatial domain, problems arise when the fields are discontinuous, for examples, at the boundary of perfect conductor where the magnetic field components are not continuous [69]. In such a case, the PSTD is not effective. Furthermore, PSTD is not suitable for highly inhomogeneous media. A combine

FDTD and PSTD method [80] was developed recently to retain the merits of each individual method.

It should be noted that as an explicit approach, PSTD is still constrained by the CFL stability condition. Furthermore, the complex computations inherited from FFT doubles the compute memory requirement and results in less saving in computation time than expected.

## **B The Multiresolution Time-Domain Method (MRTD)**

In 1996, a multi-resolution time-domain method [68] was proposed based on Battle-Lemarie wavelets, which shows an excellent capability to approximate the exact solution with negligible error at the Nyquist sampling rates in space. At the same time, Daubechies-wavelet-based technique [81], and a multigrid technique using Haar wavelets [82][83] were reported. These MRTD have been applied to analyze cavity resonators [68,82,84], microstrip lines [85,86], patch antennas [87], and nonlinear problems [88].

Basically, by applying method of moments to Maxwell's equations in its temporal form, the MRTD can be derived with the use of scaling and wavelet functions as a set of basis functions. It is worth to mention that Yee's FDTD can also be derived in the same way by choosing pulse functions for the expansion of the unknown field [89][90].

Wavelets are localized waves. Instead of oscillating forever, they drop to zero quickly. They can be obtained from an iteration of filters [91][92] and used as scaling functions and wavelets. The scaling function and wavelets have remarkable multi-resolution properties. Suppose a function can be expanded in the  $j$ -th level of scaling function, then it can also be expanded in the  $(j-1)$ -th level of scaling function and the  $(j-1)$ -th level of wavelets. Such expansion can be represented as

$$\sum_k a_{jk} \phi_{jk}(x) = \sum_k a_{j-1,k} \phi_{j-1,k}(x) + \sum_k b_{j-1,k} w_{j-1,k}(x). \quad (1.22)$$

where  $\phi_{jk}(x) = 2^{j/2} \phi(2^j x - k)$  is in scaling function,  $w_{jk}(x) = 2^{j/2} w(2^j x - k)$  is the wavelet,  $a_{jk}$  is scaling coefficient, and  $b_{jk}$  is wavelet coefficient.

Let  $V_j$  denote the space of all combinations of the  $j$ -th level scaling functions, and  $W_j$  denote the space of all combinations of the  $j$ -th level wavelets. The key statement of multiresolution can be expressed as

$$V_j = V_{j-1} \oplus W_{j-1}. \quad (1.23)$$

$V_j$  has the following properties:

$$V_j \subset V_{j+1} \quad \forall j \in \mathbb{Z}$$

$$\bigcup_{j \in \mathbb{Z}} V_j \text{ is dense in } L^2(\mathbb{R})$$

$$\bigcap_{j \in \mathbb{Z}} V_j = \emptyset$$

$$f(x) \in V_j \Leftrightarrow f(2x) \in V_{j+1} \quad \forall j \in \mathbb{Z}$$

$$f(x) \in V_j \Leftrightarrow f(x - 2^{-j}n) \in V_j \quad \forall j, n \in \mathbb{Z}$$

Moreover, it has been shown that there exists a function  $w(x)$ , the wavelets, such that the set

$$\{w_{jn}(x)\}_{n \in \mathbb{Z}} = \{2^{j/2} w(2^j x - n)\}_{n \in \mathbb{Z}} \quad j \in \mathbb{Z} \quad (1.24)$$

is orthogonal basis of  $L^2(\mathbb{R})$ .

In MRTD, the field components are expanded in terms of scaling function  $\phi_m$ .

$$E_x = \sum_{k,l,m,n=-\infty}^{+\infty} E_{l+1/2,m,n}^{\alpha x} h_k(t) \phi_{l+1/2}(x) \phi_m(y) \phi_n(z) \quad (1.25)$$

where the indices  $k,l,m,n$  are the discrete time and space indices related to the time and space coordinates via  $t = k\Delta t$ ,  $x = l\Delta x$ ,  $y = m\Delta y$ , and  $z = n\Delta z$ . The  $\Delta t$ ,  $\Delta x$ ,  $\Delta y$ , and  $\Delta z$ , represent the time and space discretization steps.

The function  $h_m(x)$  is defined as

$$h_m(x) = h\left(\frac{x}{\Delta x} - m\right) \quad (1.26)$$

with

$$h(x) = \begin{cases} 1 & \text{for } |x| < 1/2 \\ 1/2 & \text{for } |x| = 1/2 \\ 0 & \text{for } |x| > 1/2 \end{cases}$$

The function  $\phi_m(x)$  is defined as

$$\phi_m(x) = \phi\left(\frac{x}{\Delta x} - m\right) \quad (1.27)$$

where  $\phi(x)$  is the scaling function. For example,  $\phi(x)$  represents the cubic spline Battle-Lemarie scaling function in M. Krumpholz's MRTD [93][94].

The above field expansions are inserted into Maxwell's equations and sampling of the equations is carried out with pulse function as test functions in time and scaling functions as test functions in space. MRTD formulas are obtained with the following identities,

$$\int_{-\infty}^{+\infty} h_m(x) h_{m'}(x) dx = \delta_{m,m'} \Delta x \quad (1.28a)$$

$$\int_{-\infty}^{+\infty} h_m(x) \frac{\partial h_{m'+1/2}(x)}{\partial x} dx = \delta_{m,m'} - \delta_{m,m'+1} \quad (1.28b)$$

$$\int_{-\infty}^{+\infty} \phi_m(x) \phi_{m'}(x) dx = \delta_{m,m'} \Delta x \quad (1.28c)$$

$$\int_{-\infty}^{+\infty} \phi_m(x) \frac{\partial \phi_{m'+1/2}(x)}{\partial x} dx = \sum_{i=-\infty}^{+\infty} a(i) \delta_{m+1,m'} \quad (1.28d)$$

For example, for one of the scale Maxwell equations

$$\varepsilon \frac{\partial E_x}{\partial t} = \frac{\partial H_z}{\partial y} - \frac{\partial H_y}{\partial z} \quad (1.29)$$

its MRTD formula can be written as

$$\begin{aligned} \frac{\varepsilon}{\Delta t} ({}_{k+1}E_{l+1/2,m,n}^{\alpha x} - {}_k E_{l+1/2,m,n}^{\alpha x}) = \\ \frac{1}{\Delta y} \sum_{i=-\infty}^{+\infty} a(i) {}_{k+1/2}H_{l+1/2,m+i+1/2,n}^{\alpha x} - \frac{1}{\Delta z} \sum_{i=-\infty}^{+\infty} a(i) {}_{k+1/2}H_{l+1/2,m,n+i+1/2}^{\alpha x} \end{aligned} \quad (1.30)$$

The other field components can be represented by scaling function in the same way.

The MRTD algorithm is much more complicated than that of FDTD due to the field expansion. The field at one grid point is related to the field at its several neighboring points. But with more smooth function such as cubic spline Battle-Lemarie scaling function  $E^{\alpha x}$  (which has been used instead of the pulse function in FDTD), the number of the relevant points can be limited [68].

The aim of MRTD development is to reduce the dispersion of FDTD and therefore to reduce the memory requirement for space gridding. However, the stability condition for MRTD still remains and actually becomes more stringent

[95-97]. The time to spatial step ratio becomes five times less than that with the conventional FDTD [68]. The scheme itself has less physical meaning than FDTD by calculating the coefficients instead of real field quantities.

## **1.2 Motivation of the Thesis**

To further improve the efficiency of FDTD, the CFL constraint should be removed or relaxed. Although an attempt was made in 1980s with the development of the ADI-based FDTD in reference [70], it was never theoretically proven to have unconditional stability. In fact, it was never found to be completely stable without adding significant dielectric loss in an actual computation. The motivation of the thesis is to develop a really unconditionally stable FDTD technique based on ADI and thus open a new front line on the further improvement of FDTD efficiency. Since the unconditional stability is very desirable with FDTD; in particular when solving problems with very small features that lead to large variations in grid size across the problem domain, this thesis significantly advances the course of efficient FDTD development.

## **1.3 Scope and Organization of the Thesis**

This thesis introduces a new numerical time domain scheme, ADI-FDTD, without the CFL conditions and performs the extensive research on the characteristics of the ADI-FDTD. The thesis consists of the following chapters.

Chapter 2 introduces a novel alternating direction implicit method based FDTD scheme. In order to make good comparisons, Yee's FDTD scheme is firstly illustrated and then, the ADI-FDTD formulas are derived in details. Finally, numerical experiments are presented for validation of the proposed scheme.

In Chapter 3, rigorous stability analysis of the proposed ADI-FDTD is conducted to prove that the scheme is unconditionally stable. Numerical results are also



presented for validations. Error analysis shows that the time step is free from CFL condition but limited by modeling accuracy and Nyquist sampling rate.

Chapter 4 presents the numerical dispersion characteristics of ADI-FDTD which is the main contributing factor to the modeling accuracy. Based on Fourier transform theory, the numerical dispersion relation of ADI-FDTD is derived analytically. An important corollary is also established to show that ADI-FDTD has significant advantage over FDTD when dealing with structures with small components such as vias.

Chapter 5 introduces high order ADI-FDTD scheme to reduce the numerical dispersion. The fourth order ADI-FDTD scheme formulations are derived, and its unconditional stability is proved analytically. Dispersion analysis is conducted. The results show its advantages over standard ADI-FDTD.

Chapter 6 concludes the thesis by reviewing the previous chapters, and indicating the possible direction of the future work in this field.

## Chapter 2 Development of the ADI-FDTD Method for Electromagnetic Problems

### 2.1 Introduction

As mentioned in Chapter 1, the FDTD method is a well-established computational technique capable of predicting radiation and scattering in environment where shape and material parameters of objects are arbitrary. However, it suffers from serious limitations due to the substantial computer resources required to model electromagnetic problems. Such limitations are mainly due to two constraints: 1) fine mesh must be taken as a small fraction of either the minimum wavelength or minimum structure dimension to make the numerical error negligible; and 2) small time step should be chosen to satisfy the Courant-Friedrich-Levy (CFL) stability condition. Much work has been done to relax the first constraint [68,69].

To remove the second constraint, a novel unconditionally stable numerical computation scheme is developed based on FDTD and ADI technique in this chapter. The ADI [74] principle was first applied in FDTD by R. Holland [70]. The method was claimed to have no stability limitation but no analytical proof was given. In fact, this method was never found to be completely stable without adding significant dielectric loss. Different from the conventional ADI application as appeared in reference [70] and [73], the ADI in this thesis is applied in respect to a combination of mixed coordinate directions, leading to only *two* alternations in the computing direction rather than *three* alternations with the conventional ADI in three-dimensional case.

This chapter is organized in the following ways. First, fundamentals of the finite difference time domain technique are reviewed. Then, the conventional and modified ADI techniques are illustrated. And finally, a novel unconditionally stable

numerical computation scheme is proposed. The advantage of modified ADI technique is presented subsequently. The time step in the proposed FDTD is shown to exceed that of the conventional FDTD through numerical experiments.

## **2.2 FDTD Fundamentals**

The finite-difference-time-domain (FDTD) method [40] has been proven to be an effective mean that provides accurate predictions of field behaviors for varieties of electromagnetic interaction problems. It can incorporate materials of any conductivity of a real metal or of low or zero conductivity dielectric. It can model various types of materials such as magnetic materials, anisotropic plasmas and magnetic ferrites. As a result, FDTD is well-suited for a wide variety of applications including microwave circuit analysis [100-107], subpicosecond photonic device analysis [108-110], packaging and interconnection modeling [111-114], antenna design [115-117], and bioelectromagnetic application [118-120]. An extensive survey of FDTD literature may be found in reference [41].

In the following sections, a brief derivation of FDTD equations is presented, and two important aspects – stability, numerical dispersion – of the FDTD method are discussed.

### **2.2.1 Yee's Grid and FDTD Scheme**

In 1966, Yee developed the FDTD scheme which solves Maxwell's curl equation in a straightforward manner. In this numerical scheme, the continuous electromagnetic fields in a finite volume of space are sampled at certain points in a discrete manner in space and time. The electromagnetic wave propagation is modeled by advancing in time step and finite-differencing of Maxwell's equation at each spatial lattice point at corresponding time step. The field solution at the current time step is deduced from the field values at the previous time steps, which leads to a recursive time-marching or leap-frog algorithm. This approach

basically results in a simulation of actual coupled full wave solutions by the numerically sampled data that propagates in a data space (the simulation region) stored in a computer. Space and time sampling increments are selected to avoid aliasing of the continuous field distribution and to guarantee stability of the time marching algorithm. Time marching is completed when the desired late time or steady-state field behavior is observed.

In linear, lossless and isotropic medium, the differential form of Maxwell's equations may be given as

$$\nabla \times \mathbf{E} = -\mu \frac{\partial \mathbf{H}}{\partial t}, \quad (2.1a)$$

$$\nabla \times \mathbf{H} = \varepsilon \frac{\partial \mathbf{E}}{\partial t}. \quad (2.1b)$$

where  $\varepsilon$  and  $\mu$  is electrical permittivity and magnetic permeability, respectively.

The vector curl equations (2.1) can be rewritten as six scalar equations in the three-dimensional rectangular coordinate system:

$$\frac{\partial H_x}{\partial t} = \frac{1}{\mu} \left( \frac{\partial E_y}{\partial z} - \frac{\partial E_z}{\partial y} \right), \quad (2.2a)$$

$$\frac{\partial H_y}{\partial t} = \frac{1}{\mu} \left( \frac{\partial E_z}{\partial x} - \frac{\partial E_x}{\partial z} \right), \quad (2.2b)$$

$$\frac{\partial H_z}{\partial t} = \frac{1}{\mu} \left( \frac{\partial E_x}{\partial y} - \frac{\partial E_y}{\partial x} \right), \quad (2.2c)$$

$$\frac{\partial E_x}{\partial t} = \frac{1}{\varepsilon} \left( \frac{\partial H_z}{\partial y} - \frac{\partial H_y}{\partial z} \right), \quad (2.2d)$$

$$\frac{\partial E_y}{\partial t} = \frac{1}{\varepsilon} \left( \frac{\partial H_x}{\partial z} - \frac{\partial H_z}{\partial x} \right), \quad (2.2e)$$

$$\frac{\partial E_z}{\partial t} = \frac{1}{\varepsilon} \left( \frac{\partial H_y}{\partial x} - \frac{\partial H_x}{\partial y} \right). \quad (2.2f)$$

In the Yee's grid which is shown in Figure 2.1, a space point is denoted as

$$(i, j, k) = (i\Delta x, j\Delta y, k\Delta z) \quad (2.3)$$

and any function of space and time as

$$u|_{i,j,k}^n = u(i\Delta x, j\Delta y, k\Delta z, n\Delta t) \quad (2.4)$$

where  $\Delta x$ ,  $\Delta y$ ,  $\Delta z$  and  $\Delta t$  are the spatial and temporal increment steps, respectively. By using the second-order accurate central difference approximation as indicated in equation (2.5) for space and time derivatives

$$\frac{\partial(u|_{i,j,k}^n)}{\partial x} = \frac{u|_{i+1/2,j,k}^n - u|_{i-1/2,j,k}^n}{\Delta x} + O(\Delta x^2) \quad (2.5a)$$

$$\frac{\partial(u|_{i,j,k}^n)}{\partial t} = \frac{u|_{i,j,k}^{n+1/2} - u|_{i,j,k}^{n-1/2}}{\Delta t} + O(\Delta t^2) \quad (2.5b)$$

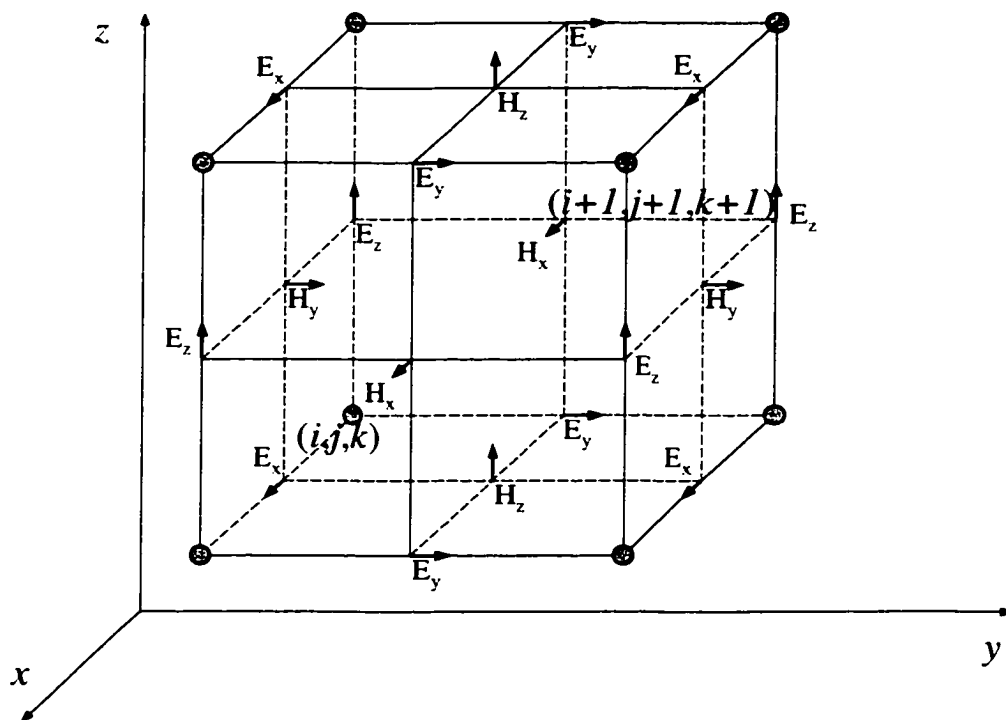


Figure 2.1 Position of electric and magnetic field components in Yee's grid.

the explicit finite difference approximation of six scalar Maxwell's equations (2.2) can be obtained as:

$$\begin{aligned}
 H_x \Big|_{i,j+\frac{1}{2},k+\frac{1}{2}}^{n+\frac{1}{2}} &= H_x \Big|_{i,j+\frac{1}{2},k+\frac{1}{2}}^{n-\frac{1}{2}} + \frac{\Delta t}{\mu} \left[ \frac{E_y \Big|_{i,j+\frac{1}{2},k+1}^n - E_y \Big|_{i,j+\frac{1}{2},k}^n}{\Delta z} \right. \\
 &\quad \left. - \frac{\Delta t}{\mu} \left[ \frac{E_z \Big|_{i+\frac{1}{2},j,k+1}^n - E_z \Big|_{i+\frac{1}{2},j,k}^n}{\Delta y} \right] \right]
 \end{aligned} \tag{2.6a}$$

$$\begin{aligned}
H_y \Big|_{i+\frac{1}{2}, j, k+\frac{1}{2}}^{n+\frac{1}{2}} &= H_y \Big|_{i+\frac{1}{2}, j, k+\frac{1}{2}}^{n-\frac{1}{2}} + \frac{\Delta t}{\mu} \left[ \frac{E_z \Big|_{i+1, j, k+\frac{1}{2}}^n - E_z \Big|_{i, j, k+\frac{1}{2}}^n}{\Delta x} \right] \\
&\quad - \frac{\Delta t}{\mu} \left[ \frac{E_x \Big|_{i+\frac{1}{2}, j, k+1}^n - E_x \Big|_{i+\frac{1}{2}, j, k}^n}{\Delta z} \right]
\end{aligned} \tag{2.6b}$$

$$\begin{aligned}
H_z \Big|_{i+\frac{1}{2}, j+\frac{1}{2}, k}^{n+\frac{1}{2}} &= H_z \Big|_{i+\frac{1}{2}, j+\frac{1}{2}, k}^{n-\frac{1}{2}} + \frac{\Delta t}{\mu} \left[ \frac{E_x \Big|_{i+\frac{1}{2}, j+1, k}^n - E_x \Big|_{i+\frac{1}{2}, j, k}^n}{\Delta y} \right] \\
&\quad - \frac{\Delta t}{\mu} \left[ \frac{E_y \Big|_{i+1, j+\frac{1}{2}, k}^n - E_y \Big|_{i, j+\frac{1}{2}, k}^n}{\Delta x} \right]
\end{aligned} \tag{2.6c}$$

$$\begin{aligned}
E_x \Big|_{i+\frac{1}{2}, j, k}^{n+1} &= E_x \Big|_{i+\frac{1}{2}, j, k}^n + \frac{\Delta t}{\varepsilon} \left[ \frac{H_z \Big|_{i+\frac{1}{2}, j+\frac{1}{2}, k}^{n+\frac{1}{2}} - H_z \Big|_{i+\frac{1}{2}, j-\frac{1}{2}, k}^{n+\frac{1}{2}}}{\Delta y} \right] \\
&\quad - \frac{\Delta t}{\varepsilon} \left[ \frac{H_y \Big|_{i+\frac{1}{2}, j, k+\frac{1}{2}}^{n+\frac{1}{2}} - H_y \Big|_{i+\frac{1}{2}, j, k-\frac{1}{2}}^{n+\frac{1}{2}}}{\Delta z} \right]
\end{aligned} \tag{2.6d}$$

$$\begin{aligned}
E_y \Big|_{i, j+\frac{1}{2}, k}^{n+1} &= E_y \Big|_{i+1/2, j, k}^n + \frac{\Delta t}{\varepsilon} \left[ \frac{H_x \Big|_{i, j+\frac{1}{2}, k+\frac{1}{2}}^{n+\frac{1}{2}} - H_x \Big|_{i, j+\frac{1}{2}, k-\frac{1}{2}}^{n+\frac{1}{2}}}{\Delta z} \right] \\
&\quad - \frac{\Delta t}{\varepsilon} \left[ \frac{H_z \Big|_{i+\frac{1}{2}, j+\frac{1}{2}, k}^{n+\frac{1}{2}} - H_z \Big|_{i-\frac{1}{2}, j+\frac{1}{2}, k}^n}{\Delta x} \right]
\end{aligned} \tag{2.6e}$$

$$E_z|_{i,j,k+\frac{1}{2}}^{n+1} = E_z|_{i,j,k+\frac{1}{2}}^n + \frac{\Delta t}{\epsilon} \left[ \frac{H_y|_{i+\frac{1}{2},j,k+\frac{1}{2}}^{n+\frac{1}{2}} - H_y|_{i-\frac{1}{2},j,k+\frac{1}{2}}^{n+\frac{1}{2}}}{\Delta x} \right] - \frac{\Delta t}{\epsilon} \left[ \frac{H_x|_{i,j+1/2,k+\frac{1}{2}}^{n+\frac{1}{2}} - H_x|_{i,j-\frac{1}{2},k+\frac{1}{2}}^n}{\Delta y} \right] \quad (2.6f)$$

Notice that in equation (2.6) and Figure 2.1, the magnetic and electric field components are interlaced within the unit cell and evaluated at alternate half-time and spatial steps. Any electric or magnetic field component at the present time step is derived from the field components at the previous time steps, which leading to a leapfrog time recursive scheme. At  $t=0$ , one can assume that all fields within the numerical sampling region are zero and an incident wave source is to be turned on in the sampling region. The waves then propagate from this source in the Yee's grid.

Yee's FDTD scheme essentially provides a simple structure of three-dimensional space being filled by an interlinked array of Farady's Law and Ampere's Law contours [46]. It is very simple in concept and implementation. In the simulation of an electromagnetic wave interaction that is defined in "open" regions where the spatial domain of the computed field is unbounded in one or more coordinate directions. A suitable boundary condition on the outer perimeter of the computational domain must be used to simulate its extension to infinity. The boundary is called the "absorbing boundary" as the waves that impinge on it are supposed to be absorbed without causing reflections. Several types of absorbing boundary conditions (ABCs) for FDTD have been developed and implemented over the years [121-124]. In 1994, Berenger developed the perfectly matched absorbing layer (PML) [78] which is based on a splitting of electric and magnetic field components in the absorbing region with the possibility of assigning losses to the individual split field components. The PML can effectively attenuate



outgoing waves over a wide frequency range and a wide range of angles of incidence. Research [41] shows that PML is remarkably robust, providing highly accurate modeling predictions for a variety of electromagnetic wave interaction problems and it is still being studied intensively to improve its performance.

### **2.2.2 Selections of Grid Size and Time Step Size**

In spite of the fact that the FDTD is popular, it is very memory and CPU-time intensive. Such intensive memory and CPU time requirements are due to the two physical constraints.

- 1) the spatial increment steps must be small enough in comparison with the wavelength (usually 10-20 steps per wavelength) in order to make the numerical dispersion error negligible. More details will be given in the next subsection.
- 2) the time step must be small enough so that it ensures the FDTD computation errors do not grow with the time and therefore the computations remain stable. More specifically , the CFL stipulates that [47]

$$u_{\max} \Delta t \leq \left[ \frac{1}{\Delta x^2} + \frac{1}{\Delta y^2} + \frac{1}{\Delta z^2} \right]^{-1/2} \quad (2.7)$$

Here  $u_{\max}$  is the maximum wave phase velocity within the model.

### **2.2.3 Numerical Dispersion**

Generally, dispersion relation describes the variation of propagating wave's phase velocity  $u_p$  with frequency  $f$ . Dispersion can be also represented as the variation of the propagating wave's wavenumber  $k = 2\pi / \lambda$  with angular

frequency  $\omega = 2\pi f$  since  $k = \omega / u_p$ . The analytical dispersion relation for a plane wave propagating in a *continuous* medium is

$$\left(\frac{\omega}{u_p}\right)^2 = \omega^2 \mu \epsilon = k_x^2 + k_y^2 + k_z^2. \quad (2.8)$$

where  $k_x$ ,  $k_y$ , and  $k_z$  are the three components of wavenumber vector along  $x$ ,  $y$  and  $z$  directions, or the spatial frequency of a wave in the  $x$ ,  $y$  and  $z$  directions.

In a FDTD grid, because the space is discretized into a computational lattice, the phase velocity of numerical wave modes in the FDTD grid can differ from the vacuum speed of light, varying with the modal wavelength, the direction of propagation, and the grid size. The dispersion caused by such numerical discretization is the so called **numerical dispersion**.

The numerical dispersion of the Yee's FDTD has been investigated intensively [125-128] and found as

$$\left(\frac{1}{c\Delta t}\right)^2 \sin^2\left(\frac{1}{2}\omega\Delta t\right) = \frac{1}{\Delta x^2} \sin^2\left(\frac{1}{2}k_x\Delta x\right) + \frac{1}{\Delta y^2} \sin^2\left(\frac{1}{2}k_y\Delta y\right) + \frac{1}{\Delta z^2} \sin^2\left(\frac{1}{2}k_z\Delta z\right) \quad (2.9)$$

in homogeneous media.

Although at the first glance, expression (2.9) bears little resemblance to the ideal case of expression (2.8), it can be shown that the two dispersion relations are identical in the limit as  $x$ ,  $y$ ,  $z$  and  $t$  all go to zero. Qualitatively, this suggests that numerical dispersion can be reduced to any degree that is desired if FDTD gridding is fine enough. In other words, when the grid sizes are small enough, the numerical solutions are close to the analytical solutions. Therefore, the first

constraint of FDTD needs to be maintained in a FDTD modeling as we mentioned above.

#### 2.2.4 Numerical Stability

Generally, the finite-difference schemes in time and space domains require that the time step be bounded in order to avoid numerical instability. Numerical instability is an undesirable possibility with explicit numerical differential equation solvers that can cause the computed results to spuriously increase without limit as time-marching continues.

To simplify the analysis, equation (2.1) can be rewrite in a compact form

$$j \frac{1}{\sqrt{\mu\epsilon}} \nabla \times \mathbf{V} = \frac{\partial \mathbf{V}}{\partial t} \quad (2.10)$$

where  $\mathbf{V} = \sqrt{\mu}\mathbf{H} + j\sqrt{\epsilon}\mathbf{E}$ .

The stability of FDTD can then be analyzed by considering the following pair of eigenvalue problems:

$$\frac{\mathbf{V}^{n+1} - \mathbf{V}^{n-1}}{\Delta t} = \Lambda \mathbf{V}^n \quad (2.11)$$

$$\frac{1}{\sqrt{\mu\epsilon}} \left[ \frac{\mathbf{a}_x}{\Delta x} \sin\left(\frac{k_x \Delta x}{2}\right) + \frac{\mathbf{a}_y}{\Delta y} \sin\left(\frac{k_y \Delta y}{2}\right) + \frac{\mathbf{a}_z}{\Delta z} \sin\left(\frac{k_z \Delta z}{2}\right) \right] \times \mathbf{V}^n = \Lambda \mathbf{V}^n \quad (2.12)$$

Equation (2.11) can be viewed as a difference system which is shown in Figure 2.2.

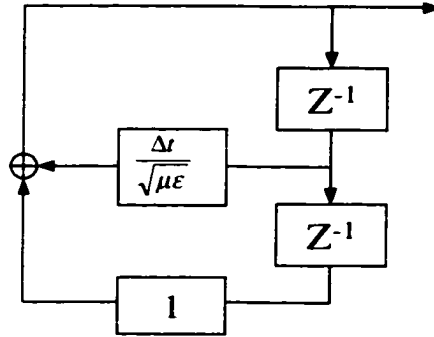


Figure 2.2 The block diagram of the difference equation.

The poles of Z-transform of the system must be within the unit circle to make the system described by (2.11) stable. This requires that  $\Lambda$  must be pure imaginary and has bounds

$$-\frac{2}{\Delta t} \leq \text{Im}(\Lambda) \leq \frac{2}{\Delta t}. \quad (2.13)$$

Let

$$V = V_0 e^{j(k_x \Delta x + k_y \Delta y + k_z \Delta z)} \quad (2.14)$$

represent an arbitrary spatial mode at  $(i, j, k)$ .  $\Lambda$  is obtained by substituting (2.14) to equation (2.12):

$$\Lambda^2 = -\frac{4}{\mu \epsilon} \left[ \frac{1}{(\Delta x)^2} \sin^2 \left( \frac{k_x \Delta x}{2} \right) + \frac{1}{(\Delta y)^2} \sin^2 \left( \frac{k_y \Delta y}{2} \right) + \frac{1}{(\Delta z)^2} \sin^2 \left( \frac{k_z \Delta z}{2} \right) \right] \quad (2.15)$$

It is obviously that for all possible  $k_x$ ,  $k_y$  and  $k_z$ , to make  $|\Lambda| \leq 1$  means

$$\text{Re}(\Lambda) = 0$$

$$-\frac{2}{\sqrt{\mu\epsilon}} \sqrt{\frac{1}{(\Delta x)^2} + \frac{1}{(\Delta y)^2} + \frac{1}{(\Delta z)^2}} \leq \text{Im}(\Lambda) \leq \frac{2}{\sqrt{\mu\epsilon}} \sqrt{\frac{1}{(\Delta x)^2} + \frac{1}{(\Delta y)^2} + \frac{1}{(\Delta z)^2}} \quad (2.16)$$

Equation (2.13) and (2.16) give the upper bound to guarantee the numerical stability:

$$\Delta t \leq \sqrt{\mu\epsilon} \left[ \frac{1}{\Delta x^2} + \frac{1}{\Delta y^2} + \frac{1}{\Delta z^2} \right]^{-1/2} \quad (2.17)$$

More details of the derivation of the stability constraint (2.17) is available in reference [47].

### 2.3 ADI Basics

In this section a very powerful method that is especially useful for solving parabolic equations is examined. This method is called the alternating direction implicit (ADI) method.

#### The Peaceman-Rachford Algorithm

ADI methods were introduced by Peaceman and Rachford in 1955 [129] for the numerical solution of elliptic and parabolic partial differential equations.

Consider solving the heat flow equation (2.18),

$$\frac{\partial u}{\partial t} = \frac{\partial^2 u}{\partial x^2} + \frac{\partial^2 u}{\partial y^2}, \quad (2.18)$$

as a good example of parabolic differential equation, over the mesh superimposed on the rectangular region  $0 \leq x \leq a$ ,  $0 \leq y \leq b$ .

By using the same space-time notation as (2.4) in Section 2.2,

$$u_{i,j}^n = u(i\Delta x, j\Delta y, n\Delta t) \quad (2.19)$$

a simple *explicit* finite-difference scheme for the solution may be written as

$$\frac{u_{i,j}^{n+1} - u_{i,j}^n}{\Delta t} = \frac{u_{i+1,j}^n - 2u_{i,j}^n + u_{i-1,j}^n}{\Delta x^2} + \frac{u_{i,j+1}^n - 2u_{i,j}^n + u_{i,j-1}^n}{\Delta y^2}. \quad (2.20)$$

Although the above explicit representation appears simple and straight forward for solutions, it is constrained by the following CFL condition for stability:

$$\frac{1}{\Delta x^2} + \frac{1}{\Delta y^2} \leq \frac{1}{2\Delta t}. \quad (2.21)$$

As a result, the time marching requires  $\Delta t$  to be extremely small. For most problems it could be an impractical method since the iterations need to be long for a solution to settle.

In the ADI approach, every time step is broken into two sub-steps, the  $n$ -th and the  $(n+1/2)$ -th steps. In the first half time step, the second derivative,  $\partial^2 u / \partial y^2$ , is approximated at the  $n$ -th iteration by the finite difference replacement and the first second order derivative,  $\partial^2 u / \partial x^2$ , replaced at an intermediate the  $(n+1/2)$ -th iteration. A set of simulation equations is then resulted that can be solved relatively easily. The equations are implicit in the x-direction. In proceeding from the intermediate iteration  $n+1/2$  to iteration  $n+1$ , the difference equation is implicit in y-direction and explicit in the x-direction. More specifically, the two sub-computations are:

$$\frac{u_{i,j}^{n+\frac{1}{2}} - u_{i,j}^n}{\Delta t / 2} = \frac{u_{i+1,j}^{n+\frac{1}{2}} - 2u_{i,j}^{n+\frac{1}{2}} + u_{i-1,j}^{n+\frac{1}{2}}}{\Delta x^2} + \frac{u_{i,j+1}^n - 2u_{i,j}^n + u_{i,j-1}^n}{\Delta y^2} \quad (2.22)$$

$$\frac{u|_{i,j}^{n+1} - u|_{i,j}^{n+\frac{1}{2}}}{\Delta t/2} = \frac{u|_{i+1,j}^{n+\frac{1}{2}} - 2u|_{i,j}^{n+\frac{1}{2}} + u|_{i-1,j}^{n+\frac{1}{2}}}{\Delta x^2} + \frac{u|_{i,j+1}^{n+1} - 2u|_{i,j}^{n+1} + u|_{i,j-1}^{n+1}}{\Delta y^2} \quad (2.23)$$

The above two sub-step computations are proven to be unconditionally stable and the proof can be shown by a procedure very similar to that used by O'Brien, Hyman, and Kaplan. The details can be found in reference [129].

## 2.4 Development of ADI Based FDTD Algorithm

In section 2.2.3, the second constraint described in equation (2.7) which is known as the CFL condition for FDTD gives the upper bound value of the time step. To remove this CFL condition, the ADI principle described above is incorporated in the FDTD, leading to an unconditionally stable FDTD scheme, called ADI-FDTD method.

### 2.4.1 Derivation of ADI-FDTD scheme

As stated in Section 2.2, in an isotropic medium with the medium permittivity  $\epsilon$  and the medium permeability  $\mu$ , the curl vector equation of Maxwell's equations can be cast into six scalar partial differential equations in the Cartesian coordinates as shown in (2.24). For simplicity, let's take the first equation as an example as shown in (2.24a).

$$\frac{\partial E_x}{\partial t} = \frac{1}{\epsilon} \left( \frac{\partial H_z}{\partial y} - \frac{\partial H_y}{\partial z} \right) \quad (2.24a)$$

$$\frac{\partial E_y}{\partial t} = \frac{1}{\epsilon} \left( \frac{\partial H_x}{\partial z} - \frac{\partial H_z}{\partial x} \right) \quad (2.24b)$$

$$\frac{\partial E_z}{\partial t} = \frac{1}{\epsilon} \left( \frac{\partial H_y}{\partial x} - \frac{\partial H_x}{\partial y} \right) \quad (2.24c)$$

$$\frac{\partial H_x}{\partial t} = \frac{1}{\mu} \left( \frac{\partial E_y}{\partial z} - \frac{\partial E_z}{\partial y} \right) \quad (2.24d)$$

$$\frac{\partial H_y}{\partial t} = \frac{1}{\mu} \left( \frac{\partial E_z}{\partial x} - \frac{\partial E_x}{\partial z} \right) \quad (2.24e)$$

$$\frac{\partial H_z}{\partial t} = \frac{1}{\mu} \left( \frac{\partial E_x}{\partial y} - \frac{\partial E_y}{\partial x} \right) \quad (2.24f)$$

By applying the ADI principle to equation (2.24a), the computation of equation (2.24a) for the FDTD solution marching from the  $n$ -th time step to the  $(n+1)$ -th time step is broken up into two computational sub-advancements: the advancement from the  $n$ -th time step to the  $(n+1/2)$ -th time step and the advancement from the  $(n+1/2)$ -th time step to the  $(n+1)$ -th time step. More specifically, the two sub-step computations are:

- 1 for the first sub-step (i.e. at the  $(n+1/2)$ -th time step), the *first* partial derivative on the right-hand side of (2.24a),  $\partial H_z / \partial y$ , is replaced with an implicit difference approximation of its unknown pivotal values at the  $(n+1/2)$ th time step; while the *second* partial derivatives on the right-hand side,  $\partial H_y / \partial z$ , is replaced with an explicit finite difference approximation in its known values at the previous  $n$ -th time step. In other words, equation (2.24a) becomes

$$\begin{aligned} & \frac{E_x \Big|_{i+\frac{1}{2},j,k}^{n+\frac{1}{2}} - E_x \Big|_{i+\frac{1}{2},j,k}^n}{\Delta t / 2} \\ &= \frac{1}{\epsilon} \left[ \frac{H_z \Big|_{i+\frac{1}{2},j+\frac{1}{2},k}^{n+\frac{1}{2}} - H_z \Big|_{i+\frac{1}{2},j-\frac{1}{2},k}^{n+\frac{1}{2}}}{\Delta y} - \frac{H_y \Big|_{i+\frac{1}{2},j,k+\frac{1}{2}}^{n+\frac{1}{2}} - H_y \Big|_{i+\frac{1}{2},j,k-\frac{1}{2}}^{n+\frac{1}{2}}}{\Delta z} \right] \end{aligned} \quad (2.25)$$



- 2 for the second sub-step (i.e. at  $(n+1)$ -th time step), the *second* term on the right-hand side,  $\partial H_y / \partial z$ , is replaced by an implicit finite-difference approximation of its unknown pivotal values at  $(n+1)$ -th time step; while the *first* term,  $\partial H_z / \partial y$ , is replaced with an explicit finite-difference approximation in its known values at the previous  $(n+1/2)$ -th time step. Similarly, equation (2.24a) evolves to

$$\begin{aligned} & \frac{E_x \Big|_{i+\frac{1}{2},j,k}^{n+1} - E_x \Big|_{i+\frac{1}{2},j,k}^{n+\frac{1}{2}}}{\Delta t / 2} \\ &= \frac{1}{\varepsilon} \left[ \frac{H_z \Big|_{i+\frac{1}{2},j+\frac{1}{2},k}^{n+\frac{1}{2}} - H_z \Big|_{i+\frac{1}{2},j-\frac{1}{2},k}^{n+\frac{1}{2}}}{\Delta y} - \frac{H_y \Big|_{i+\frac{1}{2},j,k+\frac{1}{2}}^{n+1} - H_y \Big|_{i+\frac{1}{2},j,k-\frac{1}{2}}^{n+1}}{\Delta z} \right] \end{aligned} \quad (2.26)$$

Note that the above two sub-steps represent the alternations in the FDTD recursive computation directions in the sequence of the terms, the *first* and the *second* terms. They result in the implicit formulations as the right-hand sides of the equations contain the field values which are unknown and need to be updated. The method is then termed “the Alternating Direction Implicit (ADI)” method.

Applying the same procedure to all the rest scalar differential equations as described in (2.25) and (2.26), one can obtain the complete set of the implicit unconditionally stable FDTD formulas:

For the advancement from the  $n$ th time step to the  $(n+1/2)$ th time step:

$$\begin{aligned}
& \frac{E_x \Big|_{i+\frac{1}{2},j,k}^{n+\frac{1}{2}} - E_x \Big|_{i+\frac{1}{2},j,k}^n}{\Delta t/2} \\
&= \frac{1}{\epsilon} \left[ \frac{H_z \Big|_{i-\frac{1}{2},j+\frac{1}{2},k}^{n+\frac{1}{2}} - H_z \Big|_{i+\frac{1}{2},j-\frac{1}{2},k}^{n+\frac{1}{2}}}{\Delta y} - \frac{H_y \Big|_{i+\frac{1}{2},j,k+\frac{1}{2}}^n - H_y \Big|_{i+\frac{1}{2},j,k-\frac{1}{2}}^n}{\Delta z} \right] \quad (2.27a)
\end{aligned}$$

$$\begin{aligned}
& \frac{E_y \Big|_{i,j+\frac{1}{2},k}^{n+\frac{1}{2}} - E_y \Big|_{i,j+\frac{1}{2},k}^n}{\Delta t/2} \\
&= \frac{1}{\epsilon} \left[ \frac{H_x \Big|_{i,j+\frac{1}{2},k+\frac{1}{2}}^{n+\frac{1}{2}} - H_x \Big|_{i,j+\frac{1}{2},k-\frac{1}{2}}^{n+\frac{1}{2}}}{\Delta z} - \frac{H_z \Big|_{i+\frac{1}{2},j+\frac{1}{2},k}^n - H_z \Big|_{i-\frac{1}{2},j+\frac{1}{2},k}^n}{\Delta x} \right] \quad (2.27b)
\end{aligned}$$

$$\begin{aligned}
& \frac{E_z \Big|_{i,j,k+\frac{1}{2}}^{n+\frac{1}{2}} - E_z \Big|_{i,j,k+\frac{1}{2}}^n}{\Delta t/2} \\
&= \frac{1}{\epsilon} \left[ \frac{H_y \Big|_{i+\frac{1}{2},j,k+\frac{1}{2}}^{n+\frac{1}{2}} - H_y \Big|_{i-\frac{1}{2},j,k+\frac{1}{2}}^{n+\frac{1}{2}}}{\Delta x} - \frac{H_x \Big|_{i,j+\frac{1}{2},k+\frac{1}{2}}^n - H_x \Big|_{i,j-\frac{1}{2},k+\frac{1}{2}}^n}{\Delta y} \right] \quad (2.27c)
\end{aligned}$$

$$\begin{aligned}
& \frac{H_x \Big|_{i,j+\frac{1}{2},k+\frac{1}{2}}^{n+\frac{1}{2}} - H_x \Big|_{i,j+\frac{1}{2},k+\frac{1}{2}}^n}{\Delta t/2} \\
&= \frac{1}{\mu} \left[ \frac{E_y \Big|_{i,j+\frac{1}{2},k+1}^{n+\frac{1}{2}} - E_y \Big|_{i,j+\frac{1}{2},k}^{n+\frac{1}{2}}}{\Delta z} - \frac{E_z \Big|_{i,j+1,k+\frac{1}{2}}^n - E_z \Big|_{i,j,k+\frac{1}{2}}^n}{\Delta y} \right] \quad (2.27d)
\end{aligned}$$

$$\begin{aligned}
& \frac{H_y \Big|_{i+\frac{1}{2},j,k+\frac{1}{2}}^{n+\frac{1}{2}} - H_y \Big|_{i+\frac{1}{2},j,k+\frac{1}{2}}^n}{\Delta t / 2} \\
&= \frac{1}{\mu} \left[ \frac{E_z \Big|_{i+1,j,k+\frac{1}{2}}^{n+\frac{1}{2}} - E_z \Big|_{i,j,k+\frac{1}{2}}^{n+\frac{1}{2}}}{\Delta x} - \frac{E_x \Big|_{i+\frac{1}{2},j,k+1}^n - E_x \Big|_{i+\frac{1}{2},j,k}^n}{\Delta z} \right] \quad (2.27e)
\end{aligned}$$

$$\begin{aligned}
& \frac{H_z \Big|_{i+\frac{1}{2},j+\frac{1}{2},k}^{n+\frac{1}{2}} - H_z \Big|_{i+\frac{1}{2},j+\frac{1}{2},k}^n}{\Delta t / 2} \\
&= \frac{1}{\mu} \left[ \frac{E_x \Big|_{i+\frac{1}{2},j+1,k}^{n+\frac{1}{2}} - E_x \Big|_{i+\frac{1}{2},j,k}^{n+\frac{1}{2}}}{\Delta y} - \frac{E_y \Big|_{i+1,j+\frac{1}{2},k}^n - E_y \Big|_{i,j+\frac{1}{2},k}^n}{\Delta x} \right] \quad (2.27f)
\end{aligned}$$

For the advancement from the  $(n+1/2)$ th to the  $(n+1)$ th time step

$$\begin{aligned}
& \frac{E_x \Big|_{i+\frac{1}{2},j,k}^{n+1} - E_x \Big|_{i+\frac{1}{2},j,k}^{n+\frac{1}{2}}}{\Delta t / 2} \\
&= \frac{1}{\varepsilon} \left[ \frac{H_z \Big|_{i+\frac{1}{2},j+\frac{1}{2},k}^{n+\frac{1}{2}} - H_z \Big|_{i+\frac{1}{2},j-\frac{1}{2},k}^{n+\frac{1}{2}}}{\Delta y} - \frac{H_y \Big|_{i+\frac{1}{2},j,k+\frac{1}{2}}^{n+1} - H_y \Big|_{i+\frac{1}{2},j,k-\frac{1}{2}}^{n+1}}{\Delta z} \right] \quad (2.28a)
\end{aligned}$$

$$\begin{aligned}
& \frac{E_y \Big|_{i,j+\frac{1}{2},k}^{n+1} - E_y \Big|_{i,j+\frac{1}{2},k}^{n+\frac{1}{2}}}{\Delta t / 2} \\
&= \frac{1}{\varepsilon} \left[ \frac{H_x \Big|_{i,j+\frac{1}{2},k+\frac{1}{2}}^{n+\frac{1}{2}} - H_x \Big|_{i,j+\frac{1}{2},k-\frac{1}{2}}^{n+\frac{1}{2}}}{\Delta z} - \frac{H_z \Big|_{i+\frac{1}{2},j+\frac{1}{2},k}^{n+1} - H_z \Big|_{i-\frac{1}{2},j+\frac{1}{2},k}^{n+1}}{\Delta x} \right] \quad (2.28b)
\end{aligned}$$

$$\begin{aligned}
& \frac{E_z|_{i,j,k+\frac{1}{2}}^{n+1} - E_z|_{i,j,k+\frac{1}{2}}^{n+\frac{1}{2}}}{\Delta t/2} \\
&= \frac{1}{\varepsilon} \left[ \frac{H_y|_{i+\frac{1}{2},j,k+\frac{1}{2}}^{n+\frac{1}{2}} - H_y|_{i-\frac{1}{2},j,k+\frac{1}{2}}^{n+\frac{1}{2}}}{\Delta x} - \frac{H_x|_{i,j+\frac{1}{2},k+\frac{1}{2}}^{n+1} - H_x|_{i,j-\frac{1}{2},k+\frac{1}{2}}^{n+1}}{\Delta y} \right] \quad (2.28c)
\end{aligned}$$

$$\begin{aligned}
& \frac{H_x|_{i,j+\frac{1}{2},k+\frac{1}{2}}^{n+1} - H_x|_{i,j+\frac{1}{2},k+\frac{1}{2}}^{n+\frac{1}{2}}}{\Delta t/2} \\
&= \frac{1}{\mu} \left[ \frac{E_y|_{i,j+\frac{1}{2},k+1}^{n+\frac{1}{2}} - E_y|_{i,j+\frac{1}{2},k}^{n+\frac{1}{2}}}{\Delta z} - \frac{E_z|_{i,j+1,k+\frac{1}{2}}^{n+1} - E_z|_{i,j,k+\frac{1}{2}}^{n+1}}{\Delta y} \right] \quad (2.28d)
\end{aligned}$$

$$\begin{aligned}
& \frac{H_y|_{i+\frac{1}{2},j,k+\frac{1}{2}}^{n+1} - H_y|_{i+\frac{1}{2},j,k+\frac{1}{2}}^{n+\frac{1}{2}}}{\Delta t/2} \\
&= \frac{1}{\mu} \left[ \frac{E_z|_{i+1,j,k+\frac{1}{2}}^{n+\frac{1}{2}} - E_z|_{i,j,k+\frac{1}{2}}^{n+\frac{1}{2}}}{\Delta x} - \frac{E_x|_{i+\frac{1}{2},j,k+1}^{n+1} - E_x|_{i+\frac{1}{2},j,k}^{n+1}}{\Delta z} \right] \quad (2.28e)
\end{aligned}$$

$$\begin{aligned}
& \frac{H_z|_{i+\frac{1}{2},j+\frac{1}{2},k}^{n+1} - H_z|_{i+\frac{1}{2},j+\frac{1}{2},k}^{n+\frac{1}{2}}}{\Delta t/2} \\
&= \frac{1}{\mu} \left[ \frac{E_x|_{i+\frac{1}{2},j+1,k}^{n+\frac{1}{2}} - E_x|_{i+\frac{1}{2},j,k}^{n+\frac{1}{2}}}{\Delta y} - \frac{E_y|_{i+1,j+\frac{1}{2},k}^{n+1} - E_y|_{i,j+\frac{1}{2},k}^{n+1}}{\Delta x} \right] \quad (2.28f)
\end{aligned}$$

The notations  $E_\alpha|_{i,j,k}^n$  and  $H_\alpha|_{i,j,k}^n$  with  $\alpha = x, y, z$  are the field components with their grid positions being the same as those with the conventional FDTD of the Yee's scheme.

Attention should be paid to the fact that there is no time-step difference (or lagging) between electric and magnetic field components in the formulations.

#### **2.4.2 Advantages of modified ADI technique**

The above ADI procedure is different from the conventional ADI procedure as appeared in [70-74]. In the conventional ADI procedure, the alternations in the computation direction are performed in each spatial coordinate direction, respectively. In the two-dimensional case, there are two spatial coordinates, e.g.  $x$  and  $y$ . Therefore, the computation for each temporal cycle (or each time step) is then broken into two sub-step computations as shown in reference [73]. The first sub-step computation is performed in respect to the  $x$  direction while the second computation is performed in respect with the  $y$  direction. In the three-dimensional case, the computation for each cycle is then broken up into three computational sub-steps as indicated in reference [70] since there are three spatial coordinates,  $x$ ,  $y$  and  $z$ . In the proposed method, however, the number of the sub-steps is only *two* for each time step even in three dimensions. The reason is that in the proposed method, the ADI is applied in terms of the sequence of the terms on the right-hand side of the equations (the *first* and the *second* terms), rather than in terms of the coordinate directions. For instance, in equation (2.27a-c), the magnetic field components  $H_z$ ,  $H_x$ , and  $H_y$ , which are the first terms of the right-hand side, are implicitly computed in respect to the  $y$ ,  $z$  and  $x$  directions (mixed directions in the first sub-step), respectively, while the second terms of the right-hand side are all explicit for those equations. At the second sub-step, the first terms of the right-hand side in the equation (2.28a-c),  $H_z$ ,  $H_x$ , and  $H_y$ , are computed explicitly while the second terms become implicit. The reduction in the number of the sub-steps certainly saves the computation time.

### 2.4.3 Efficient Computation Approach

The unknown field components are coupled in equations (2.27) and (2.28) and are therefore, not easy to handle. These equations may be rearranged more efficiently for computations. For instance, consider equation (2.27a) where both sides of the equations contain the unknown field components  $E_x$  and  $H_z$ . By substituting equation (2.27f) into equation (2.27a), one can obtain:

$$\begin{aligned}
& -\left(\frac{\Delta t^2}{4\mu\epsilon\Delta y^2}\right)E_x\Big|_{i+\frac{1}{2},j+1,k}^{n+\frac{1}{2}} + \left(1 + \frac{\Delta t^2}{2\mu\epsilon\Delta y^2}\right)E_x\Big|_{i+\frac{1}{2},j,k}^{n+\frac{1}{2}} - \left(\frac{\Delta t^2}{4\mu\epsilon\Delta y^2}\right)E_x\Big|_{i+\frac{1}{2},j-1,k}^{n+\frac{1}{2}} \\
& = E_x\Big|_{i+\frac{1}{2},j,k}^n - \frac{\Delta t^2}{4\mu\epsilon\Delta y\Delta x}\left(E_y\Big|_{i+1,j+\frac{1}{2},k}^n - E_y\Big|_{i,j+\frac{1}{2},k}^n - E_y\Big|_{i+1,j-\frac{1}{2},k}^n + E_y\Big|_{i,j-\frac{1}{2},k}^n\right) \\
& + \frac{\Delta t}{2\epsilon\Delta y}\left(H_z\Big|_{i+\frac{1}{2},j+\frac{1}{2},k}^n - H_z\Big|_{i+\frac{1}{2},j-\frac{1}{2},k}^n\right) - \frac{\Delta t}{2\epsilon\Delta z}\left(H_y\Big|_{i+\frac{1}{2},j,k+\frac{1}{2}}^n - H_y\Big|_{i+\frac{1}{2},j,k-\frac{1}{2}}^n\right)
\end{aligned} \tag{2.29a}$$

In the above equation, all the field components on the right-hand side are of known values at the previous time steps, while the field components on the left-hand side are of the same field components,  $E_x$ , but at three adjacent grid points. The unknown variables are decoupled. If written in a matrix form, it will result in a banded matrix with three non-zero values.

The same decoupling procedures can be applied to equations (2.27b)-(2.28f) and similar equations can be obtained for the other field components as shown in equations (2.29b-30.f) that follow:

For the first sub-step,

$$\begin{aligned}
& -\left(\frac{\Delta t^2}{4\mu\epsilon\Delta z^2}\right)E_y\Big|_{i,j+\frac{1}{2},k+1}^{n+\frac{1}{2}} + \left(1 + \frac{\Delta t^2}{2\mu\epsilon\Delta z^2}\right)E_y\Big|_{i,j+\frac{1}{2},k}^{n+\frac{1}{2}} - \left(\frac{\Delta t^2}{4\mu\epsilon\Delta z^2}\right)E_y\Big|_{i,j+\frac{1}{2},k-1}^{n+\frac{1}{2}} \\
& = E_y\Big|_{i,j+\frac{1}{2},k}^n - \frac{\Delta t^2}{4\mu\epsilon\Delta z\Delta y}\left(E_z\Big|_{i,j+1,k+\frac{1}{2}}^n - E_z\Big|_{i,j,k+\frac{1}{2}}^n - E_z\Big|_{i,j+1,k-\frac{1}{2}}^n + E_z\Big|_{i,j,k-\frac{1}{2}}^n\right) \\
& + \frac{\Delta t}{2\epsilon\Delta z}\left(H_x\Big|_{i,j+\frac{1}{2},k+\frac{1}{2}}^n - H_x\Big|_{i,j+\frac{1}{2},k-\frac{1}{2}}^n\right) - \frac{\Delta t}{2\epsilon\Delta x}\left(H_z\Big|_{i+\frac{1}{2},j+\frac{1}{2},k}^n - H_z\Big|_{i-\frac{1}{2},j+\frac{1}{2},k}^n\right)
\end{aligned} \tag{2.29b}$$

$$\begin{aligned}
& -\left(\frac{\Delta t^2}{4\mu\epsilon\Delta x^2}\right)E_z|_{i+1,j,k+\frac{1}{2}}^{n+\frac{1}{2}} + \left(1 + \frac{\Delta t^2}{2\mu\epsilon\Delta x^2}\right)E_z|_{i,j,k+\frac{1}{2}}^{n+\frac{1}{2}} - \left(\frac{\Delta t^2}{4\mu\epsilon\Delta x^2}\right)E_z|_{i-1,j,k+\frac{1}{2}}^{n+\frac{1}{2}} \\
& = E_z|_{i,j,k+\frac{1}{2}}^n - \frac{\Delta t^2}{4\mu\epsilon\Delta x\Delta z}\left(E_x|_{i+\frac{1}{2},j,k+1}^n - E_x|_{i+\frac{1}{2},j,k}^n - E_x|_{i-\frac{1}{2},j,k+1}^n + E_x|_{i-\frac{1}{2},j,k}^n\right) \\
& + \frac{\Delta t}{2\epsilon\Delta x}\left(H_y|_{i+\frac{1}{2},j,k+\frac{1}{2}}^n - H_y|_{i-\frac{1}{2},j,k+\frac{1}{2}}^n\right) - \frac{\Delta t}{2\epsilon\Delta y}\left(H_x|_{i,j+\frac{1}{2},k+\frac{1}{2}}^n - H_x|_{i,j+\frac{1}{2},k-\frac{1}{2}}^n\right)
\end{aligned} \tag{2.29c}$$

$$\begin{aligned}
& -\left(\frac{\Delta t^2}{4\mu\epsilon\Delta z^2}\right)H_x|_{i,j+\frac{1}{2},k+\frac{1}{2}}^{n+\frac{1}{2}} + \left(1 + \frac{\Delta t^2}{2\mu\epsilon\Delta z^2}\right)H_x|_{i,j+\frac{1}{2},k+\frac{1}{2}}^{n+\frac{1}{2}} - \left(\frac{\Delta t^2}{4\mu\epsilon\Delta z^2}\right)H_x|_{i,j+\frac{1}{2},k-\frac{1}{2}}^{n+\frac{1}{2}} \\
& = H_x|_{i,j+\frac{1}{2},k+\frac{1}{2}}^n - \frac{\Delta t^2}{4\mu\epsilon\Delta z\Delta x}\left(H_z|_{i+\frac{1}{2},j+\frac{1}{2},k+1}^n - H_z|_{i-\frac{1}{2},j+\frac{1}{2},k+1}^n - H_z|_{i+\frac{1}{2},j+\frac{1}{2},k}^n + H_z|_{i-\frac{1}{2},j+\frac{1}{2},k}^n\right) \\
& + \frac{\Delta t}{2\mu\Delta z}\left(E_y|_{i,j+\frac{1}{2},k+1}^n - E_y|_{i,j+\frac{1}{2},k}^n\right) - \frac{\Delta t}{2\mu\Delta y}\left(E_z|_{i,j+1,k+\frac{1}{2}}^n - E_z|_{i,j,k+\frac{1}{2}}^n\right)
\end{aligned} \tag{2.29d}$$

$$\begin{aligned}
& -\left(\frac{\Delta t^2}{4\mu\epsilon\Delta x^2}\right)H_y|_{i+\frac{1}{2},j,k+\frac{1}{2}}^{n+\frac{1}{2}} + \left(1 + \frac{\Delta t^2}{2\mu\epsilon\Delta x^2}\right)H_y|_{i+\frac{1}{2},j,k+\frac{1}{2}}^{n+\frac{1}{2}} - \left(\frac{\Delta t^2}{4\mu\epsilon\Delta x^2}\right)H_y|_{i-\frac{1}{2},j,k+\frac{1}{2}}^{n+\frac{1}{2}} \\
& = H_y|_{i+\frac{1}{2},j,k+\frac{1}{2}}^n - \frac{\Delta t^2}{4\mu\epsilon\Delta x\Delta y}\left(H_x|_{i+1,j+\frac{1}{2},k+\frac{1}{2}}^n - H_x|_{i+1,j-\frac{1}{2},k+\frac{1}{2}}^n - H_x|_{i,j+\frac{1}{2},k+\frac{1}{2}}^n + H_x|_{i,j-\frac{1}{2},k+\frac{1}{2}}^n\right) \\
& + \frac{\Delta t}{2\mu\Delta x}\left(E_z|_{i+1,k+\frac{1}{2}}^n - E_z|_{i,k+\frac{1}{2}}^n\right) - \frac{\Delta t}{2\mu\Delta z}\left(E_x|_{i+\frac{1}{2},j,k+1}^n - E_x|_{i+\frac{1}{2},j,k}^n\right)
\end{aligned} \tag{2.29e}$$

$$\begin{aligned}
& -\left(\frac{\Delta t^2}{4\mu\epsilon\Delta y^2}\right)H_z|_{i+\frac{1}{2},j+\frac{1}{2},k}^{n+\frac{1}{2}} + \left(1 + \frac{\Delta t^2}{2\mu\epsilon\Delta y^2}\right)H_z|_{i+\frac{1}{2},j+\frac{1}{2},k}^{n+\frac{1}{2}} - \left(\frac{\Delta t^2}{4\mu\epsilon\Delta y^2}\right)H_z|_{i+\frac{1}{2},j-\frac{1}{2},k}^{n+\frac{1}{2}} \\
& = H_z|_{i+\frac{1}{2},j+\frac{1}{2},k}^n - \frac{\Delta t^2}{4\mu\epsilon\Delta y\Delta z}\left(H_y|_{i+\frac{1}{2},j+1,k+\frac{1}{2}}^n - H_y|_{i+\frac{1}{2},j+1,k-\frac{1}{2}}^n - H_y|_{i+\frac{1}{2},j,k+\frac{1}{2}}^n + H_y|_{i+\frac{1}{2},j,k-\frac{1}{2}}^n\right) \\
& + \frac{\Delta t}{2\mu\Delta y}\left(E_x|_{i+\frac{1}{2},j+1,k}^n - E_x|_{i+\frac{1}{2},j,k}^n\right) - \frac{\Delta t}{2\mu\Delta x}\left(E_y|_{i+1,j+\frac{1}{2},k}^n - E_y|_{i,j+\frac{1}{2},k}^n\right)
\end{aligned} \tag{2.29f}$$

For the second sub-step,

$$\begin{aligned}
& -\left(\frac{\Delta t^2}{4\mu\epsilon\Delta z^2}\right)E_x|_{i+\frac{1}{2},j,k+1}^{n+1} + \left(1 + \frac{\Delta t^2}{2\mu\epsilon\Delta z^2}\right)E_x|_{i+\frac{1}{2},j,k}^{n+1} - \left(\frac{\Delta t^2}{4\mu\epsilon\Delta z^2}\right)E_x|_{i+\frac{1}{2},j,k-1}^{n+1} \\
& = E_x|_{i+\frac{1}{2},j,k}^{n+\frac{1}{2}} - \frac{\Delta t^2}{4\mu\epsilon\Delta z\Delta x} \left( E_z|_{i+1,j,k+\frac{1}{2}}^{n+\frac{1}{2}} - E_z|_{i,j,k+\frac{1}{2}}^{n+\frac{1}{2}} - E_z|_{i+1,j,k-\frac{1}{2}}^{n+\frac{1}{2}} + E_z|_{i,j,k-\frac{1}{2}}^{n+\frac{1}{2}} \right) \\
& + \frac{\Delta t}{2\epsilon\Delta y} \left( H_z|_{i+\frac{1}{2},j+\frac{1}{2},k}^{n+\frac{1}{2}} - H_z|_{i+\frac{1}{2},j-\frac{1}{2},k}^{n+\frac{1}{2}} \right) - \frac{\Delta t}{2\epsilon\Delta z} \left( H_y|_{i+\frac{1}{2},j,k+\frac{1}{2}}^{n+\frac{1}{2}} - H_y|_{i+\frac{1}{2},j,k-\frac{1}{2}}^{n+\frac{1}{2}} \right)
\end{aligned} \tag{2.30a}$$

$$\begin{aligned}
& -\left(\frac{\Delta t^2}{4\mu\epsilon\Delta x^2}\right)E_y|_{i+1,j+\frac{1}{2},k}^{n+1} + \left(1 + \frac{\Delta t^2}{2\mu\epsilon\Delta x^2}\right)E_x|_{i,j+\frac{1}{2},k}^{n+1} - \left(\frac{\Delta t^2}{4\mu\epsilon\Delta x^2}\right)E_x|_{i-1,j+\frac{1}{2},k}^{n+1} \\
& = E_y|_{i,j+\frac{1}{2},k}^{n+\frac{1}{2}} - \frac{\Delta t^2}{4\mu\epsilon\Delta x\Delta y} \left( E_x|_{i+\frac{1}{2},j+1,k}^{n+\frac{1}{2}} - E_x|_{i+\frac{1}{2},j,k}^{n+\frac{1}{2}} - E_x|_{i-\frac{1}{2},j+1,k}^{n+\frac{1}{2}} + E_x|_{i-\frac{1}{2},j,k}^{n+\frac{1}{2}} \right) \\
& + \frac{\Delta t}{2\epsilon\Delta z} \left( H_x|_{i,j+\frac{1}{2},k+\frac{1}{2}}^{n+\frac{1}{2}} - H_x|_{i,j+\frac{1}{2},k-\frac{1}{2}}^{n+\frac{1}{2}} \right) - \frac{\Delta t}{2\epsilon\Delta x} \left( H_z|_{i+\frac{1}{2},j+\frac{1}{2},k}^{n+\frac{1}{2}} - H_z|_{i-\frac{1}{2},j+\frac{1}{2},k}^{n+\frac{1}{2}} \right)
\end{aligned} \tag{2.30b}$$

$$\begin{aligned}
& -\left(\frac{\Delta t^2}{4\mu\epsilon\Delta y^2}\right)E_z|_{i+1,j,k+\frac{1}{2}}^{n+1} + \left(1 + \frac{\Delta t^2}{2\mu\epsilon\Delta y^2}\right)E_z|_{i,j,k+\frac{1}{2}}^{n+1} - \left(\frac{\Delta t^2}{4\mu\epsilon\Delta y^2}\right)E_z|_{i-1,j,k+\frac{1}{2}}^{n+1} \\
& = E_z|_{i,j,k+\frac{1}{2}}^{n+\frac{1}{2}} - \frac{\Delta t^2}{4\mu\epsilon\Delta y\Delta z} \left( E_y|_{i,j+\frac{1}{2},k+1}^{n+\frac{1}{2}} - E_y|_{i,j+\frac{1}{2},k}^{n+\frac{1}{2}} - E_y|_{i,j-\frac{1}{2},k+1}^{n+\frac{1}{2}} + E_y|_{i,j-\frac{1}{2},k}^{n+\frac{1}{2}} \right) \\
& + \frac{\Delta t}{2\epsilon\Delta x} \left( H_y|_{i+\frac{1}{2},j,k+\frac{1}{2}}^{n+\frac{1}{2}} - H_y|_{i-\frac{1}{2},j,k+\frac{1}{2}}^{n+\frac{1}{2}} \right) - \frac{\Delta t}{2\epsilon\Delta y} \left( H_x|_{i,j+\frac{1}{2},k+\frac{1}{2}}^{n+\frac{1}{2}} - H_x|_{i,j+\frac{1}{2},k-\frac{1}{2}}^{n+\frac{1}{2}} \right)
\end{aligned} \tag{2.30c}$$

$$\begin{aligned}
& -\left(\frac{\Delta t^2}{4\mu\epsilon\Delta y^2}\right)H_x|_{i,j+\frac{1}{2},k+\frac{1}{2}}^{n+1} + \left(1 + \frac{\Delta t^2}{2\mu\epsilon\Delta y^2}\right)H_x|_{i,j+\frac{1}{2},k+\frac{1}{2}}^{n+1} - \left(\frac{\Delta t^2}{4\mu\epsilon\Delta y^2}\right)H_x|_{i,j-\frac{1}{2},k+\frac{1}{2}}^{n+1} \\
& = H_x|_{i,j+\frac{1}{2},k+\frac{1}{2}}^{n+\frac{1}{2}} - \frac{\Delta t^2}{4\mu\epsilon\Delta y\Delta x} \left( H_y|_{i+\frac{1}{2},j+1,k+\frac{1}{2}}^{n+\frac{1}{2}} - H_y|_{i+\frac{1}{2},j+1,k+\frac{1}{2}}^{n+\frac{1}{2}} - H_y|_{i+\frac{1}{2},j,k+\frac{1}{2}}^{n+\frac{1}{2}} + H_y|_{i-\frac{1}{2},j,k+\frac{1}{2}}^{n+\frac{1}{2}} \right) \\
& + \frac{\Delta t}{2\mu\Delta z} \left( E_y|_{i,j+\frac{1}{2},k+1}^{n+\frac{1}{2}} - E_y|_{i,j+\frac{1}{2},k}^{n+\frac{1}{2}} \right) - \frac{\Delta t}{2\mu\Delta y} \left( E_z|_{i,j+1,k+\frac{1}{2}}^{n+\frac{1}{2}} - E_z|_{i,j,k+\frac{1}{2}}^{n+\frac{1}{2}} \right)
\end{aligned} \tag{2.30d}$$

$$\begin{aligned}
& -\left(\frac{\Delta t^2}{4\mu\epsilon\Delta z^2}\right)H_y|_{i+\frac{1}{2},j,k+\frac{1}{2}}^{n+1} + \left(1 + \frac{\Delta t^2}{2\mu\epsilon\Delta z^2}\right)H_y|_{i+\frac{1}{2},j,k+\frac{1}{2}}^{n+1} - \left(\frac{\Delta t^2}{4\mu\epsilon\Delta z^2}\right)H_y|_{i+\frac{1}{2},j,k-\frac{1}{2}}^{n+1} \\
& = H_y|_{i+\frac{1}{2},j,k+\frac{1}{2}}^{n+\frac{1}{2}} - \frac{\Delta t^2}{4\mu\epsilon\Delta z\Delta y} \left( H_z|_{i+\frac{1}{2},j+\frac{1}{2},k+1}^{n+\frac{1}{2}} - H_z|_{i+\frac{1}{2},j-\frac{1}{2},k+1}^{n+\frac{1}{2}} - H_z|_{i+\frac{1}{2},j+\frac{1}{2},k}^{n+\frac{1}{2}} + H_z|_{i+\frac{1}{2},j-\frac{1}{2},k}^{n+\frac{1}{2}} \right) \\
& + \frac{\Delta t}{2\mu\Delta x} \left( E_z|_{i+1,j,k+\frac{1}{2}}^{n+\frac{1}{2}} - E_z|_{i,j,k+\frac{1}{2}}^{n+\frac{1}{2}} \right) - \frac{\Delta t}{2\mu\Delta z} \left( E_x|_{i+\frac{1}{2},j,k+1}^{n+\frac{1}{2}} - E_x|_{i+\frac{1}{2},j,k}^{n+\frac{1}{2}} \right)
\end{aligned} \tag{2.30e}$$



$$\begin{aligned}
& - \left( \frac{\Delta t^2}{4\mu\epsilon\Delta x^2} \right) H_z \Big|_{i+\frac{1}{2}, j+\frac{1}{2}, k}^{n+\frac{1}{2}} + \left( 1 + \frac{\Delta t^2}{2\mu\epsilon\Delta x^2} \right) H_z \Big|_{i+\frac{1}{2}, j+\frac{1}{2}, k}^{n+\frac{1}{2}} - \left( \frac{\Delta t^2}{4\mu\epsilon\Delta x^2} \right) H_z \Big|_{i-\frac{1}{2}, j+\frac{1}{2}, k}^{n+\frac{1}{2}} \\
& = H_z \Big|_{i+\frac{1}{2}, j+\frac{1}{2}, k}^{n+\frac{1}{2}} - \frac{\Delta t^2}{4\mu\epsilon\Delta x\Delta z} \left( H_x \Big|_{i+1, j+\frac{1}{2}, k+\frac{1}{2}}^{n+\frac{1}{2}} - H_x \Big|_{i+1, j+\frac{1}{2}, k-\frac{1}{2}}^{n+\frac{1}{2}} - H_x \Big|_{i, j+\frac{1}{2}, k+\frac{1}{2}}^{n+\frac{1}{2}} + H_x \Big|_{i, j+\frac{1}{2}, k-\frac{1}{2}}^{n+\frac{1}{2}} \right) \quad (2.30f) \\
& + \frac{\Delta t}{2\mu\Delta y} \left( E_x \Big|_{i+\frac{1}{2}, j+1, k}^{n+\frac{1}{2}} - E_x \Big|_{i+\frac{1}{2}, j, k}^{n+\frac{1}{2}} \right) - \frac{\Delta t}{2\mu\Delta x} \left( E_y \Big|_{i+1, j+\frac{1}{2}, k}^{n+\frac{1}{2}} - E_y \Big|_{i, j+\frac{1}{2}, k}^{n+\frac{1}{2}} \right)
\end{aligned}$$

Another easy way to obtain all the above equations is to permute the indices of the equation (2.29a). The resulting equations form a linear system of equations that can be solved with available numerical packages. In the following paragraphs, we will describe the approach to the solutions in a matrix form.

The above equations, (2.29) and (2.30), for all field components can be summarized in a simple matrix form:

$$M_1 X^{n+\frac{1}{2}} = P_1 X^n \quad (\text{for advancement from } n\text{-th to } (n+1/2)\text{-th time step}) \quad (2.31a)$$

$$M_2 X^{n+1} = P_2 X^{n+\frac{1}{2}} \quad (\text{for advancement from } (n+1/2)\text{-th to } (n+1)\text{-th time step}) \quad (2.31b)$$

Here vector  $X^n$  is a one-column vector containing all the field components ( $E_x$ ,  $E_y$ ,  $E_z$ ,  $H_x$ ,  $H_y$ ,  $H_z$ ) at the  $n$ -th time step.  $M_1$ ,  $M_2$ ,  $P_1$  and  $P_2$  are the coefficient matrices with their elements related to values of spatial and temporal steps as dictated by equation (2.29) and (2.30). They are all sparse matrices.  $M_1$  and  $M_2$  are associated with the left-hand side of equations (2.29) and (2.30) while  $P_1$  and  $P_2$  are associated with the right-hand side of the equations. It can be observed from equations (2.29) and (2.30) that each row of  $M_1$  and  $M_2$  contains only three non-zero elements at maximum. Matrix operations on them can be fast, in particular, the inverse of  $M_1$  and  $M_2$ .

Recursive equations (2.31) can be solved either implicitly or explicitly. Since the inverse of the sparse matrix  $M_1$  and  $M_2$  can be found relatively easily, an explicit method may be used. They are,

$$X^{n+\frac{1}{2}} = M_1^{-1} P_1 X^n \quad (2.32)$$

$$X^{n+1} = M_2^{-1} P_2 X^{n+\frac{1}{2}} \quad (2.33)$$

Combination of the above two equations ends up with:

$$X^{n+1} = M_2^{-1} P_2 M_1^{-1} P_1 X^n \quad (2.34)$$

or,

$$X^{n+1} = QX^n \quad (2.35)$$

with  $Q = M_2^{-1} P_2 M_1^{-1} P_1$ .

Although the above approach looks simple and easy to implement, the computation requirement could be very large. For a large-scale problem such as mesh size of  $100 \times 100 \times 100$ , the dimension of matrix  $M_1$  and  $M_2$  will be huge (e.g. a million by a million), leading to a computational disaster if we calculate the inverse the matrix  $M_1$  and  $M_2$  which are unnecessarily sparse. In addition, huge amount of computation will be required for matrix multiplying to get  $Q$ .

In a practical simulation, a more efficient approach can be applied. By analyzing the first sub-step in equation (2.27), it could be found that three magnetic field components  $H_x$ ,  $H_y$  and  $H_z$  can be calculated directly from three electric field components  $E_x$ ,  $E_y$  and  $E_z$  updated with equation (2.27). In other words, after all the electric field components are obtained, magnetic field components can then be updated directly from equations (2.27) with the electric field components

already known. Thus, magnetic field components can be solved in a simple way without any matrix multiplying or inversion. The process also holds for the second sub-step computation.

To compute  $E_x$ ,  $E_y$  and  $E_z$ , a special procedure can be applied.

Consider equation (2.29a) which can be simplified as

$$a_j u_{j-1} + b_j u_j + c_j u_{j+1} = d_j \quad (2.36)$$

where  $u_j$  represents  $E_x|_{i+\frac{1}{2},j,k}^{n+\frac{1}{2}}$  and  $a_j$ ,  $b_j$ ,  $c_j$ , and  $d_j$  represent correspondent known coefficient values in equation (2.29a).

Assume that  $j$  sweeps from 0 to  $N+1$ , and  $u_0 = 0$  and  $u_{N+1} = 0$  on the boundary. Application of equation (2.36) in the order of ascending  $j$  leads to a set of  $N$  simultaneous equations

$$\left\{ \begin{array}{l} b_1 u_1 + c_1 u_2 = d_1 \\ a_2 u_1 + b_2 u_2 + c_2 u_3 = d_2 \\ \dots\dots \\ a_r u_{r-1} + b_r u_r + c_r u_{r+1} = d_r \\ \dots\dots \\ a_{N-1} u_{N-2} + b_{N-1} u_{N-1} + c_{N-1} u_N = d_{N-1} \\ a_N u_{N-1} + b_N u_N = d_N \end{array} \right. \quad (2.37)$$

from which  $N$  unknown values  $u_j (j = 1 \dots N)$  can be determined.

The matrix expression of (2.37) can be given by

$$Au = d \quad (2.38)$$

where

$$A = \begin{bmatrix} b_1 & c_1 & 0 & \dots & & 0 \\ a_2 & b_2 & c_2 & 0 & \dots & 0 \\ & & \dots & & & \\ & & a_r & b_r & c_r & \\ & & & \dots & & \\ 0 & \dots & 0 & a_{N-1} & b_{N-1} & c_{N-1} \\ 0 & \dots & & 0 & a_N & b_N \end{bmatrix}$$

$$u = [u_1 \quad u_2 \quad \dots \quad u_N]^T$$

$$d = [d_1 \quad d_2 \quad \dots \quad d_N]^T$$

Two different approaches can be used in solving the above equation.

#### A) Inverse matrix

Notice that the size of  $A$  is much smaller than that of  $M_1$  or  $M_2$  since it accounts for variation in one dimension (i.e.  $j$  in this case). For a  $100 \times 100 \times 100$  problem, the size of  $A$  is  $100 \times 100$  which is  $1/10^8$  of the size of  $M_1$  or  $M_2$ . Therefore, the computation of the inverse of the matrix requires much less memory. Furthermore,  $A^{-1}$  may be used once only to calculate the field values at the left-most grid point  $u_1$ . Once  $u_1$  is obtained, forward substitutions can be applied in (2.37) to find the other components. More specifically, the second leftmost value at  $j = 1$ , at the  $(n + \frac{1}{2})$ -th time step, can be obtained directly from

$$u_2 = \frac{1}{c_1}(d_1 - b_1 u_1) \quad (2.39)$$

The rest  $u$ 's can then be easily calculated by applying (2.36)

$$u_{j+1} = \frac{1}{c_j} (d_j - b_j u_j - a_j u_{j-1}) \quad (2.40)$$

with a sequence of ascending  $j$  that allows one to find  $u_{j+1}$  from  $u_j$  and  $u_{j-1}$ . In such a way, for the most of the computations, we avoid the application of  $A^{-1}$  that is not necessarily very sparse. Thus, the computation efficiency is improved.

### B) Direct Solution

Alternatively, by using the Gaussian elimination method,  $u$  can be obtained directly without involvement of  $A^{-1}$ . Hence, time consuming calculation  $A^{-1}$  can be totally avoided.

Our experiences show that, for a linear, lossless and isotropic medium, approach A) is more efficient because it is only calculated once and can be used in each time step advance and only the first row of  $A^{-1}$  is needed,.

## 2.5 Two-Dimensional ADI-FDTD Formulation

For the 2D electromagnetic problem, the ADI-FDTD formulation can be further simplified. For example, the following are the TM and the TE algorithms for a two-dimensional space region containing a finite number of media having distinct electrical properties.

For TE to  $z$  polarization, the Maxwell's equations are:

$$\frac{\partial E_x}{\partial t} = \frac{1}{\epsilon} \left( \frac{\partial H_z}{\partial y} \right), \quad (2.41a)$$

$$\frac{\partial E_y}{\partial t} = \frac{1}{\epsilon} \left( -\frac{\partial H_z}{\partial x} \right), \quad (2.41b)$$

$$\frac{\partial H_z}{\partial t} = \frac{1}{\mu} \left( \frac{\partial E_x}{\partial y} - \frac{\partial E_y}{\partial x} \right), \quad (2.41c)$$

The corresponding ADI-FDTD formulas are then:

1) for first sub-step

$$\frac{E_x \Big|_{i+\frac{1}{2},j}^{n+\frac{1}{2}} - E_x \Big|_{i+\frac{1}{2},j}^n}{\Delta t/2} = \frac{1}{\varepsilon} \left[ \frac{H_z \Big|_{i+\frac{1}{2},j+\frac{1}{2}}^{n+\frac{1}{2}} - H_z \Big|_{i+\frac{1}{2},j-\frac{1}{2}}^{n+\frac{1}{2}}}{\Delta y} \right] \quad (2.42a)$$

$$\frac{E_y \Big|_{i,j+\frac{1}{2},k}^{n+\frac{1}{2}} - E_y \Big|_{i,j+\frac{1}{2},k}^n}{\Delta t/2} = \frac{1}{\varepsilon} \left[ -\frac{H_z \Big|_{i+\frac{1}{2},j+\frac{1}{2},k}^n - H_z \Big|_{i-\frac{1}{2},j+\frac{1}{2},k}^n}{\Delta x} \right] \quad (2.42b)$$

$$\begin{aligned} & \frac{H_z \Big|_{i+\frac{1}{2},j+\frac{1}{2},k}^{n+\frac{1}{2}} - H_z \Big|_{i+\frac{1}{2},j+\frac{1}{2},k}^n}{\Delta t/2} \\ &= \frac{1}{\mu} \left[ \frac{E_x \Big|_{i+\frac{1}{2},j+1,k}^{n+\frac{1}{2}} - E_x \Big|_{i+\frac{1}{2},j,k}^{n+\frac{1}{2}}}{\Delta y} - \frac{E_y \Big|_{i+1,j+\frac{1}{2},k}^n - E_y \Big|_{i,j+\frac{1}{2},k}^n}{\Delta x} \right] \end{aligned} \quad (2.42c)$$

2) for the second sub-step:

$$\frac{E_x \Big|_{i+\frac{1}{2},j,k}^{n+1} - E_x \Big|_{i+\frac{1}{2},j,k}^{n+\frac{1}{2}}}{\Delta t/2} = \frac{1}{\varepsilon} \left[ \frac{H_z \Big|_{i+\frac{1}{2},j+\frac{1}{2},k}^{n+\frac{1}{2}} - H_z \Big|_{i+\frac{1}{2},j-\frac{1}{2},k}^{n+\frac{1}{2}}}{\Delta y} \right] \quad (2.43a)$$

$$\frac{E_y \Big|_{i,j+\frac{1}{2},k}^{n+1} - E_y \Big|_{i,j+\frac{1}{2},k}^{n+\frac{1}{2}}}{\Delta t/2} = \frac{1}{\varepsilon} \left[ -\frac{H_z \Big|_{i+\frac{1}{2},j+\frac{1}{2},k}^{n+1} - H_z \Big|_{i-\frac{1}{2},j+\frac{1}{2},k}^{n+1}}{\Delta x} \right] \quad (2.43b)$$

$$\begin{aligned}
& \frac{H_z \Big|_{i+\frac{1}{2}, j+\frac{1}{2}, k}^{n+1} - H_z \Big|_{i+\frac{1}{2}, j+\frac{1}{2}, k}^{n+\frac{1}{2}}}{\Delta t / 2} \\
&= \frac{1}{\mu} \left[ \frac{E_x \Big|_{i+\frac{1}{2}, j+1, k}^{n+\frac{1}{2}} - E_x \Big|_{i+\frac{1}{2}, j, k}^{n+\frac{1}{2}}}{\Delta y} - \frac{E_y \Big|_{i+1, j+\frac{1}{2}, k}^{n+1} - E_y \Big|_{i, j+\frac{1}{2}, k}^{n+1}}{\Delta x} \right] \quad (2.43c)
\end{aligned}$$

Notice that in the TE ADI-FDTD formulation, the same set of equations can also be obtained by applying the original ADI technique instead of the modified one. For example, equations (2.39a-c) of the first sub-step are implicit in the y-direction and equations (2.40a-c) of the second sub-step are implicit in x-direction [73]. Hence, there is no difference between the modified ADI and original ADI in the two-dimensional case.

For the two-dimensional TM case, the Maxwell's equations become

$$\frac{\partial E_z}{\partial t} = \frac{1}{\epsilon} \left( \frac{\partial H_y}{\partial x} - \frac{\partial H_x}{\partial y} \right). \quad (2.44a)$$

$$\frac{\partial H_x}{\partial t} = \frac{1}{\mu} \left( -\frac{\partial E_z}{\partial y} \right), \quad (2.44b)$$

$$\frac{\partial H_y}{\partial t} = \frac{1}{\mu} \left( \frac{\partial E_z}{\partial x} \right). \quad (2.44c)$$

The corresponding ADI-FDTD formulations are,

1) for the first sub-step:

$$\begin{aligned}
& \frac{E_z \Big|_{i,j,k+\frac{1}{2}}^{n+\frac{1}{2}} - E_z \Big|_{i,j,k+\frac{1}{2}}^n}{\Delta t / 2} \\
&= \frac{1}{\epsilon} \left[ \frac{H_y \Big|_{i+\frac{1}{2},j,k+\frac{1}{2}}^{n+\frac{1}{2}} - H_y \Big|_{i-\frac{1}{2},j,k+\frac{1}{2}}^{n+\frac{1}{2}}}{\Delta x} - \frac{H_x \Big|_{i,j+\frac{1}{2},k+\frac{1}{2}}^n - H_x \Big|_{i,j-\frac{1}{2},k+\frac{1}{2}}^n}{\Delta y} \right] \quad (2.45a)
\end{aligned}$$

$$\frac{H_x \Big|_{i,j+\frac{1}{2},k+\frac{1}{2}}^{n+\frac{1}{2}} - H_x \Big|_{i,j+\frac{1}{2},k+\frac{1}{2}}^n}{\Delta t / 2} = \frac{1}{\mu} \left[ -\frac{E_z \Big|_{i,j+1,k+\frac{1}{2}}^n - E_z \Big|_{i,j,k+\frac{1}{2}}^n}{\Delta y} \right] \quad (2.45b)$$

$$\frac{H_y \Big|_{i+\frac{1}{2},j,k+\frac{1}{2}}^{n+\frac{1}{2}} - H_y \Big|_{i+\frac{1}{2},j,k+\frac{1}{2}}^n}{\Delta t / 2} = \frac{1}{\mu} \left[ \frac{E_z \Big|_{i+1,j,k+\frac{1}{2}}^{n+\frac{1}{2}} - E_z \Big|_{i,j,k+\frac{1}{2}}^{n+\frac{1}{2}}}{\Delta x} \right] \quad (2.45c)$$

2) for the second sub-step:

$$\begin{aligned}
& \frac{E_z \Big|_{i,j,k+\frac{1}{2}}^{n+1} - E_z \Big|_{i,j,k+\frac{1}{2}}^{n+\frac{1}{2}}}{\Delta t / 2} \\
&= \frac{1}{\epsilon} \left[ \frac{H_y \Big|_{i+\frac{1}{2},j,k+\frac{1}{2}}^{n+\frac{1}{2}} - H_y \Big|_{i-\frac{1}{2},j,k+\frac{1}{2}}^{n+\frac{1}{2}}}{\Delta x} - \frac{H_x \Big|_{i,j+\frac{1}{2},k+\frac{1}{2}}^{n+1} - H_x \Big|_{i,j-\frac{1}{2},k+\frac{1}{2}}^{n+1}}{\Delta y} \right] \quad (2.46a)
\end{aligned}$$

$$\frac{H_x \Big|_{i,j+\frac{1}{2},k+\frac{1}{2}}^{n+1} - H_x \Big|_{i,j+\frac{1}{2},k+\frac{1}{2}}^{n+\frac{1}{2}}}{\Delta t / 2} = \frac{1}{\mu} \left[ -\frac{E_z \Big|_{i,j+1,k+\frac{1}{2}}^{n+1} - E_z \Big|_{i,j,k+\frac{1}{2}}^{n+1}}{\Delta y} \right] \quad (2.46b)$$

$$\frac{H_y \Big|_{i+\frac{1}{2},j,k+\frac{1}{2}}^{n+1} - H_y \Big|_{i+\frac{1}{2},j,k+\frac{1}{2}}^{n+\frac{1}{2}}}{\Delta t / 2} = \frac{1}{\mu} \left[ \frac{E_z \Big|_{i+1,j,k+\frac{1}{2}}^{n+\frac{1}{2}} - E_z \Big|_{i,j,k+\frac{1}{2}}^{n+\frac{1}{2}}}{\Delta x} \right] \quad (2.46c)$$



Similar to the TE case, above equations may be obtained by directly applying the conventional ADI technique.

For the two-dimensional TE and TM cases, the same efficient computation approaches as presented in the previous section for the 3D cases can also be used to accelerate simulation speed.

## 2.6 Simulations and Results

To demonstrate the validity of the proposed ADI-FDTD method, one homogeneous and one inhomogeneous rectangular cavities were computed with both the ADI-FDTD and the conventional Yee's FDTD. The reasons of choosing the cavities are that the analytical solutions are readily available for comparison.

### Homogeneous Air-filled Cavity

The results illustrated in Table 1.1 show the first four resonant frequencies of an air-filled cavity. The air-filled cavity has the dimension  $9\text{mm} \times 6\text{mm} \times 15\text{mm}$ . For both ADI-FDTD scheme and Yee's FDTD scheme, a mesh with  $\Delta l = 0.6\text{mm}$  was used resulting in  $15 \times 10 \times 25$  grid points. Note that that a time step  $\Delta t_{FDTD} = 0.8\text{ps}$  and a larger time step  $\Delta t_i = 3 \times \Delta t_{FDTD} = 2.4\text{ps}$  were chosen for FDTD and ADI-FDTD, respectively. It can be seen that the errors for both methods are comparable. And yet a saving factor of 1.55 in CPU time with the proposed ADI-FDTD was achieved in this case.

**Table 1.1: Comparisons of Results with the conventional FDTD and ADI-FDTD**

Analytic Results (GHz)	Conventional FDTD scheme		ADI-FDTD scheme	
	Simulation results (GHz)	Relative error	Simulation results (GHz)	Relative error
19.427	19.451	0.12%	19.400	0.14%
26.022	25.972	0.19%	25.961	0.23%
31.652	31.455	0.62%	31.553	0.31%
34.776	34.613	0.47%	34.577	0.57%

### Inhomogeneous Half-filled Cavity

The geometry of the inhomogeneous half-filled cavity is depicted in Figure 2.3. One half of the cavity is filled with air and the other half with the dielectric material of a relative permittivity of  $\epsilon_r = 64$ . The cavity has the dimension of  $1\text{m} \times 2\text{m} \times 1.5\text{m}$ . Again a uniform mesh with  $\Delta l = 0.1\text{m}$  was used, leading to a mesh of  $10 \times 20 \times 15$  grid points.

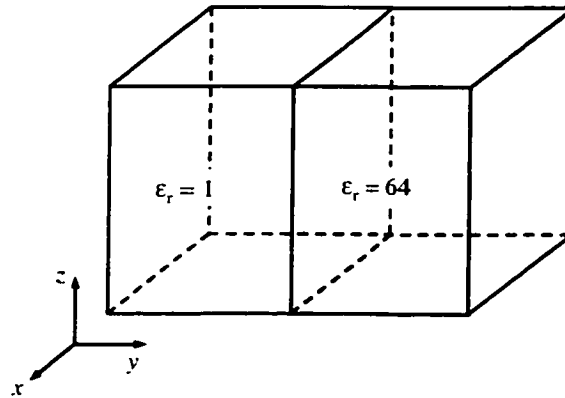


Figure 2.3 The cavity half filled with air and the other half filled with dielectric material.

For the comparison purpose, both the ADI-FDTD and the conventional FDTD were used to simulate the cavity. This time, a time step  $\Delta t_{FDTD} = 1.5 \times 10^{-10} \text{ s}$  was chosen with the conventional FDTD, while a larger time step  $\Delta t_i = 4 \times \Delta t_{FDTD} = 6 \times 10^{-10} \text{ s}$  was chosen with the proposed ADI-FDTD. With such time step ratio, we found, by trial and error, that the two methods presented similar accuracy. Therefore, the two methods are compared at the same accuracy level. 20000 iterations were run with the conventional FDTD method while 5000 iterations with the ADI-FDTD. The iterations present the same

physical time period since the time step with the conventional FDTD is one-fourth of the time step with ADI-FDTD. Table 1.2 shows the first five resonant frequencies obtained with the two methods. The errors for the two methods are at the same level.

**Table 1.2: Comparisons of Results with the conventional FDTD and ADI-FDTD**

Analytic Results (MHz)	Conventional FDTD scheme		ADI-FDTD scheme	
	Simulation results (MHz)	Relative error	Simulation results (MHz)	Relative error
18.627	18.610	0.11%	18.587	0.21%
27.172	27.12	0.19%	27.046	0.46%
29.374	29.225	0.51%	29.155	0.88%
32.881	32.671	0.64%	32.626	0.77%
35.069	34.946	0.35%	34.832	0.67%

On a Pentium III 450 MHz PC, it took 545.83 seconds to finish the simulation with the ADI-FDTD and 873.34 seconds with the conventional FDTD. We then concluded preliminarily that a saving factor with the ADI-FDTD in CPU time is about 1.6 when the conventional FDTD is used as a reference.

### Computational Expenditures

Since the Yee's grid is used with the ADI-FDTD method, the number of field components at all the grid points are the same as that with the conventional FDTD. However, due to the fact that E and H field components are not interlaced in time anymore, the memory requirement is almost double of that for the conventional FDTD method as indicated in equations (2.29) and (2.30).

In addition, more components are involved in the recursive computation at each time step with the proposed FDTD method. The CPU time for each time step with the ADI-FDTD is then larger than that with the conventional FDTD method. However, since a larger time step can be used with the ADI-FDTD, the total number of iterations required with the ADI-FDTD could be reduced. The opposite

effects of the more CPU time for each time step and the reduced number of iterations on the overall CPU time will be studied, in particular, numerically, in the next chapter.

## **2.7 Discussion and Conclusions**

In this Chapter, a new three-dimensional ADI-FDTD free of the CFL stability condition is presented for solving electromagnetic problems. In the new scheme, the Yee's grid is used with the application of the alternative direction implicit technique in formulating the algorithm. As a result, the memory requirement is about twice that for the conventional FDTD while the time step is no longer restricted by the numerical stability. In comparison with earlier work reported by reference [70], the proposed ADI-FDTD reduces the number of sub-step by a factor of three to two, which means 33% time saving in a single run.

To avoid time consuming computation of inverting a matrix, an efficient computation technique is presented for practical implementation. Numerical verifications are presented to demonstrate the validity of the proposed method without the CFL condition. Preliminary experiments indicated that with the same accuracy, the proposed method uses four times fewer of iterations and is 1.6 times faster than the conventional FDTD. Note that parts of this chapter have been published in the technical journals [99][130].

## **Chapter 3 Numerical Stability Analysis: Proof of unconditional stability**

### **3.1 Introduction**

The numerical algorithm for Maxwell's curl equations defined by conventional FDTD systems require that time increment  $\Delta t$  has a specific bound relative to the lattice space increments  $\Delta x$ ,  $\Delta y$  and  $\Delta z$ . This bound is necessary to avoid numerical instability, an undesirable possibility with explicit differential equation solvers that can cause the computed results to spuriously increase without limit as time-marching continues.

The new ADI-based FDTD algorithm developed in Chapter 2 shows numerically the stability even beyond the CFL point of the conventional FDTD. Original ADI technique has been applied to solve parabolic differential equation [74], and proved stable. As described in Chapter 2, the ADI technique applied to the proposed ADI-FDTD is different from the original one. Rather than alternating the coordinate directions from which ADI get its name, the modified ADI technique used in the ADI-FDTD is applied by alternating the sequence of the terms on the right-hand side of the equations (the *first* and the *second* terms). Hence, the stability of the new scheme need to be investigated rigorously to demonstrate that the proposed scheme is unconditionally stable. In other words, although the preliminary numerical experiments show that the new ADI-FDTD is stable even when the time step beyond hundreds of times the limit of the conventional FDTD, a theoretical proof that ADI-FDTD is unconditionally stable is required and is given in this chapter.

### 3.2 Unconditional stability of Three-dimensional ADI-FDTD Algorithm

Generally, for a recursive scheme or system,

$$\mathbf{F}^{n+1} = \mathbf{A} \cdot \mathbf{F}^n \quad (3.1)$$

its numerical stability can be determined with the so-called *Fourier* method as described in reference [22]. Instantaneous values of electric and magnetic fields distributed in space across a grid are first *Fourier*-transformed into the waves in the spatial spectral domain to represent a spectrum of spatial sinusoidal modes. By checking the eigenvalues associated with the spectral-domain waves in the system, one can determine the stability conditions of the system. If magnitudes of all the eigenvalues are less than or equal to unity, the scheme is stable. If one of them is larger than one, the scheme is potentially unstable. The *Fourier* method is applied in this chapter and the analysis is presented in the following paragraphs.

Mathematically, the spatial Fourier transform of the instantaneous electric and magnetic fields can be expressed in the  $i$ ,  $j$ , and  $k$  coordinates to provide a spectrum of sinusoidal modes. The results are often called three-dimensional spatial-frequency waves, or eigenmodes of the grid. More specifically, assume that the spatial frequencies to be  $k_x$ ,  $k_y$  and  $k_z$  along the  $x$ ,  $y$  and  $z$  directions.

The field components in the spatial spectral domain can then be written as

$$E_x \Big|_{i+\frac{1}{2},j,k}^n = E_x^n e^{-j(k_x(i+\frac{1}{2})\Delta x + k_y j\Delta y + k_z k\Delta z)} \quad (3.2a)$$

$$E_y \Big|_{i,j+\frac{1}{2},k}^n = E_y^n e^{-j(k_x i\Delta x + k_y(j+\frac{1}{2})\Delta y + k_z k\Delta z)} \quad (3.2b)$$

$$E_z \Big|_{i,j,k+\frac{1}{2}}^n = E_z^n e^{-j(k_x i\Delta x + k_y j\Delta y + k_z(k+\frac{1}{2})\Delta z)} \quad (3.2c)$$

$$H_x \Big|_{i,j+\frac{1}{2},k+\frac{1}{2}}^n = H_x^n e^{-j(k_x i \Delta x + k_y (j+\frac{1}{2}) \Delta y + k_z (k+\frac{1}{2}) \Delta z)} \quad (3.2d)$$

$$H_y \Big|_{i+\frac{1}{2},j,k+\frac{1}{2}}^n = H_y^n e^{-j(k_x (i+\frac{1}{2}) \Delta x + k_y j \Delta y + k_z (k+\frac{1}{2}) \Delta z)} \quad (3.2e)$$

$$H_z \Big|_{i+\frac{1}{2},j+\frac{1}{2},k}^n = H_z^n e^{-j(k_x (i+\frac{1}{2}) \Delta x + k_y (j+\frac{1}{2}) \Delta y + k_z k \Delta z)} \quad (3.2f)$$

Substitution of equations (3.2a-3.2f) into (2.29a), respectively, can lead to equation (3.3) in the spatial spectral domain in terms of  $k_x$ ,  $k_y$ ,  $k_z$ ,  $\Delta t$ ,  $\Delta x$ ,  $\Delta y$ , and  $\Delta z$ .

$$\begin{aligned} & - \left( \frac{\Delta t^2}{4\mu\epsilon\Delta y^2} \right) E_x^{n+\frac{1}{2}} e^{-j(k_x (i+\frac{1}{2}) \Delta x + k_y (j+1) \Delta y + k_z k \Delta z)} + \left( 1 + \frac{\Delta t^2}{2\mu\epsilon\Delta y^2} \right) E_x^{n+\frac{1}{2}} e^{-j(k_x (i+\frac{1}{2}) \Delta x + k_y j \Delta y + k_z k \Delta z)} \\ & - \left( \frac{\Delta t^2}{4\mu\epsilon\Delta y^2} \right) E_x^{n+\frac{1}{2}} e^{-j(k_x (i+\frac{1}{2}) \Delta x + k_y (j-1) \Delta y + k_z k \Delta z)} \\ & = E_x^n e^{-j(k_x (i+\frac{1}{2}) \Delta x + k_y j \Delta y + k_z k \Delta z)} \\ & + \frac{\Delta t}{2\epsilon\Delta y} \left( H_z^n e^{-j(k_x (i+\frac{1}{2}) \Delta x + k_y (j+\frac{1}{2}) \Delta y + k_z k \Delta z)} - H_z^n e^{-j(k_x (i+\frac{1}{2}) \Delta x + k_y (j-\frac{1}{2}) \Delta y + k_z k \Delta z)} \right) \\ & - \frac{\Delta t}{2\epsilon\Delta z} \left( H_y^n e^{-j(k_x (i+\frac{1}{2}) \Delta x + k_y j \Delta y + k_z (k+\frac{1}{2}) \Delta z)} - H_y^n e^{-j(k_x (i+\frac{1}{2}) \Delta x + k_y j \Delta y + k_z (k-\frac{1}{2}) \Delta z)} \right) \\ & - \frac{\Delta t^2}{4\mu\epsilon\Delta x\Delta y} \left( E_y^n e^{-j(k_x (i+1) \Delta x + k_y (j+\frac{1}{2}) \Delta y + k_z k \Delta z)} - E_y^n e^{-j(k_x i \Delta x + k_y (j+\frac{1}{2}) \Delta y + k_z k \Delta z)} \right. \\ & \left. - E_y^n e^{-j(k_x (i+1) \Delta x + k_y (j-\frac{1}{2}) \Delta y + k_z k \Delta z)} + E_y^n e^{-j(k_x i \Delta x + k_y (j-\frac{1}{2}) \Delta y + k_z k \Delta z)} \right) \end{aligned} \quad (3.3)$$

Factoring out the  $e^{-j(k_x i \Delta x + k_y j \Delta y + k_z k \Delta z)}$  term that is common to both sides, one can simplify the above equation to equation (3.4):

$$\begin{aligned}
& -\left(\frac{\Delta t^2}{4\mu\epsilon\Delta y^2}\right)E_x^{n+\frac{1}{2}}e^{-j(k_y\Delta y)} + \left(1 + \frac{\Delta t^2}{2\mu\epsilon\Delta y^2}\right)E_x^{n+\frac{1}{2}} \\
& -\left(\frac{\Delta t^2}{4\mu\epsilon\Delta y^2}\right)E_x^{n+\frac{1}{2}}e^{-j(k_y(-1)\Delta y)} \\
& = E_x^n - \frac{\Delta t^2}{4\mu\epsilon\Delta x\Delta y} \left( \begin{array}{l} E_y^n e^{-j(k_x(1/2)\Delta x + k_y(\frac{1}{2})\Delta y)} - E_y^n e^{-j(k_x(-1/2)\Delta x + k_y(\frac{1}{2})\Delta y)} \\ - E_y^n e^{-j(k_x(1/2)\Delta x + k_y(-\frac{1}{2})\Delta y)} + E_y^n e^{-j(k_x(-1/2)\Delta x + k_y(-\frac{1}{2})\Delta y)} \end{array} \right) \\
& + \frac{\Delta t}{2\epsilon\Delta y} \left( H_z^n e^{-j(k_y\frac{1}{2}\Delta y)} - H_z^n e^{-j(k_y(-\frac{1}{2})\Delta y)} \right) - \frac{\Delta t}{2\epsilon\Delta z} \left( H_y^n e^{-j(k_z\frac{1}{2}\Delta z)} - H_y^n e^{-j(k_z(-\frac{1}{2})\Delta z)} \right)
\end{aligned} \tag{3.4}$$

Applying Euler's identity to the complex exponentials yields:

$$\begin{aligned}
& -\left(\frac{\Delta t^2}{4\mu\epsilon\Delta y^2}\right)E_x^{n+\frac{1}{2}}2\cos(k_y\Delta y) + \left(1 + \frac{\Delta t^2}{2\mu\epsilon\Delta y^2}\right)E_x^{n+\frac{1}{2}} \\
& = E_x^n + \frac{\Delta t}{2\epsilon\Delta y} \left( H_z^n (-2j\sin(k_y\Delta y/2)) \right) - \frac{\Delta t}{2\epsilon\Delta z} \left( H_y^n (-2j\sin(k_z\Delta z/2)) \right) \\
& - \frac{\Delta t^2}{4\mu\epsilon\Delta x\Delta y} \left( E_y^n (-2j\sin(k_y\Delta y/2))(-2j\sin(k_x\Delta x/2)) \right)
\end{aligned} \tag{3.5}$$

With

$$1 - \cos\theta = 2\sin^2(\theta/2), \tag{3.6}$$

equation (3.5) becomes:

$$\begin{aligned}
& \left(1 + \frac{\sin^2(k_y\Delta y)\Delta t^2}{\mu\epsilon\Delta y^2}\right)E_x^{n+\frac{1}{2}} \\
& = E_x^n - j\frac{\sin(k_y\Delta y/2)\Delta t}{\epsilon\Delta y} H_z^n + j\frac{\sin(k_z\Delta z/2)\Delta t}{\epsilon\Delta z} H_y^n \\
& + \frac{\sin(k_x\Delta x/2)\sin(k_y\Delta y/2)\Delta t^2}{\mu\epsilon\Delta x\Delta y} E_y^n
\end{aligned} \tag{3.7a}$$

In a similar manner, substituting the eigenmode expressions of equations (3.2) into equation (2.29b-f) for the first sub-step yields,



$$\begin{aligned}
& \left(1 + \frac{\sin^2(k_z \Delta z) \Delta t^2}{\mu \epsilon \Delta z^2}\right) E_y^{n+\frac{1}{2}} \\
&= E_y^n - j \frac{\sin(k_z \Delta z / 2) \Delta t}{\epsilon \Delta z} H_x^n + j \frac{\sin(k_x \Delta x / 2) \Delta t}{\epsilon \Delta x} H_z^n \\
&+ \frac{\sin(k_y \Delta y / 2) \sin(k_z \Delta z / 2) \Delta t^2}{\mu \epsilon \Delta y \Delta z} E_z^n
\end{aligned} \tag{3.7b}$$

$$\begin{aligned}
& \left(1 + \frac{\sin^2(k_x \Delta x) \Delta t^2}{\mu \epsilon \Delta x^2}\right) E_z^{n+\frac{1}{2}} \\
&= E_z^n - j \frac{\sin(k_x \Delta x / 2) \Delta t}{\epsilon \Delta x} H_y^n + j \frac{\sin(k_y \Delta y / 2) \Delta t}{\epsilon \Delta y} H_x^n \\
&- \frac{\sin(k_z \Delta z / 2) \sin(k_x \Delta x / 2) \Delta t^2}{\mu \epsilon \Delta z \Delta x} E_x^n
\end{aligned} \tag{3.7c}$$

$$\begin{aligned}
& \left(1 + \frac{\sin^2(k_z \Delta z) \Delta t^2}{\mu \epsilon \Delta z^2}\right) H_x^{n+\frac{1}{2}} \\
&= H_x^n - j \frac{\sin(k_z \Delta z / 2) \Delta t}{\epsilon \Delta z} E_y^n + j \frac{\sin(k_y \Delta y / 2) \Delta t}{\epsilon \Delta y} E_z^n \\
&+ \frac{\sin(k_z \Delta z / 2) \sin(k_x \Delta x / 2) \Delta t^2}{\mu \epsilon \Delta z \Delta x} H_z^n
\end{aligned} \tag{3.7d}$$

$$\begin{aligned}
& \left(1 + \frac{\sin^2(k_x \Delta x) \Delta t^2}{\mu \epsilon \Delta x^2}\right) H_y^{n+\frac{1}{2}} \\
&= H_y^n - j \frac{\sin(k_x \Delta x / 2) \Delta t}{\epsilon \Delta x} E_z^n + j \frac{\sin(k_z \Delta z / 2) \Delta t}{\epsilon \Delta z} E_x^n \\
&+ \frac{\sin(k_x \Delta x / 2) \sin(k_y \Delta y / 2) \Delta t^2}{\mu \epsilon \Delta x \Delta y} H_x^n
\end{aligned} \tag{3.7e}$$

$$\begin{aligned}
& \left(1 + \frac{\sin^2(k_y \Delta y) \Delta t^2}{\mu \epsilon \Delta y^2}\right) H_z^{n+\frac{1}{2}} \\
&= H_z^n - j \frac{\sin(k_y \Delta y / 2) \Delta t}{\epsilon \Delta y} E_z^n + j \frac{\sin(k_x \Delta x / 2) \Delta t}{\epsilon \Delta x} E_y^n \\
&+ \frac{\sin(k_y \Delta y / 2) \sin(k_z \Delta z / 2) \Delta t^2}{\mu \epsilon \Delta y \Delta z} H_y^n
\end{aligned} \tag{3.7f}$$

For the equation (2.30) for the second sub-step computation, similar expressions can be obtained as,

$$\begin{aligned}
& \left(1 + \frac{\sin^2(k_z \Delta z) \Delta t^2}{\mu \epsilon \Delta z^2}\right) E_x^{n+1} \\
&= E_x^n - j \frac{\sin(k_y \Delta y / 2) \Delta t}{\epsilon \Delta y} H_z^{n+\frac{1}{2}} + j \frac{\sin(k_z \Delta z / 2) \Delta t}{\epsilon \Delta z} H_y^{n+\frac{1}{2}} \\
&+ \frac{\sin(k_x \Delta x / 2) \sin(k_z \Delta z / 2) \Delta t^2}{\mu \epsilon \Delta z \Delta x} E_z^{n+\frac{1}{2}}
\end{aligned} \tag{3.8a}$$

$$\begin{aligned}
& \left(1 + \frac{\sin^2(k_x \Delta x) \Delta t^2}{\mu \epsilon \Delta x^2}\right) E_y^{n+1} \\
&= E_y^{n+\frac{1}{2}} - j \frac{\sin(k_z \Delta z / 2) \Delta t}{\epsilon \Delta z} H_x^{n+\frac{1}{2}} + j \frac{\sin(k_x \Delta x / 2) \Delta t}{\epsilon \Delta x} H_z^{n+\frac{1}{2}} \\
&+ \frac{\sin(k_x \Delta x / 2) \sin(k_y \Delta y / 2) \Delta t^2}{\mu \epsilon \Delta x \Delta y} E_x^{n+\frac{1}{2}}
\end{aligned} \tag{3.8b}$$

$$\begin{aligned}
& \left(1 + \frac{\sin^2(k_y \Delta y) \Delta t^2}{\mu \epsilon \Delta y^2}\right) E_z^{n+1} \\
&= E_z^{n+\frac{1}{2}} - j \frac{\sin(k_x \Delta x / 2) \Delta t}{\epsilon \Delta x} H_y^{n+\frac{1}{2}} + j \frac{\sin(k_y \Delta y / 2) \Delta t}{\epsilon \Delta y} H_x^{n+\frac{1}{2}} \\
&+ \frac{\sin(k_y \Delta y / 2) \sin(k_z \Delta z / 2) \Delta t^2}{\mu \epsilon \Delta y \Delta z} E_y^{n+\frac{1}{2}}
\end{aligned} \tag{3.8c}$$

$$\begin{aligned}
& \left(1 + \frac{\sin^2(k_y \Delta y) \Delta t^2}{\mu \epsilon \Delta y^2}\right) H_x^{n+1} \\
&= H_x^{n+\frac{1}{2}} - j \frac{\sin(k_z \Delta z / 2) \Delta t}{\epsilon \Delta z} E_y^{n+\frac{1}{2}} + j \frac{\sin(k_y \Delta y / 2) \Delta t}{\epsilon \Delta y} E_z^{n+\frac{1}{2}} \\
&+ \frac{\sin(k_x \Delta x / 2) \sin(k_y \Delta y / 2) \Delta t^2}{\mu \epsilon \Delta x \Delta y} H_y^{n+\frac{1}{2}}
\end{aligned} \tag{3.8d}$$

$$\begin{aligned}
& \left(1 + \frac{\sin^2(k_z \Delta z) \Delta t^2}{\mu \epsilon \Delta z^2}\right) H_y^{n+1} \\
&= H_y^{n+\frac{1}{2}} - j \frac{\sin(k_x \Delta x / 2) \Delta t}{\epsilon \Delta x} E_z^{n+\frac{1}{2}} + j \frac{\sin(k_z \Delta z / 2) \Delta t}{\epsilon \Delta z} E_x^{n+\frac{1}{2}} \\
&+ \frac{\sin(k_y \Delta y / 2) \sin(k_z \Delta z / 2) \Delta t^2}{\mu \epsilon \Delta y \Delta z} H_z^{n+\frac{1}{2}}
\end{aligned} \tag{3.8e}$$

$$\begin{aligned}
& \left(1 + \frac{\sin^2(k_x \Delta x) \Delta t^2}{\mu \epsilon \Delta x^2}\right) H_z^{n+1} \\
&= H_z^{n+\frac{1}{2}} - j \frac{\sin(k_y \Delta y / 2) \Delta t}{\epsilon \Delta y} E_x^{n+\frac{1}{2}} + j \frac{\sin(k_x \Delta x / 2) \Delta t}{\epsilon \Delta x} E_y^{n+\frac{1}{2}} \\
&+ \frac{\sin(k_z \Delta z / 2) \sin(k_x \Delta x / 2) \Delta t^2}{\mu \epsilon \Delta z \Delta x} H_x^{n+\frac{1}{2}}
\end{aligned} \tag{3.8f}$$

Denote the field vector in the spatial spectral domain as:

$$\mathbf{F}^n = \begin{bmatrix} E_x^n \\ E_y^n \\ E_z^n \\ H_x^n \\ H_y^n \\ H_z^n \end{bmatrix}, \tag{3.9}$$

Then the time-marching relation of all six field components can be summarized and written in a matrix form as followings.

For the first sub-step computation,

$$\mathbf{F}^{n+\frac{1}{2}} = \mathbf{A}_1 \cdot \mathbf{F}^n \quad (3.10)$$

where

$$\mathbf{A}_1 = \begin{bmatrix} \frac{1}{Q_y} & \frac{W_x \cdot W_y}{\mu \epsilon Q_y} & 0 & 0 & \frac{jW_z}{\epsilon Q_y} & \frac{-jW_y}{\epsilon Q_y} \\ 0 & \frac{1}{Q_z} & \frac{W_z \cdot W_y}{\mu \epsilon Q_z} & \frac{-jW_z}{\epsilon Q_z} & 0 & \frac{jW_x}{\epsilon Q_z} \\ \frac{W_x \cdot W_z}{\mu \epsilon Q_x} & 0 & \frac{1}{Q_x} & \frac{jW_y}{\epsilon Q_x} & \frac{-jW_x}{\epsilon Q_x} & 0 \\ 0 & \frac{-jW_z}{\mu Q_z} & \frac{jW_z}{\mu Q_z} & \frac{1}{Q_z} & 0 & \frac{W_x \cdot W_z}{\mu \epsilon Q_z} \\ \frac{jW_z}{\mu Q_x} & 0 & \frac{-jW_x}{\mu Q_x} & \frac{W_x \cdot W_y}{\mu \epsilon Q_x} & \frac{1}{Q_x} & 0 \\ \frac{-jW_y}{\mu Q_y} & \frac{jW_x}{\mu Q_y} & 0 & 0 & \frac{W_z \cdot W_y}{\mu \epsilon Q_y} & \frac{1}{Q_y} \end{bmatrix} \quad (3.11)$$

$$W_\alpha = \frac{\Delta r}{\Delta \alpha} \cdot \sin\left(\frac{k_\alpha \Delta \alpha}{2}\right), \quad \alpha = x, y, z$$

$$Q_\alpha = 1 + \frac{W_\alpha^2}{\mu \epsilon}, \quad \alpha = x, y, z$$

For the second sub-step computation,

$$\mathbf{F}^{n+1} = \mathbf{A}_2 \cdot \mathbf{F}^{n+\frac{1}{2}} \quad (3.12)$$

where

$$A_2 = \begin{bmatrix} \frac{1}{Q_z} & 0 & \frac{W_z \cdot W_x}{\mu \epsilon Q_z} & 0 & \frac{jW_z}{\epsilon Q_z} & \frac{-jW_y}{\epsilon Q_z} \\ \frac{W_x \cdot W_y}{\mu \epsilon Q_x} & \frac{1}{Q_x} & 0 & \frac{-jW_z}{\epsilon Q_x} & 0 & \frac{jW_x}{\epsilon Q_x} \\ 0 & \frac{W_y \cdot W_z}{\mu \epsilon Q_y} & \frac{1}{Q_y} & \frac{jW_y}{\epsilon Q_y} & \frac{-jW_x}{\epsilon Q_y} & 0 \\ 0 & \frac{-jW_z}{\mu Q_y} & \frac{jW_y}{\mu Q_y} & \frac{1}{Q_y} & \frac{W_x \cdot W_y}{\mu \epsilon Q_y} & 0 \\ \frac{jW_z}{\mu Q_z} & 0 & \frac{-jW_x}{\mu Q_z} & 0 & \frac{1}{Q_z} & \frac{W_y \cdot W_z}{\mu \epsilon Q_z} \\ -jW_y & \frac{jW_x}{\mu Q_x} & 0 & \frac{W_x \cdot W_z}{\mu \epsilon Q_x} & 0 & \frac{1}{Q_x} \\ \frac{jW_z}{\mu Q_x} & \frac{jW_x}{\mu Q_x} & 0 & \frac{W_x \cdot W_z}{\mu \epsilon Q_x} & 0 & \frac{1}{Q_x} \end{bmatrix} \quad (3.13)$$

where  $W_\alpha$  and  $Q_\alpha$  have the same definition as defined in equation (3.11).

Substitution of equation (3.10) into equation (3.12) leads to:

$$F^{n+1} = \Lambda F^n = A_2 A_1 F^n \quad (3.14)$$

With the use of Maple V5.2, one has:

$$A = \begin{bmatrix} \frac{A_1 + B_1}{Q_x Q_y Q_z} & \frac{2\mu \epsilon W_x W_y}{Q_x Q_y} & \frac{2\mu \epsilon W_x W_z}{Q_y Q_z} & \frac{-2j\mu W}{Q_x Q_y} & \frac{2j\mu^2 \epsilon W_z}{Q_y Q_z} & \frac{2j\mu D_1}{Q_x Q_y Q_z} \\ \frac{2\mu \epsilon W_y W_x}{Q_z Q_x} & \frac{A_2 + B_2}{Q_x Q_y Q_z} & \frac{2\mu \epsilon W_y W_z}{Q_y Q_z} & \frac{2j\mu D_2}{Q_x Q_y Q_z} & \frac{-2j\mu W}{Q_y Q_z} & \frac{2j\mu^2 \epsilon W_x}{Q_z Q_x} \\ \frac{2\mu \epsilon W_z W_x}{Q_z Q_x} & \frac{2\mu \epsilon W_z W_y}{Q_x Q_y Q_z} & \frac{A_3 + B_3}{Q_y Q_z} & \frac{2j\mu^2 \epsilon W_y}{Q_x Q_y} & \frac{2j\mu D_3}{Q_y Q_z} & \frac{-2j\mu W}{Q_z Q_x} \\ \frac{-2j\epsilon W}{Q_x Q_z} & \frac{2j\epsilon D_2}{Q_x Q_y} & \frac{2j\mu \epsilon^2 W_y}{Q_y Q_z} & \frac{A_1 + B_3}{Q_x Q_y} & \frac{2\mu \epsilon W_x W_y}{Q_x Q_y Q_z} & \frac{2\mu \epsilon W_z W_x}{Q_z Q_x} \\ \frac{2j\mu \epsilon^2 W_z}{Q_x Q_z} & \frac{-2j\epsilon W}{Q_x Q_y Q_z} & \frac{2j\epsilon D_3}{Q_y Q_z} & \frac{2\mu \epsilon W_x W_y}{Q_x Q_y} & \frac{A_2 + B_1}{Q_y Q_z} & \frac{2\mu \epsilon W_y W_z}{Q_z Q_x} \\ \frac{2j\epsilon D_1}{Q_z Q_x} & \frac{2j\mu \epsilon^2 W_x}{Q_y Q_x} & \frac{-2j\epsilon W}{Q_x Q_y Q_z} & \frac{2\mu \epsilon W_z W_x}{Q_x Q_y} & \frac{2\mu \epsilon W_y W_z}{Q_x Q_y Q_z} & \frac{A_3 + B_2}{Q_z Q_x} \\ \frac{Q_x Q_y Q_z}{Q_x Q_y} & \frac{Q_x Q_y}{Q_z Q_y} & \frac{Q_z Q_y}{Q_x Q_y} & \frac{Q_x Q_y}{Q_x Q_y} & \frac{Q_y Q_z}{Q_y Q_z} & \frac{Q_x Q_y Q_z}{Q_x Q_y Q_z} \end{bmatrix} \quad (3.15)$$

where

$$W = W_x W_y W_z$$

$$A_1 = \mu^3 \varepsilon^3 + \mu^2 \varepsilon^2 (W_x^2 - W_y^2 - W_z^2) + W_x^2 W_y^2 W_z^2$$

$$A_2 = \mu^3 \varepsilon^3 + \mu^2 \varepsilon^2 (W_y^2 - W_z^2 - W_x^2) + W_x^2 W_y^2 W_z^2$$

$$A_3 = \mu^3 \varepsilon^3 + \mu^2 \varepsilon^2 (W_z^2 - W_x^2 - W_y^2) + W_x^2 W_y^2 W_z^2$$

$$B_1 = \mu \varepsilon (W_x^2 W_y^2 - W_y^2 W_z^2 - W_z^2 W_x^2)$$

$$B_2 = \mu \varepsilon (W_y^2 W_z^2 - W_z^2 W_x^2 - W_x^2 W_y^2) \quad (3.16)$$

$$B_3 = \mu \varepsilon (W_z^2 W_x^2 - W_x^2 W_y^2 - W_y^2 W_z^2)$$

$$D_1 = W_y (W_x^2 W_z^2 - \mu^2 \varepsilon^2)$$

$$D_2 = W_z (W_y^2 W_x^2 - \mu^2 \varepsilon^2)$$

$$D_3 = W_x (W_z^2 W_y^2 - \mu^2 \varepsilon^2)$$

The eigenvalues of the  $\Lambda$  can be found as:

$$\lambda_1 = \lambda_2 = 1$$

$$\lambda_3 = \lambda_5 = \frac{T + jS}{R} \quad (3.17)$$

$$\lambda_4 = \lambda_6 = \lambda_3^* = \frac{T - jS}{R}$$

with

$$R = (\mu \varepsilon + W_x^2)(\mu \varepsilon + W_y^2)(\mu \varepsilon + W_z^2) \quad (3.18)$$

$$S = \sqrt{4\mu\epsilon(\mu\epsilon W_x^2 + \mu\epsilon W_y^2 + \mu\epsilon W_z^2 + W_x^2 W_y^2 + W_y^2 W_z^2 + W_z^2 W_x^2)(\mu^3 \epsilon^3 + W_x^2 W_y^2 W_z^2)}$$

$$T = \mu^3 \epsilon^3 - \mu\epsilon(\mu\epsilon W_x^2 + \mu\epsilon W_y^2 + \mu\epsilon W_z^2 + W_x^2 W_y^2 + W_y^2 W_z^2 + W_z^2 W_x^2) + W_x^2 W_y^2 W_z^2$$

The first two eigenvalues obviously have magnitude of unity and the magnitudes of the rest eigenvalues need to be checked out.

It can be shown that the following equation is true.

$$R^2 = S^2 + T^2 \quad (3.19)$$

Because  $R$ ,  $S$  and  $T$  in the expressions for  $\lambda_3$ ,  $\lambda_4$ ,  $\lambda_5$  and  $\lambda_6$  are real numbers, the magnitudes of the remaining four eigenvalues are

$$|\lambda_3| = |\lambda_4| = |\lambda_5| = |\lambda_6| = \left| \frac{T + jS}{R} \right| = \left| \frac{T - jS}{R} \right| = \sqrt{\frac{T^2 + S^2}{R^2}} = 1. \quad (3.20)$$

In other words, the four eigenvalues also have magnitudes of unity. Therefore, we conclude that the proposed ADI-FDTD scheme is unconditionally stable regardless of the time step  $\Delta t$ . The CFL stability condition is then removed.

### 3.3 Stability Analysis of the Two-Dimensional ADI-FDTD Formulations

The stability analysis discussed above is now applied to the two-dimensional TE and TM cases which only involve three field components. Because the detailed derivation is similar to that of three-dimensional case, only the results are presented.

For the TE method as described by (2.42) and (2.43),

$$\mathbf{F}^{n+1} = \mathcal{A}_2 \cdot \mathbf{F}^{n+\frac{1}{2}} = \mathcal{A}_2 \mathcal{A}_1 \mathbf{F}^n = \mathcal{A} \mathbf{F}^n \quad (3.21)$$

where  $F^n$  is defined in a different way

$$F^n = \begin{bmatrix} E_x^n \\ E_y^n \\ H_z^n \end{bmatrix} \quad (3.22)$$

and

$$A_1 = \begin{bmatrix} \frac{1}{Q_y} & \frac{W_x W_y}{\mu \epsilon Q_y} & \frac{-jW_y}{\epsilon Q_y} \\ 0 & 1 & \frac{jW_x}{\epsilon} \\ \frac{-jW_y}{\mu Q_y} & \frac{jW_x}{\mu Q_y} & \frac{1}{Q_y} \end{bmatrix} \quad (3.23)$$

$$A_2 = \begin{bmatrix} 1 & 0 & -j\frac{W_y}{\epsilon} \\ \frac{W_x W_y}{\mu \epsilon Q_x} & \frac{1}{Q_x} & \frac{jW_x}{\epsilon Q_x} \\ \frac{-jW_y}{\mu Q_x} & \frac{jW_x}{\mu Q_x} & \frac{1}{Q_x} \end{bmatrix} \quad (3.24)$$

$$A = \begin{bmatrix} \frac{\mu^2 \epsilon^2 + \mu \epsilon (W_x^2 - W_y^2) + W_x^2 W_y^2}{\mu^2 \epsilon^2 Q_x Q_y} & \frac{2W_x W_y}{\mu \epsilon Q_x Q_y} & \frac{-2jW_y}{\epsilon Q_x Q_y} \\ \frac{2W_x W_y}{\mu \epsilon Q_x} & \frac{\mu \epsilon - W_x^2}{\mu \epsilon Q_x} & \frac{2jW_x}{\epsilon Q_x} \\ \frac{-2jW_y}{\mu Q_x Q_y} & \frac{2jW_x}{\mu Q_x Q_y} & \frac{\mu^2 \epsilon^2 - \mu \epsilon (W_x^2 + W_y^2) - W_x^2 W_y^2}{\mu^2 \epsilon^2 Q_x Q_y} \end{bmatrix} \quad (3.25)$$

$$W_\alpha = \frac{\Delta l}{\Delta \alpha} \cdot \sin\left(\frac{k_\alpha \Delta \alpha}{2}\right), \quad \alpha = x, y \quad (3.26)$$

$$Q_\alpha = 1 + \frac{W_\alpha^2}{\mu \epsilon}, \quad \alpha = x, y \quad (3.27)$$



The eigenvalues of the  $\Lambda$  can then be found as:

$$\begin{aligned}\lambda_1 &= 1 \\ \lambda_2 &= \frac{T + jS}{R} \\ \lambda_3 &= \frac{T - jS}{R}\end{aligned}\tag{3.28}$$

with

$$\begin{aligned}R &= (\mu\epsilon + W_x^2)(\mu\epsilon + W_y^2) \\ S &= \sqrt{4\mu^2\epsilon^2(\mu\epsilon W_x^2 + \mu\epsilon W_y^2 + W_x^2 W_y^2)} \\ T &= \mu^2\epsilon^2 - \mu\epsilon W_x^2 - \mu\epsilon W_y^2 - W_x^2 W_y^2\end{aligned}\tag{3.29}$$

The first eigenvalue is one which has magnitude of unity. Noting that  $R$ ,  $S$  and  $T$  are the real numbers, we have

$$|\lambda_2| = |\lambda_3| = \left| \frac{T + jS}{R} \right| = \left| \frac{T - jS}{R} \right| = \sqrt{\frac{T^2 + S^2}{R^2}} = 1\tag{3.30}$$

Therefore, the magnitudes of all three eigenvalues are unity. As a result, the proposed ADI-FDTD scheme is unconditionally stable regardless of the time step  $\Delta t$  in two-dimensional TE case.

For the TM wave, the definition of  $F^n$  is different because three other different field components  $E_z$ ,  $H_x$  and  $H_y$  are considered,

$$\mathbf{F}^n = \begin{bmatrix} E_z^n \\ H_x^n \\ H_y^n \end{bmatrix}. \quad (3.31)$$

$\Lambda_1$ ,  $\Lambda_2$  and  $\Lambda$  can be found as:

$$\Lambda_1 = \begin{bmatrix} \frac{1}{Q_x} & \frac{jW_y}{\epsilon Q_x} & -\frac{jW_x}{\epsilon Q_x} \\ \frac{jW_y}{\mu} & 1 & \frac{jW_x}{\epsilon Q_x} \\ -\frac{jW_x}{\mu Q_x} & \frac{W_x W_y}{\mu \epsilon Q_x} & \frac{1}{Q_x} \end{bmatrix} \quad (3.32)$$

$$\Lambda_2 = \begin{bmatrix} \frac{1}{Q_y} & \frac{jW_y}{\epsilon Q_y} & -\frac{jW_x}{\epsilon Q_y} \\ \frac{jW_y}{\mu Q_y} & 1 & \frac{W_x W_y}{\mu \epsilon Q_y} \\ -\frac{jW_x}{\mu} & 0 & 1 \end{bmatrix} \quad (3.33)$$

$$\Lambda = \begin{bmatrix} \frac{\mu^2 \epsilon^2 - \mu \epsilon (W_x^2 + W_y^2) - W_x^2 W_y^2}{\mu^2 \epsilon^2 Q_x Q_y} & \frac{2jW_y}{\epsilon Q_x Q_y} & -\frac{2jW_x}{\epsilon Q_x Q_y} \\ \frac{2jW_y}{\mu Q_x Q_y} & \frac{\mu^2 \epsilon^2 + \mu \epsilon (W_x^2 - W_y^2) + W_x^2 W_y^2}{\mu^2 \epsilon^2 Q_x Q_y} & \frac{2W_x W_y}{\mu \epsilon Q_x Q_y} \\ -\frac{2jW_x}{\mu Q_x} & \frac{2W_x W_y}{\mu \epsilon Q_x} & \frac{\mu \epsilon - W_x^2}{\mu \epsilon Q_x} \end{bmatrix} \quad (3.34)$$

where the definition of  $W_\alpha$  and  $Q_\alpha$  are the same as by equation (3.26) and (3.27), respectively.

Again, The three eigenvalues can be obtained as

$$\lambda_1 = 1$$

$$\lambda_2 = \frac{T + jS}{R} \quad (3.35)$$

$$\lambda_3 = \frac{T - jS}{R}$$

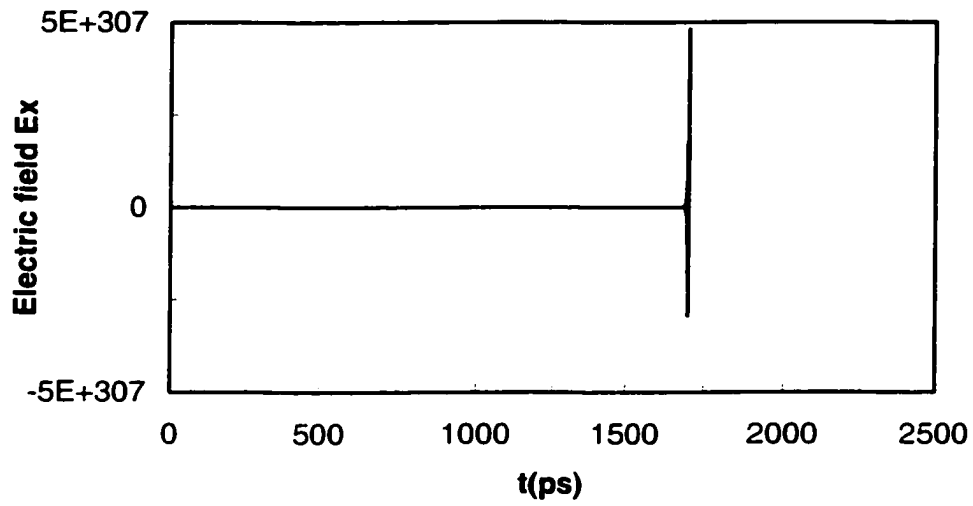
$R$ ,  $S$  and  $T$  are the same as (3.29). Therefore three eigenvalues have unity magnitudes and the scheme is unconditional stable as well.

### **3.4 Numerical experiment and Result**

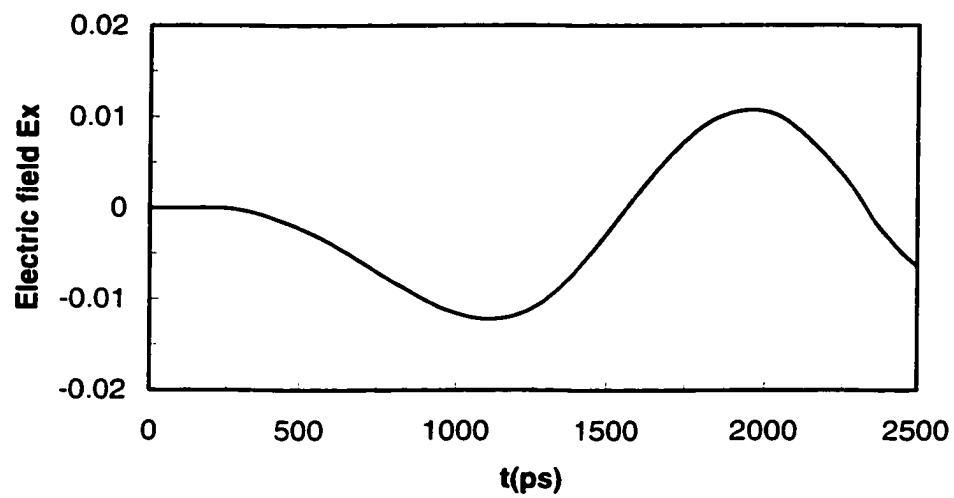
The ADI-FDTD is theoretically proven unconditionally stable in both three-dimensional and two-dimensional case. The CFL condition inherent in the conventional FDTD is completely removed. Numerical verification is carried out to confirm the result. In following sections, the numerical validations of unconditional stability of ADI-FDTD are presented. A study on time step selection without CFL condition is also made with respect to the numerical errors. The preliminary error analysis shows that the time step in ADI-FDTD is now limited by modeling accuracy and the Nyquist sampling rate.

#### **3.4.1 Numerical Verification of the Stability**

Simulations were run for both homogeneous and inhomogeneous cavities again with both the conventional FDTD and the ADI-FDTD having a time step that exceeds the limit defined by the CFL condition (2.7).

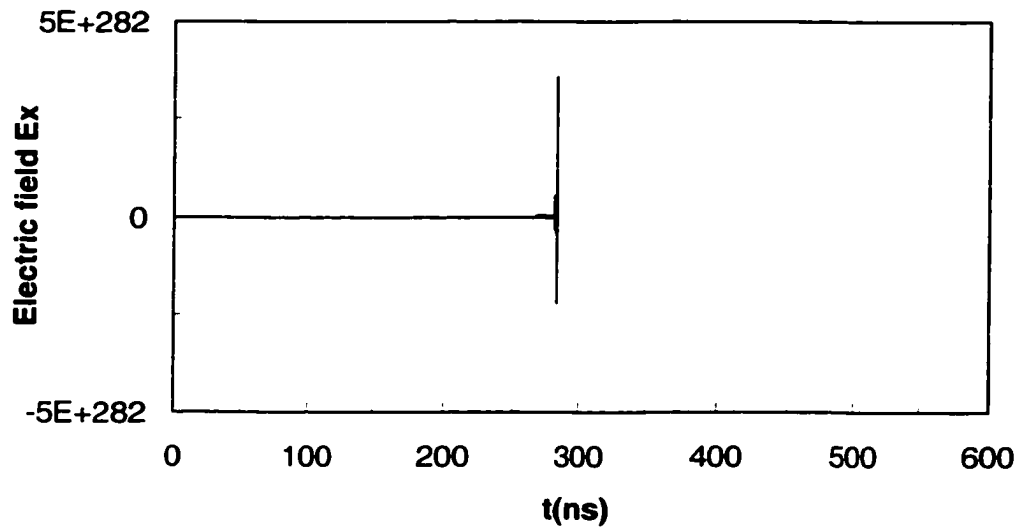


(a)

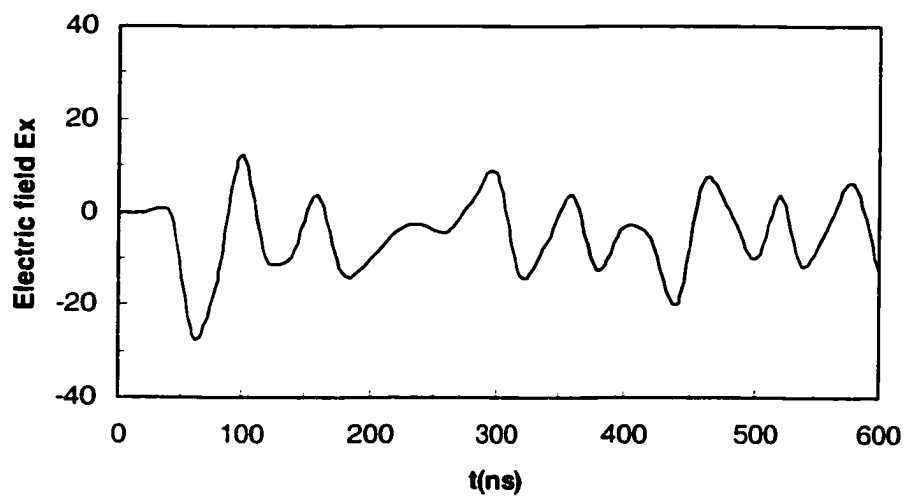


(b)

Figure 3.1 Time-domain electric fields with the conventional FDTD and the proposed FDTD. (a) The conventional FDTD solutions that becomes unstable with  $\Delta t_j = 1.2$  ps; (b) The proposed FDTD solution with  $\Delta t_i = 120$  ps .



(a)



(b)

Figure 3.2 Time-domain electric fields at the center of the cavity recorded with the conventional FDTD and the proposed ADI-FDTD. The conventional FDTD solutions that become unstable with  $\Delta t_j = 2 \times 10^{-10} s$ ; The proposed ADI-FDTD solution with  $\Delta t_j = 200 \times 10^{-10} s$ .

Figures 3.1 and 3.2 show the electric field recorded at the center of the both cavities. In the homogeneous case,  $\Delta t_{FDTD} = 1.2 \times 10^{-12} s$  (larger than the CFL limit  $\Delta t_{FDTDMAX} = \frac{\Delta l}{c\sqrt{3}} = 1.155 \times 10^{-12} s$ ) was chosen with the conventional FDTD, while a time step 100 times larger,  $\Delta t_i = 1.2 \times 10^{-10} s$ , was used with the ADI-FDTD scheme. In the inhomogeneous case, time step  $\Delta t_{FDTD} = 2 \times 10^{-10} s$  and  $\Delta t_i = 2 \times 10^{-8} s$ , both larger than the CFL limit  $\Delta t_{FDTDMAX} = \frac{\Delta l}{c\sqrt{3}} = 1.92 \times 10^{-10} s$ , were used in for the conventional FDTD and ADI-FDTD, respectively. It can be seen, in both cases, the conventional FDTD quickly becomes unstable as shown in Figure 3.1a and Figure 3.2a, while the proposed FDTD remains with the stable solution as shown in Figure 3.1b and Figure 3.2b. The simulation with a much longer period was also done with the proposed scheme. No instability was observed.

### 3.4.2 Numerical Accuracy Versus Time Step

Since the proposed ADI-FDTD has been proven to be always stable, the selection of the time step is then no longer restricted by stability. As a result, it is interesting and meaningful to investigate how the large time step will affect accuracy. The same two cavities are used again for the numerical experiments.

**Table 3.1: The Proposed ADI-FDTD simulation results with different  $\Delta t$**

Analytical Result (MHz)	The proposed ADI-FDTD scheme					
	$\Delta t_{i1} = 4\Delta t_{FDTD}$		$\Delta t_{i2} = 6\Delta t_{FDTD}$		$\Delta t_{i3} = 8\Delta t_{FDTD}$	
	Result (MHz)	Relative error	Result (MHz)	Relative error	Result (MHz)	Relative error
18.627	18.587	0.21%	18.556	0.38%	18.511	0.62%

For the comparison purpose, both the conventional FDTD and proposed ADI-FDTD are used to simulate the cavity. This time, a single value of the time step

$\Delta t_{FDTD} = 1.5 \times 10^{-10} s$  is chosen with the conventional FDTD, while various values of time step  $\Delta t_i$  are used with the ADI-FDTD to check for the accuracy. Table 3.1 presents the simulation results for the dominant mode in the cavity. As can be seen, the relative errors of the ADI-FDTD increase with the time step. These errors are completely due to modeling accuracy of the numerical algorithm, such as the numerical dispersion. The gain for the increased errors is, however, the reduction in the number of the iterations and therefore the shortening of the CPU time. In the experiments, for an error of 0.38%, the CPU time with the proposed ADI-FDTD is about half of that with the conventional FDTD. For an error of 0.62%, the CPU time is cut to one third of the conventional FDTD time. Note that the shortening of the CPU time is not linearly proportional to the increase in the size of the time step or the reduction in the number of the iterations. The reason is that the CPU time required for each time-step computation with the proposed FDTD is more than that with the conventional FDTD since more components are involved in the computations as shown in equation (2.27).

Figure 3.3 illustrates the relative errors for the dominant mode of the cavity computed using the conventional FDTD and the proposed FDTD with variable time steps. For clarity, relative time-step,  $\Delta t / \Delta t_{FDTDMAX}$ , is used. As can be seen, at low  $\Delta t / \Delta t_{FDTDMAX}$ , the errors of both the conventional FDTD and the ADI-FDTD are almost the same. However, after  $\Delta t / \Delta t_{FDTDMAX} = 1.0$ , the conventional FDTD solutions become diverge (unstable) while the ADI-FDTD continues to produce stable results with increasing errors. Such errors may or may not be acceptable depending on the applications and users' specifications.

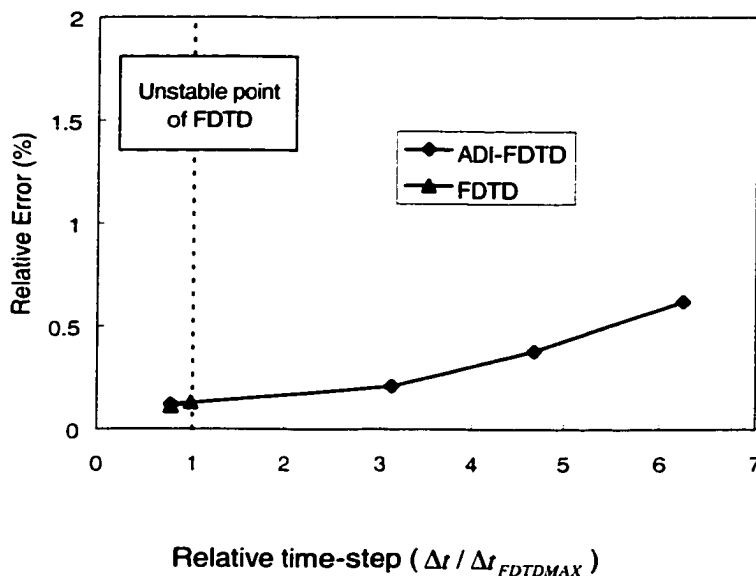


Figure 3.3 Relative errors of the conventional FDTD and the proposed FDTD as the function of relative time step  $\Delta t / \Delta t_{FDTD\_MAX}$ . Dash line represents the unstable point of the conventional FDTD scheme.

### 3.5 Discussion and Conclusion

In this chapter, the unconditional stability of proposed ADI-FDTD has been proven analytically and demonstrated numerically. Numerical results also shows that the proposed scheme is indeed stable even when time step is a hundred times of the CFL limit of the conventional FDTD. It can be expected that because of the removal of the CFL constraint on time step, various efficient modeling techniques, such as multigridging scheme, can be implemented in a way easier than before [68].

With the CFL limit removed in ADI-FDTD, the time step of ADI-FDTD is no longer restricted by the numerical stability but by the modeling accuracy of the algorithm and the Nyquist sampling limit. Therefore, study of the modeling accuracy of ADI-FDTD becomes significant and will lead a criteria in terms of proper and efficient



application of ADI-FDTD. One of the major factors that affect modeling accuracy is the numerical dispersion which is investigated extensively in next chapter.

## Chapter 4 Numerical Dispersion Analysis

### 4.1 Introduction

As pointed out in chapter 2, the conventional FDTD method is an *explicit* marching-in-time technique and its time-step is limited by the well-known CFL stability condition. Consequently, the FDTD may require a large number of iterations in certain applications especially when small time step is required, e.g. structures with fine geometry such as small via [46]. As shown in chapter 3, in the proposed ADI-FDTD scheme the CFL stability condition is removed. The time step is not limited by the CFL condition anymore but by the accuracy of modeling results and the Nyquist sampling limit. Hence, the number of iterations can be reduced significantly compared to the conventional FDTD in simulating the same structure. It will be shown that ADI-FDTD has advantage in this case.

Like any numerical method, numerical dispersion is inherent in FDTD scheme. It is the result of the spatial discretization where the phase velocity of numerical modes in a FDTD grid is forced to vary with grid size, time step, wave propagation direction, and modal wavelength. This numerical dispersion can lead to nonphysical results such as pulse distortion and artificial anisotropics. To estimate the errors induced by numerical dispersion, numerical dispersion relation of any discrete lattice need to be studied. For the conventional FDTD scheme, numerical dispersion has been investigated extensively [125]-[128].

In this chapter, a thorough study of the numerical dispersion characteristics of the proposed unconditionally stable ADI-FDTD will be presented. In a similar manner of stability analysis in Chapter 3, Fourier numerical wave modes are assumed to propagate at arbitrary angles in the space lattice. The numerical dispersion of ADI-FDTD is then derived and the effect of the time and spatial steps on the numerical dispersion are investigated and compared with the conventional Yee's FDTD.

In addition, dispersion analysis was made for structures that contain components of fine geometry such as thin circuit board layers and vias. For these structures, very fine local mesh is normally required in order to obtain sufficient modeling resolution. The dispersion analysis shows that under these circumstances, the time step of the unconditionally stable FDTD can be chosen much larger than that of the conventional Yee's FDTD scheme without sacrificing the accuracy. As a result, the simulation time can be reduced significantly.

#### 4.2 Numerical Dispersion of Three-dimensional ADI-FDTD Algorithm

To derive the numerical dispersion of the FDTD method, the Fourier transform of the FDTD formulations in the *spatial* domain along the  $x$ ,  $y$ , and  $z$  directions is taken and the propagation waves are assumed to be monochromatic. After some manipulations, a relation for the field components in the mixed *temporal* and *spatial* domains can be obtained and the dispersion is determined. The details of the procedure can be found in reference [46].

The same procedure is used to derive the numerical dispersion relation of ADI-FDTD. Detailed derivation is given as follows.

The *spatial spectral domain* representation of the proposed ADI-FDTD has been obtained in Chapter 3 for the stability analysis as shown in equation (3.14). As derived, the relationship between the field components at the  $(n+1)$ -th time step and the  $n$ -th time step in the *spatial spectral domain* is:

$$\mathbf{F}^{n+1} = \Lambda \mathbf{F}^n \quad (4.1)$$

Note that  $\Lambda$  is a 6 by 6 matrix that contains  $k_x \Delta x$ ,  $k_y \Delta y$ , and  $k_z \Delta z$ .  $k_x$ ,  $k_y$ , and  $k_z$  are the spatial frequencies along the  $x$ ,  $y$  and  $z$  directions, respectively, or the  $x$ ,  $y$  and  $z$  components of the numerical wave number vector.  $\Delta x$ ,  $\Delta y$  and  $\Delta z$  are the

spatial discretization steps along the  $x$ ,  $y$ , and  $z$  directions, respectively.  $F^n$  represents a vector that contains all the six field components in the spatial spectral domain:

$$F^n = \begin{bmatrix} E_x^n \\ E_y^n \\ E_z^n \\ H_x^n \\ H_y^n \\ H_z^n \end{bmatrix} \quad (4.2)$$

Now assume the electromagnetic fields to be monochromatic traveling wave:

$$\begin{aligned} E_\alpha^n &= E_\alpha e^{j\omega n \Delta t} \\ H_\alpha^n &= H_\alpha e^{j\omega n \Delta t} \end{aligned} \quad \alpha = x, y, z \quad (4.3)$$

where  $\omega$  is the angular frequency and  $\Delta t$  is the time step.

With equation (4.3), the column vector  $F$  which has six field components can now be written as

$$F^n = F e^{j\omega \Delta t n} \quad (4.4)$$

where

$$F = \begin{bmatrix} E_x \\ E_y \\ E_z \\ H_x \\ H_y \\ H_z \end{bmatrix}$$

After some linear algebra manipulation, equation (4.1) becomes:

$$(e^{j\omega\Delta t} \mathbf{I} - \mathbf{A})\mathbf{F} = 0 \quad (4.5)$$

Here  $\mathbf{I}$  is a 6 by 6 identity matrix.

Since solutions of equation (4.5) should be nontrivial, the determinant of coefficient matrix should be zero. That is,

$$\det(e^{j\omega\Delta t} \mathbf{I} - \mathbf{A}) = 0. \quad (4.6)$$

It describes the dispersion relation of the ADI-FDTD method.

The dispersion relation (4.6) can be further simplified and represented with its eigenvalues. The six eigenvalues the of  $\mathbf{A}$  are found as:

$$\begin{aligned} \lambda_1 &= \lambda_2 = 1 \\ \lambda_3 &= \lambda_4 = \frac{T + jS}{R} \\ \lambda_5 &= \lambda_6 = \lambda_3^* = \frac{T - jS}{R} \end{aligned} \quad (4.7)$$

where

$$\begin{aligned} R &= (\mu\epsilon + W_x^2)(\mu\epsilon + W_y^2)(\mu\epsilon + W_z^2) \\ S &= \sqrt{4\mu\epsilon(\mu\epsilon W_x^2 + \mu\epsilon W_y^2 + \mu\epsilon W_z^2 + W_x^2 W_y^2 + W_y^2 W_z^2 + W_z^2 W_x^2)(\mu^3 \epsilon^3 + W_x^2 W_y^2 W_z^2)} \\ T &= \mu^3 \epsilon^3 - \mu\epsilon(\mu\epsilon W_x^2 + \mu\epsilon W_y^2 + \mu\epsilon W_z^2 + W_x^2 W_y^2 + W_y^2 W_z^2 + W_z^2 W_x^2) + W_x^2 W_y^2 W_z^2 \end{aligned} \quad (4.8)$$

Therefore, (4.6) can be explicitly written as:

$$(e^{j\omega\Delta t} - 1)^2 (e^{j\omega\Delta t} - \lambda_3)^2 (e^{j\omega\Delta t} - \lambda_3^*)^2 = 0 \quad (4.9)$$

or,

$$(e^{j\omega\Delta t} - 1)^2 [e^{j2\omega\Delta t} - (\lambda_3 + \lambda_3^*)e^{j\omega\Delta t} + 1]^2 = 0 \quad (4.10)$$

It leads to:

$$\omega = 0 \quad (4.11)$$

and

$$\begin{aligned} \sin^2(\omega\Delta t) &= \frac{S^2}{R^2} \\ &= \frac{4\mu\epsilon(\mu\epsilon W_x^2 + \mu\epsilon W_y^2 + \mu\epsilon W_z^2 + W_x^2 W_y^2 + W_y^2 W_z^2 + W_z^2 W_x^2)(\mu^3 \epsilon^3 + W_x^2 W_y^2 W_z^2)}{(\mu\epsilon + W_x^2)^2 (\mu\epsilon + W_y^2)^2 (\mu\epsilon + W_z^2)^2} \end{aligned} \quad (4.12)$$

The first solution  $\omega = 0$  is the stationary solution that corresponds to the electrostatic and magnetostatic solutions. It is a representation of the non-propagating solutions in the unconditionally stable ADI-FDTD mesh. The second solution (4.12), however, corresponds to the propagating modes of the ADI-FDTD mesh. It reveals the dispersion relationship among the numerical wave numbers in the  $x$ ,  $y$  and  $z$  directions, the wave angular frequency, the grid size and time step.

In order to evaluate the errors caused by the numerical dispersion of the ADI-FDTD, reference solutions are needed for comparisons. In our case, two reference solutions are used: (A) the analytical dispersion relationship in the continuous medium that the ADI-FDTD is simulating and (B) the dispersion solutions of the conventional Yee's FDTD scheme that is constrained by the CFL stability conditions.

The analytical dispersion relation for a plane wave in the continuous medium is

$$\omega^2 \mu \varepsilon = k_x^2 + k_y^2 + k_z^2 \quad (4.13)$$

while the numerical dispersion of the Yee's FDTD is [47]

$$\left( \frac{1}{c\Delta t} \right)^2 \sin^2\left(\frac{1}{2}\omega\Delta t\right) = \frac{1}{\Delta x^2} \sin^2\left(\frac{1}{2}k_x\Delta x\right) + \frac{1}{\Delta y^2} \sin^2\left(\frac{1}{2}k_y\Delta y\right) + \frac{1}{\Delta z^2} \sin^2\left(\frac{1}{2}k_z\Delta z\right) \quad (4.14)$$

### 4.3 Convergence of ADI-FDTD Solutions

For an ADI-FDTD solution to be valid approximations to the exact solutions of Maxwell's equations, the numerical dispersion of the proposed ADI-FDTD scheme has to converge to the analytical dispersion relation. The numerical dispersion of ADI-FDTD as shown in equation (4.12) looks much more complicated and bears little resemblance to the ideal analytical dispersion relation as shown in equation (4.13). However, it can be proven that equation (4.12) will converge to equation (4.13) as  $\Delta x, \Delta y, \Delta z$  and  $\Delta t$  all go to zero.

The numerical dispersion relation of ADI-FDTD (4.12) can be reorganized as

$$\begin{aligned} & \frac{\sin^2(\omega\Delta t)}{\Delta t^2} \mu \varepsilon \\ &= \frac{4\mu^2 \varepsilon^2 (\mu \varepsilon V_x^2 + \mu \varepsilon V_y^2 + \mu \varepsilon V_z^2 + \Delta t^2 (V_x^2 V_y^2 + V_y^2 V_z^2 + V_z^2 V_x^2)) (\mu^3 \varepsilon^3 + \Delta t^6 V_x^2 V_y^2 V_z^2)}{(\mu \varepsilon + \Delta t^2 V_x^2)^2 (\mu \varepsilon + \Delta t^2 V_y^2)^2 (\mu \varepsilon + \Delta t^2 V_z^2)^2} \end{aligned} \quad (4.15)$$

where

$$V_\alpha = \frac{1}{\Delta \alpha} \cdot \sin\left(\frac{k_\alpha \Delta \alpha}{2}\right), \quad \alpha = x, y, z. \quad (4.16)$$

Then, by taking the limit of both left and right hand sides for  $\Delta x \rightarrow 0$ ,  $\Delta y \rightarrow 0$ ,  $\Delta z \rightarrow 0$ , and  $\Delta t \rightarrow 0$ :

$$\lim_{\Delta x, \Delta y, \Delta z, \Delta t \rightarrow 0} \frac{\sin^2(\omega \Delta t)}{\Delta t^2} \mu \epsilon = \omega^2 \mu \epsilon \quad (4.17a)$$

$$\begin{aligned} & \lim_{\Delta x, \Delta y, \Delta z, \Delta t \rightarrow 0} \frac{4\mu^2 \epsilon^2 (\mu \epsilon V_x^2 + \mu \epsilon V_y^2 + \mu \epsilon V_z^2 + \Delta t^2 (V_x^2 V_y^2 + V_y^2 V_z^2 + V_z^2 V_x^2)) (\mu^3 \epsilon^3 + \Delta t^6 V_x^2 V_y^2 V_z^2)}{(\mu \epsilon + \Delta t^2 V_x^2)^2 (\mu \epsilon + \Delta t^2 V_y^2)^2 (\mu \epsilon + \Delta t^2 V_z^2)^2} \\ & = k_x^2 + k_y^2 + k_z^2 \end{aligned} \quad (4.17b)$$

The analytical dispersion is resulted. In other words,

$$\lim_{\Delta x, \Delta y, \Delta z, \Delta t \rightarrow 0} (\text{equation(4.12)}) = (\omega^2 \mu \epsilon = k_x^2 + k_y^2 + k_z^2). \quad (4.18)$$

Thus, the validity of the ADI-FDTD approximations for the solution of Maxwell's equation is shown.

In conclusion, similar to that of the conventional FDTD, the solutions of the ADI-FDTD will converge to the analytical solutions as grid and time steps go to zero. That is, the unconditionally stable ADI-FDTD will present the approximate solutions which can be close enough to the analytical solutions if small spatial and time steps are used for the simulation. Nevertheless, compared to the numerical dispersion described by equation (4.14) for the conventional FDTD, the numerical dispersion (4.12) of ADI-FDTD exhibits a more complicated relation between time step and cell size. It needs to be studied thoroughly.

#### 4.4 Numerical Dispersion of Two-dimensional TE and TM Case

For the two-dimensional ADI-FDTD, similar numerical dispersion relations can be found. As derived in the previous section, equation (3.1) is a general form of dispersion of the ADI-FDTD time-marching scheme in the spatial spectral domain

$$\mathbf{F}^{n+1} = \mathbf{A} \mathbf{F}^n. \quad (4.19)$$



By assuming the numerical modes to be monochromatic, the dispersion relation of TE ADI-FDTD can be expressed in terms of eigenvalues of  $\mathcal{A}$ ,

$$(e^{j\omega\Delta t} - \lambda_1)(e^{j\omega\Delta t} - \lambda_2)(e^{j\omega\Delta t} - \lambda_3) = 0 \quad (4.20)$$

where  $\lambda_1$ ,  $\lambda_2$  and  $\lambda_3$  can be found in (3.28).

Similarly, we have two solutions,

$$\omega = 0 \quad (4.21)$$

and

$$\sin^2(\omega\Delta t) = \frac{S^2}{R^2} = \frac{4\mu^2\epsilon^2(\mu\epsilon W_x^2 + \mu\epsilon W_y^2 + W_x^2 W_y^2)}{(\mu\epsilon + W_x^2)^2 (\mu\epsilon + W_y^2)^2} \quad (4.22)$$

As discussed in the previous section, the first solution (4.21) represents the non-propagating solution in the unconditionally stable ADI-FDTD mesh, and the second solution (4.22) corresponds to the propagating solution.

The eigenvalues for  $\mathcal{A}$  in the TM case are found to be the same as in the TE case. Therefore, the numerical dispersion for the TM modes has the identical expression, which is

$$\sin^2(\omega\Delta t) = \frac{S^2}{R^2} = \frac{4\mu^2\epsilon^2(\mu\epsilon W_x^2 + \mu\epsilon W_y^2 + W_x^2 W_y^2)}{(\mu\epsilon + W_x^2)^2 (\mu\epsilon + W_y^2)^2}. \quad (4.23)$$

Actually, numerical dispersion for the TE and the TM cases can also be obtained by setting  $\Delta z$  to 0 in the dispersion relation for the three-dimensional case shown in equation (4.12).

## 4.5 Dispersion Characteristics of the ADI-FDTD scheme - Numerical Result

Several aspects of the numerical dispersion of the ADI-FDTD scheme are studied. They include 1) the effects of the propagation direction on the dispersion, 2) the effects of the larger time step on the dispersion, 3) three-dimensional view of the numerical dispersion, and 4) dispersion on the  $k_x - k_y$  plane.

### 4.5.1 *Effects of the propagation direction on the dispersion*

To investigate the effects of wave propagation direction on the dispersion characteristics, one can assume that wave propagates at angle  $\phi$  and  $\theta$  in the spherical coordinate. The  $x$ -,  $y$ - and  $z$ - components of the wavevector then have the following form,

$$k_x = k \sin \theta \sin \phi$$

$$k_y = k \sin \theta \cos \phi \tag{4.24}$$

$$k_z = k \cos \theta$$

By substituting equation (4.24) into the dispersion relation (4.12), numerical wavenumber  $k$  can be found numerically using the Newton's method for given  $\phi$  and  $\theta$ . The process can be more convenient when the grid size is normalized to the wavelength. For simplicity, uniform cells are considered here ( $\Delta x = \Delta y = \Delta z = \delta$ ).

Figure 4.1 shows the variations of the numerical phase velocity with the wave propagation angles for the unconditionally stable ADI-FDTD, while Figure 4.2 for the conventional FDTD of the Yee's scheme.

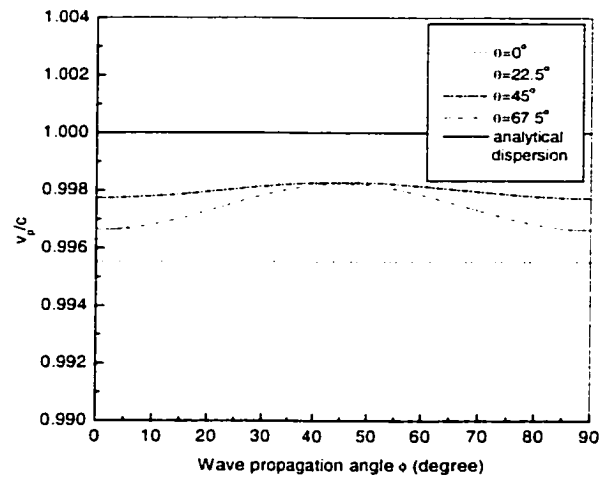


Figure 4.1 Numerical wave phase velocity versus wave propagation angle in the ADI-FDTD grid with  $\delta = \lambda/20$  and  $\Delta t = \delta/c/5$ .

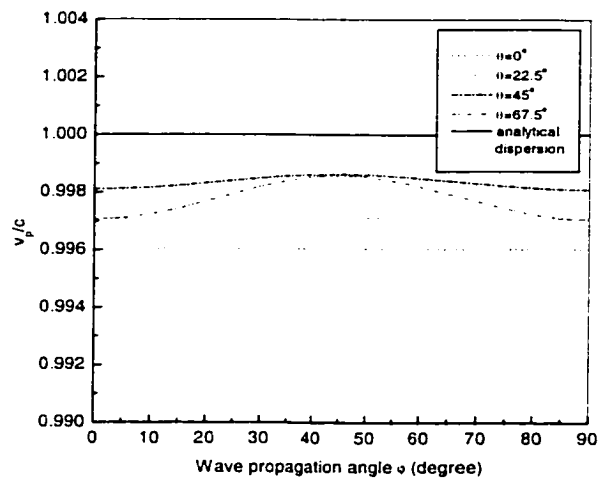


Figure 4.2 Numerical wave phase velocity with wave propagation angle in the grid for the conventional FDTD grid with at  $\delta = \lambda/20$  and  $\Delta t = \delta/c/5$ .

In both cases, a uniform grid resolution  $\delta = \lambda/20$  and a time step  $\Delta t = \delta/c/5$  was taken. From Figure 4.1, it is seen that the numerical phase velocity is maximum when wave propagates at  $45^\circ$  (with least differences or errors from the analytical dispersion relation) and minimum when wave propagates at  $0^\circ$  and  $90^\circ$  (with largest differences or errors). This represents a numerical anisotropy that is inherent in the ADI-FDTD algorithm (like any other FDTD schemes). In comparisons between Figure 4.1 and Figure 4.2, one can see that the dispersion errors of the ADI-FDTD and the conventional FDTD are both small. The maximum numerical dispersion error is 0.42% for the ADI-FDTD scheme in comparison with 0.40% for the conventional FDTD. It suggests that the dispersion characteristic of the ADI-FDTD and the conventional FDTD is very comparable with a small time step. This is expected since the ADI-FDTD differs from FDTD in its application of the implicit finite-difference. When the time step and cell size go to zero, the differences between the implicit finite difference in the ADI-FDTD technique and the explicit finite-difference in the conventional FDTD tends to zero. Therefore, dispersion behaviors of the two methods will be similar when small cell sizes and time steps are used. In general, below the maximum time step defined by the CFL condition, both the ADI-FDTD and the conventional FDTD present the same level of the accuracy. This has been numerically shown in [131].

#### **4.5.2            *Effects of the large time step on the numerical dispersion***

Since the time step in the ADI-FDTD scheme is no longer restricted by the CFL condition, it is then important and meaningful to see how large a time step can impact numerical dispersion. In our studies, three different time steps are selected for the dispersion analysis:  $\Delta t = \delta/c/\sqrt{3}$  (CFL limit),  $\Delta t = \delta/c(\sqrt{3})$  times of the CFL limit), and  $\Delta t = 1.5\delta/c$  (2.6 times of the CFL limit). For each time step, the spatial resolution  $\delta = \lambda/20$  was maintained.

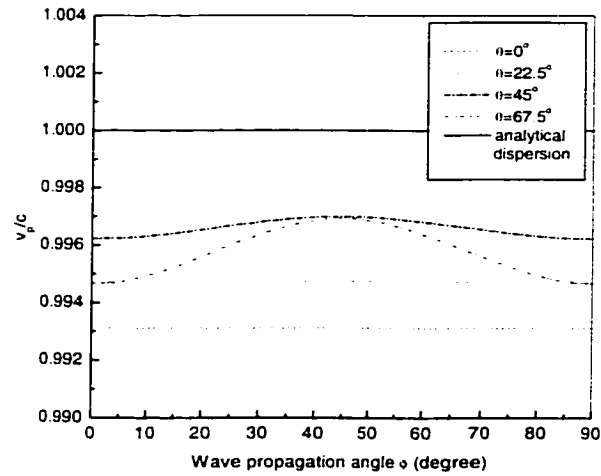


Figure 4.3 Numerical wave phase velocity versus wave propagation angle in the ADI-FDTD grid with at  $\delta = \lambda/20$  and  $\Delta t = \delta/c/\sqrt{3}$  (CFL limit)

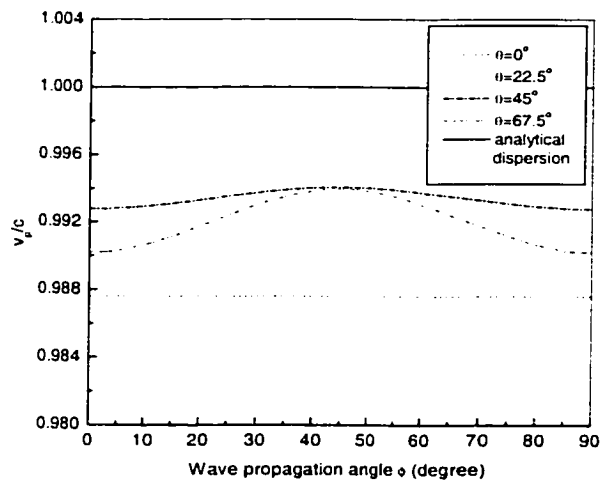


Figure 4.4 Numerical wave phase velocity versus wave propagation angle in the ADI-FDTD grid with  $\delta = \lambda/20$  and  $\Delta t = \delta/c$  (1.73 times of CFL limit).

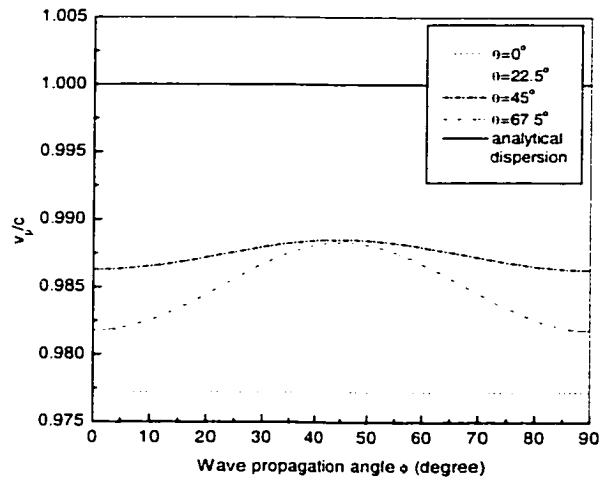


Figure 4.5 Numerical wave phase velocity with wave propagation angle in the unconditionally stable FDTD grid with at  $\delta = \lambda / 20$  and  $\Delta t = 1.5\delta / c$  (2.6 times of CFL limit).

Figures 4.3-4.5 illustrate how the time step affects the numerical phase velocity. It is obvious that the curves in different figures are basically in the same shape. However, the difference between numerical velocity and the analytical dispersion relation (as determined by (4.13)) increases when the time step is increased. With the time step equal to the CFL limit, the maximum velocity error is about 0.6%, while with the time step of 2.6 times of the CFL limit, the error is 2.2%. This is an indication that the time step can not be too large. Its selection is dependent on the accuracy that can be tolerated by the user's error specifications. In other words, a tradeoff should be made between simulation accuracy and speed when one chooses the time step. Our numerical experience suggests that the time step could be made four times larger than that of the conventional FDTD in most cases with acceptable accuracy. Note that although the time step could be 4 times larger, the saving in the overall CPU time is only about 1.6 times as mentioned in chapter 3.

### 4.5.3 *The three dimensional view of the numerical dispersion*

So far, the numerical dispersion analysis is limited to a two-dimensional perspective. The analytical dispersion relation described by equation (4.13), nevertheless, represents a sphere if plotted in the three-dimension coordinate system of the wave-number vector  $(k_x, k_y, k_z)$ . If the solutions of the ADI-FDTD are the approximation of the analytical solutions, its numerical dispersion should also be an approximation to the sphere. The degree of the approximation will be very much dependent on the time step and spatial steps. The surface determined by a numerical dispersion will have distortions from the perfect sphere (i.e. the analytical dispersion relation). Consequently, it will be very useful to examine a numerical dispersion graphically in the three dimensional system  $(k_x, k_y, k_z)$  with different time steps. It will give us an overall view of the numerical dispersion behaviors of the ADI-FDTD method.

Figures 4.6 and Figure 4.7 show the different dispersion characteristics of the unconditionally stable ADI-FDTD scheme with the different time steps. The spatial step  $\delta = \lambda/20$  is fixed. Figure 4.6 shows the result with time step  $\Delta t = \delta/c/\sqrt{3}$ . The surface in Figure 4.6 forms a closed 3D surface that is very close to a sphere. It means that the dispersion characteristic is quite close to that of the analytical one. Figure 4.7 shows the dispersion surface when the time step is increased to  $\Delta t = 2\delta/c$ . Noticeable distortions from the sphere can be easily seen in Figure 4.7. It indicates that the degree of the ADI-FDTD approximation to the analytical solutions is worse.

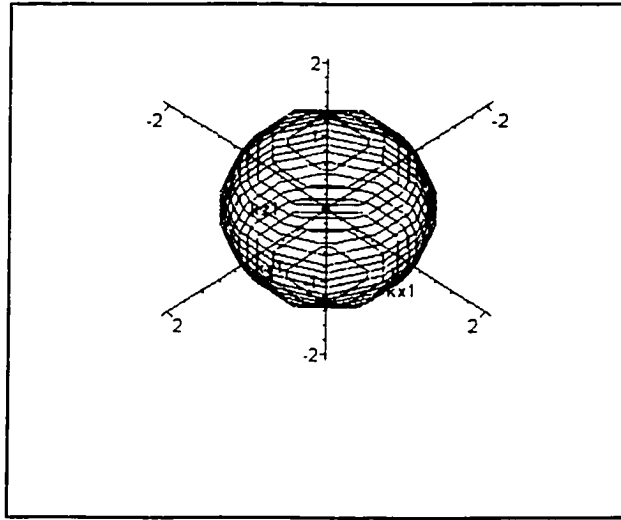


Figure 4.6 Dispersion characteristics with grid size  $\delta = \lambda/20$  and  $\Delta t = \delta/c$  (1.73 times of CFL limit).



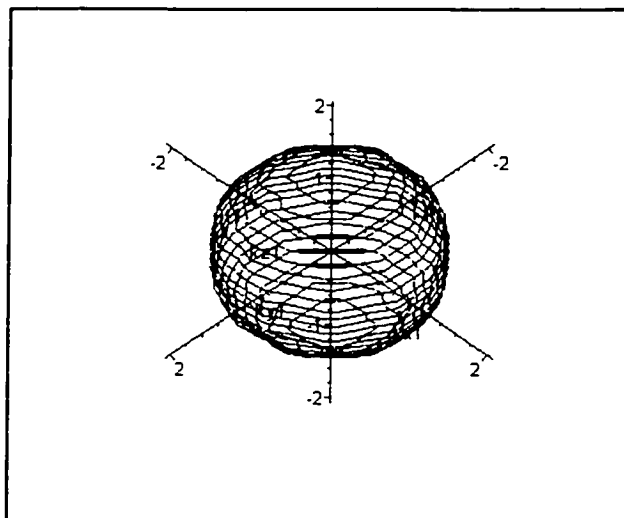


Figure 4.7 Dispersion characteristics with grid size  $\delta = \lambda / 20$  and  $\Delta t = 2\delta / c$  (3.46 times of CFL limit).

#### 4.5.4 Dispersion on the $k_x$ - $k_y$ plane

In order to view dispersion characteristics more closely and precisely, the dispersion is shown on the cut of the  $k_x$ - $k_y$  plane. In this case, only  $k_x$  and  $k_y$  need to be considered ( $\theta = 90^\circ, k_z = k \cos\theta = 0$ ). Equation (4.12) is then simplified to

$$\sin^2(\omega\Delta t) = \frac{4\mu^2\varepsilon^2 \left( \mu\varepsilon \left( \frac{\Delta t}{\delta} \cos(k_x\delta) \right)^2 + \mu\varepsilon \left( \frac{\Delta t}{\delta} \sin(k_y\delta) \right)^2 + \left( \frac{\Delta t}{\delta} \cos(k_x\delta) \right)^2 \left( \frac{\Delta t}{\delta} \sin(k_y\delta) \right)^2 \right)}{\left( \mu\varepsilon + \left( \frac{\Delta t}{\delta} \cos(k_x\delta) \right)^2 \right)^2 \left( \mu\varepsilon + \left( \frac{\Delta t}{\delta} \sin(k_y\delta) \right)^2 \right)^2} \quad (4.22)$$

Here, we assume uniform cells ( $\Delta x = \Delta y = \Delta z = \delta$ ) for simplicity.

Figures 4.8-4.12 shows the numerical dispersion characteristics for a plane wave propagating in the x-y plane with different time steps.

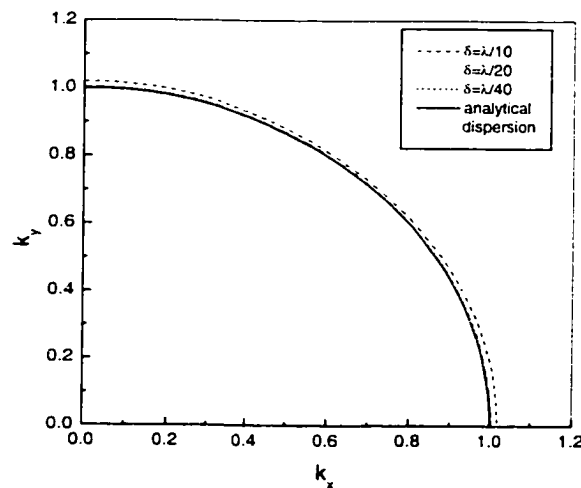


Figure 4.8 Dispersion characteristics of different mesh sizes at time step  $\Delta t = \delta/c/5$ .

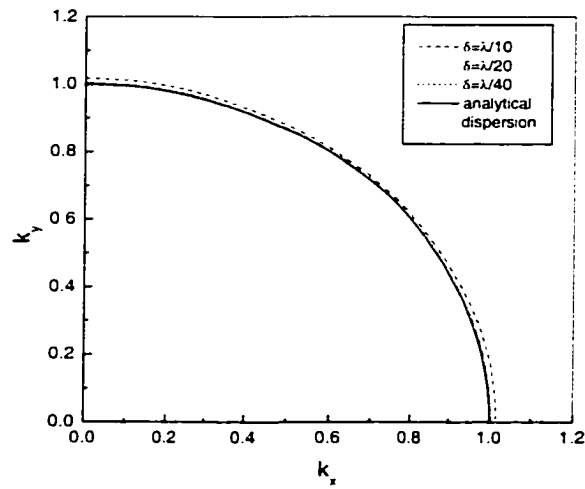


Figure 4.9 Dispersion characteristics of different mesh sizes at time step  $\Delta t = \delta / c / 5$  for FDTD.

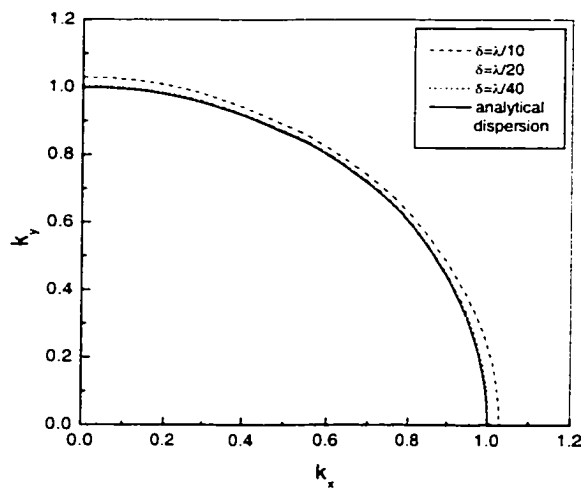


Figure 4.10 Dispersion characteristics of different mesh sizes at time step  $\Delta t = \delta / c / \sqrt{3}$  (CFL limit)

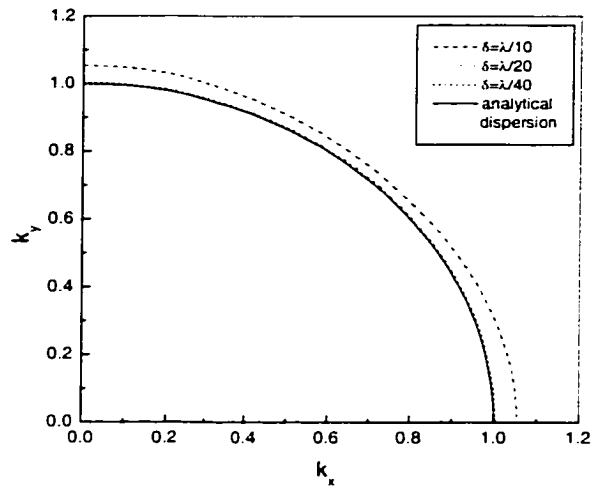


Figure 4.11 Dispersion characteristics of different mesh sizes at time step  $\Delta t = \delta / c$  (1.73 times of CFL limit).

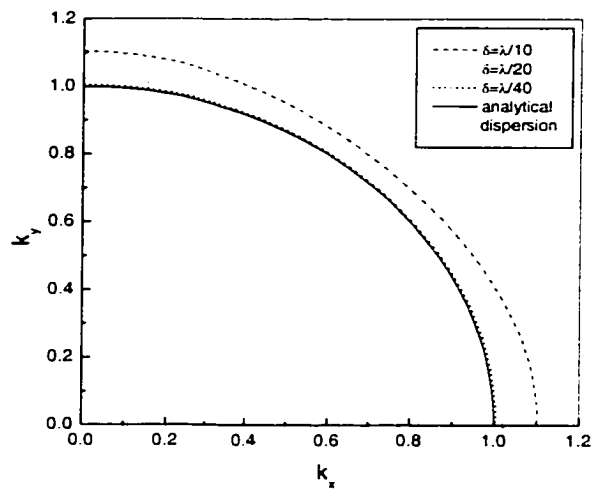


Figure 4.12 Dispersion characteristics of different mesh sizes at time step  $\Delta t = 1.5\delta / c$  (2.6 times of CFL limit).

In each figure, three different mesh sizes are considered: dense ( $\delta = \lambda / 40$ ), normal ( $\delta = \lambda / 20$ ) and coarse ( $\delta = \lambda / 10$ ). Figure 4.8 shows a good match between the dispersion characteristics of the unconditionally stable ADI-FDTD

and the analytical dispersion relation when  $\Delta t = \delta / c / 5$ . More precisely, the maximum dispersion error is 0.11%, 0.44% and 1.8% for dense, normal and coarse mesh respectively. Figure 4.9 shows the dispersion characteristics of FDTD under the same condition with the maximum dispersion error being 0.1%, 0.4% and 1.6% for dense, normal and coarse mesh respectively. The difference between Figure 4.8 and 4.9 is very small. This again demonstrates that the dispersion error differences between ADI-FDTD and the conventional FDTD are comparable when time step is small. In Figure 4.10, 4.11 and 4.12, however, the difference between numerical dispersion of ADI-FDTD and the analytical dispersion increases as the time step becomes bigger. More specifically, when  $\Delta t = 1.5\delta / c$  maximum numerical dispersion error reaches 0.57%, 2.3% and 10% for dense, normal and coarse mesh, respectively. As can be seen, the grid resolution plays an important role in the numerical dispersion. The coarser the mesh, the larger the errors. In particular, Figure 4.12 shows a significant error between the analytical dispersion relation and the numerical dispersion of ADI-FDTD when the coarse grid is used. The error can go up to 10%. However, for the dense grid, the difference between the numerical dispersion of ADI-FDTD and analytical dispersion is negligible.

#### **4.6 An Important corollary**

The curves shown in Figure 4.12 have an important implication in terms of the application of the unconditionally stable ADI-FDTD when fine structures are encountered and multigridding schemes are required. In other words, certain electromagnetic structures including RF circuits contain very small and fine structures (thin layer) where the fields need to be counted for. Modeling such structures requires a small mesh size due to the dispersion errors. In the conventional FDTD scheme such a small mesh size leads to a small time step throughout the whole solution domain because of the CFL stability condition. Hence, the computation time can increase dramatically. However, in the

unconditionally stable ADI-FDTD, the problem does not exist since the CFL constraint is removed and the time step can be chosen to be larger in the fine mesh region while the accuracy is not sacrificed. The reason is that from Figure 4.12, one can see that for a fine mesh, a large time step can be used and yet the numerical dispersion errors are still very small. In the following paragraphs, a quantitative analysis of the local dispersion error is provided for the case where a multigridding technique is preferred for modeling.

Suppose that the largest coarse grid size is  $\delta_a$  and the local fine grid size is  $\delta_l$  as shown in Figure 4.13.

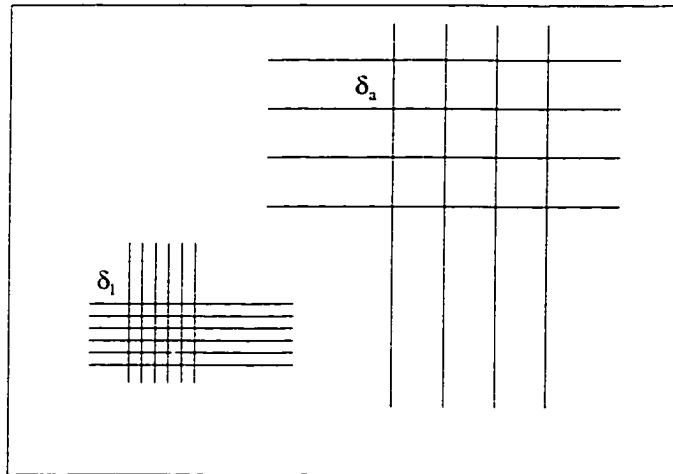


Figure 4.13 Multigridding meshes.

The ratio of the coarse grid size to the local grid size  $r$  is then:

$$r = \frac{\delta_a}{\delta_l} \quad (4.23)$$

The local dispersion characteristics can then be computed in terms of the ratio. Suppose that  $\delta_a = \lambda/20$  is used and different time steps are chosen:  $\Delta t = \delta_a / c / \sqrt{3}$  ( $r$  times of CFL limit),  $\Delta t = \delta_a / c$  ( $1.7^*r$  times of CFL limit) and  $\Delta t = 1.5\delta_a / c$  ( $2.6^*r$  times of CFL limit). The different multigriding meshes with  $r = 1$  (no mesh refinement),  $r = 10$ , and  $r = 20$  are used, respectively. The corresponding dispersion characteristics are computed and shown in Figure 4.14 to Figure 4.16.

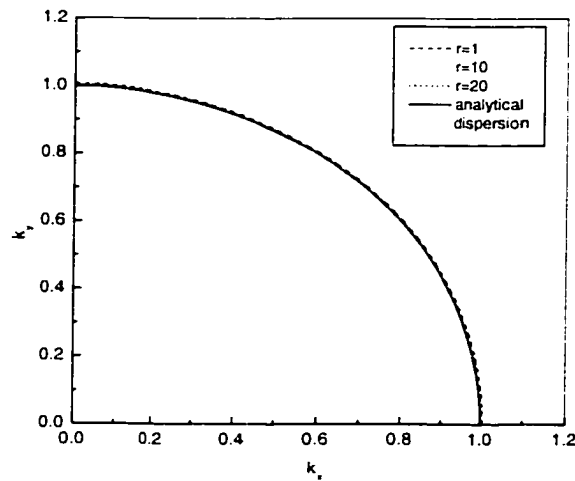


Figure 4.14 Dispersion characteristics of different  $r$  at time step  $\Delta t = \delta_a / c / \sqrt{3}$  (CFL limit).

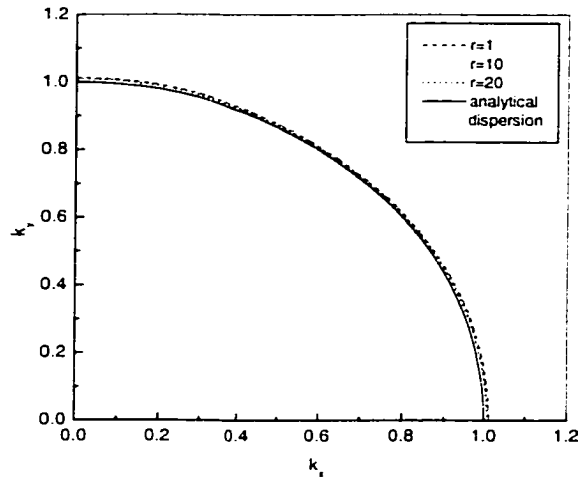


Figure 4.15 Dispersion characteristics of different  $r$  at time step  $\Delta t = \delta_a / c$  (1.73 times of the CFL limit)

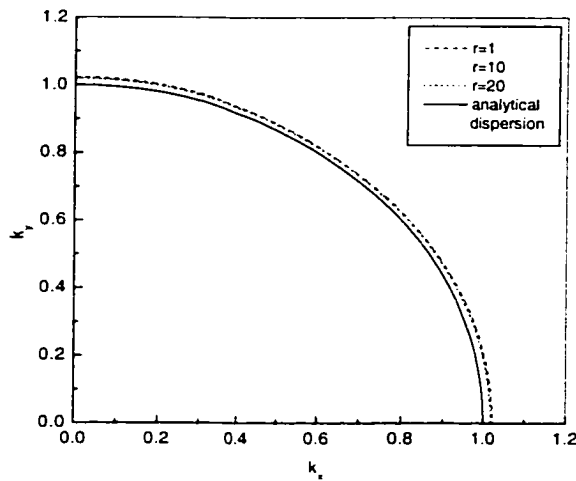


Figure 4.16 Dispersion characteristics of different  $s$  at time step  $\Delta t = 1.5\delta_a / c$  (2.6 times of CFL limit)

As it can be seen, the deviations of numerical dispersion from the analytical dispersion are reduced as  $r$  increases. That is, when  $r$  is increased (i.e. the mesh becomes finer), the errors of the local fine mesh due to the numerical dispersion



are actually decreased. This leads to an important corollary: *the dispersion errors of the fine mesh ( $r>1$ ) for the small structures will always be smaller than that of the coarse mesh ( $r=1$ ) if the time step is taken to be the same for both meshes.* As a result, in a multigriding technique with the unconditionally stable FDTD, one can take the time step for the fine mesh the same as the time step for the coarse mesh as long as the dispersion errors of the coarse mesh are acceptable for accuracy.  $\Delta t$  is only restricted by the coarse size  $\delta_a$  in terms of accuracy. Such a conclusion is very useful in the multigriding arrangement in terms of saving of the computation time. For example, if  $\Delta t = \delta_a / c / \sqrt{3}$  is chosen for the coarse mesh and ( $r>1$ ) is used for a local refined mesh, the number of iterations with the unconditionally stable FDTD is reduced by  $r$  times in comparison with the conventional FDTD of the Yee's scheme where  $\Delta t$  has to be made less than  $\delta_a / (c\sqrt{3}r)$ . The simulation speed is significantly increased.

#### **4.7 Discussion and Conclusion**

The numerical dispersion of the recently developed unconditionally stable ADI-FDTD scheme has been derived in an analytical form. It has been used to investigate the impact of different spatial and time steps on the numerical dispersion. It is found that for a time step smaller than the CFL limit, the dispersion errors of the ADI-FDTD is only slightly higher than that of the conventional FDTD. That is, with a small time step, the unconditionally stable ADI-FDTD is at the same accuracy level as the conventional FDTD. For a larger time step, however, the dispersion errors are increased as the time step is increased. Consequently, the tradeoff between the modeling accuracy and the computation speed has to be made when a time step is chosen.

The dispersion analysis also shows that a much bigger time step can be used without sacrificing the accuracy in a fine mesh with the unconditionally stable ADI-FDTD scheme. If a part of the solution domain requires a fine mesh or grid,

the time step need not to be necessarily small. The same time step used for the coarse grid can still be used and the accuracy for the local fine mesh will not be worse than that for the coarse. In other words, the selection of the time step is only dependent on the required accuracy of the coarse mesh applied. This is a very unique feature with the unconditionally stable ADI-FDTD since it will reduce significantly the number of iterations in comparisons with the use of the conventional FDTD or even the Battle-Lemarie multiresolution time-domain scheme (MRTD) [68] that has excellent dispersion performance. The reason is that the time steps with either the conventional FDTD or MRTD have to satisfy the CFL stability conditions. The fine meshes thus require the application of small time steps. However, this is not the case with the ADI-FDTD since it does not have CFL condition.

## **Chapter 5 A High Order ADI-FDTD Method for Reducing Dispersion**

### **5.1 Introduction**

The newly developed ADI-FDTD method is based on ADI method and the resulting formulation is unconditionally stable. The selection of the time step is now only dependent on the modeling accuracy required and Nyquist sampling limit. Dispersion analysis and numerical experiment show that the scheme has advantages over conventional FDTD [99][130]. As described before, although the ADI-FDTD is free from the CFL constraint, the numerical dispersion becomes more serious when modeling electrically large structures.

High order finite difference schemes can be used to combat the numerical dispersion in FDTD. Dispersion analyses for the high-order schemes were conducted in the literatures [132-134] demonstrating the high phase accuracy over the conventional low-order FDTD.

Based on the idea, a fourth-order ADI-FDTD method is developed for the solutions of Maxwell's equations in the time domain in this chapter. The same staggered mesh as that used in the second order ADI-FDTD is used, and the stability and dispersion performance of the scheme is investigated. Analysis shows that the forth-order ADI-FDTD is also unconditionally stable, with its numerical dispersion and anisotropy lower than those of the second order ADI-FDTD developed in the previous chapter. Dispersion analysis shows that the scheme can be applied with a coarse grid to reduce the memory consumption.

## 5.2 Fourth Order ADI-FDTD Formulation

The ADI-FDTD presented in the previous chapters is second order in spatial domain because the spatial derivatives in the Maxwell's equations are approximated by central finite difference, for example,

$$\frac{\partial H_z|_{i,j,k}^n}{\partial y} = \frac{H_z|_{i+\frac{1}{2},j+\frac{1}{2},k}^n - H_z|_{i+\frac{1}{2},j-\frac{1}{2},k}^n}{\Delta y} + O(\Delta y^2). \quad (5.1)$$

When fourth order central finite difference approximation is applied,

$$\frac{\partial H_z|_{i,j,k}^n}{\partial y} = \frac{1}{24\Delta y} \left[ \begin{array}{l} -H_z|_{i+\frac{1}{2},j+\frac{3}{2},k}^n + 27H_z|_{i+\frac{1}{2},j+\frac{1}{2},k}^n \\ -27H_z|_{i+\frac{1}{2},j-\frac{1}{2},k}^n + H_z|_{i+\frac{1}{2},j-\frac{3}{2},k}^n \end{array} \right] + O(\Delta y^4). \quad (5.2)$$

Replacing all the spatial derivatives in ADI-FDTD formulations (2.27-2.28) with the fourth order central finite difference correspondences, the fourth order ADI-FDTD formulas are obtained. Again, two-step computations are needed. For instance, for the x component of electric field to advance from the  $n$ -th time step to the  $(n+1/2)$ -th time step, the formula can be written as

$$\begin{aligned} & \frac{E_x|_{i+\frac{1}{2},j,k}^{n+\frac{1}{2}} - E_x|_{i+\frac{1}{2},j,k}^n}{\Delta t/2} \\ &= \frac{1}{\epsilon} \left\{ \frac{1}{24\Delta y} \left[ -H_z|_{i+\frac{1}{2},j+\frac{3}{2},k}^{n+\frac{1}{2}} + 27H_z|_{i+\frac{1}{2},j+\frac{1}{2},k}^{n+\frac{1}{2}} - 27H_z|_{i+\frac{1}{2},j-\frac{1}{2},k}^{n+\frac{1}{2}} + H_z|_{i+\frac{1}{2},j-\frac{3}{2},k}^{n+\frac{1}{2}} \right] \right. \\ & \quad \left. - \frac{1}{24\Delta z} \left[ -H_y|_{i+\frac{1}{2},j,k+\frac{3}{2}}^n + 27H_y|_{i+\frac{1}{2},j,k+\frac{1}{2}}^n - 27H_y|_{i+\frac{1}{2},j,k-\frac{1}{2}}^n + H_y|_{i+\frac{1}{2},j,k-\frac{3}{2}}^n \right] \right\} \end{aligned} \quad (5.3)$$

For the advancement from the  $(n+1/2)$ -th to the  $(n+1)$ -th time step, we have

$$\begin{aligned}
& \frac{E_x|_{i+\frac{1}{2},j,k}^{n+1} - E_x|_{i+\frac{1}{2},j,k}^{n+\frac{1}{2}}}{\Delta t/2} \\
&= \frac{1}{\epsilon} \left\{ \frac{1}{24\Delta y} \left[ H_z|_{i+\frac{1}{2},j+\frac{1}{2},k}^{n+\frac{1}{2}} + 27H_z|_{i+\frac{1}{2},j+\frac{1}{2},k}^{n+\frac{1}{2}} - 27H_z|_{i+\frac{1}{2},j-\frac{1}{2},k}^{n+\frac{1}{2}} + H_z|_{i+\frac{1}{2},j-\frac{1}{2},k}^{n+\frac{1}{2}} \right] \right. \\
&\quad \left. - \frac{1}{24\Delta z} \left[ -H_y|_{i+\frac{1}{2},j,k+\frac{1}{2}}^{n+1} + 27H_y|_{i+\frac{1}{2},j,k+\frac{1}{2}}^{n+1} - 27H_y|_{i+\frac{1}{2},j,k-\frac{1}{2}}^{n+1} + H_y|_{i+\frac{1}{2},j,k-\frac{1}{2}}^{n+1} \right] \right\} \quad (5.4)
\end{aligned}$$

The same procedures can be applied to all the other field components and similar equations can be obtained.

After some algebra manipulation, similar to that applied for the second-order ADI-FDTD, the fourth order ADI-FDTD scheme can be written in a compact matrix form as

$$\begin{cases} \mathbf{M}_1 \mathbf{X}^{n+\frac{1}{2}} = \mathbf{P}_1 \mathbf{X}^n \\ \mathbf{M}_2 \mathbf{X}^{n+1} = \mathbf{P}_2 \mathbf{X}^{n+\frac{1}{2}} \end{cases} \quad (5.5)$$

$\mathbf{X}^n$  is a column vector which contains all the field components inside simulation region at the n-th time step.  $\mathbf{M}_1$ ,  $\mathbf{M}_2$ ,  $\mathbf{P}_1$ , and  $\mathbf{P}_2$  are the coefficient matrices with their elements related to the values of spatial and temporal steps.  $\mathbf{M}_1$  and  $\mathbf{M}_2$  are sparse matrices. In particular, each row of these two matrices contains seven non-zero elements, which is more than that of the second-order scheme (three non-zero elements each row). Each step is advanced by solving the linear matrix problem. In practical implementation, by applying similar computation techniques developed in chapter 2, most computations on inverse matrix can be avoided and the simulation performance can be improved significantly.

### 5.3 Numerical Stability and Dispersion Analysis

Now assume every field component in the spatial spectral domain to be:

$$F_{\alpha} \Big|_{i+\frac{1}{2},j,k}^n = F_{\alpha}^n e^{-j(k_x \Delta x + k_y \Delta y + k_z \Delta z)} \quad (5.6)$$

where  $F$  represents either  $E$  or  $H$  and  $\alpha = x, y, z$ .  $\Delta x$ ,  $\Delta y$ ,  $\Delta z$ , and  $\Delta t$  are spatial and temporal steps, and  $k_x$ ,  $k_y$ , and  $k_z$  are spatial frequencies.

The fourth-order ADI-FDTD formulations (equations (5.3) and (5.4) together with the similar equations for the other field components) can be written in a matrix form by summarizing all the equations together in the spatial spectral domain and placing the field components of different time step at the different side of the equations:

$$L_1 F^{n+\frac{1}{2}} = R_1 F^n \quad (\text{for advancement from the } n\text{th to } (n+1/2)\text{th time step}) \quad (5.7)$$

$$L_2 F^{n+1} = R_2 F^{n+\frac{1}{2}} \quad (\text{for advancement from the } (n+1/2)\text{th to } (n+1)\text{th time step}) \quad (5.8)$$

Here vector  $F^n$  is a 6 by 1 vector containing the six field components at the  $n$ -th time step in the spatial spectral domain.  $L_1$ ,  $L_2$ ,  $R_1$  and  $R_2$  are the coefficient matrices with their elements related to spatial and temporal steps,  $\Delta x$ ,  $\Delta y$ ,  $\Delta z$ , and  $\Delta t$ , and spatial frequencies  $k_x$ ,  $k_y$ , and  $k_z$ .

Combination of the above two equations ends up with:

$$F^{n+1} = L_2^{-1} R_2 L_1^{-1} R_1 F^n = \mathcal{A} F^n \quad (5.9)$$

It is interesting to note that  $\mathcal{A}$  has similar expression as that of standard second-order ADI-FDTD except that  $W_{\alpha}$  ( $\alpha = x, y, z$ ) are now defined as:

$$W_{\alpha} = \frac{\Delta t}{\Delta \alpha} \cdot \left[ 27 \sin\left(\frac{k_{\alpha} \Delta \alpha}{2}\right) - \sin\left(\frac{3k_{\alpha} \Delta \alpha}{2}\right) \right], \quad \alpha = x, y, z \quad (5.10)$$

In general,

$$\Lambda = \begin{bmatrix}
\frac{A_1 + B_1}{Q_x Q_y Q_z} & \frac{2\mu\epsilon W_x W_y}{Q_x Q_y} & \frac{2\mu\epsilon W_x W_z}{Q_y Q_z} & \frac{-2j\mu W}{Q_x Q_y} & \frac{2j\mu^2 \epsilon W_z}{Q_y Q_z} & \frac{2j\mu D_1}{Q_x Q_y Q_z} \\
\frac{2\mu\epsilon W_y W_x}{Q_z Q_x} & \frac{A_2 + B_2}{Q_x Q_y Q_z} & \frac{2\mu\epsilon W_y W_z}{Q_y Q_z} & \frac{2j\mu D_2}{Q_x Q_y Q_z} & \frac{-2j\mu W}{Q_y Q_z} & \frac{2j\mu^2 \epsilon W_x}{Q_x Q_y Q_z} \\
\frac{2\mu\epsilon W_z W_x}{Q_z Q_x} & \frac{2\mu\epsilon W_z W_y}{Q_x Q_y Q_z} & \frac{A_3 + B_3}{Q_y Q_z} & \frac{2j\mu^2 \epsilon W_y}{Q_x Q_y Q_z} & \frac{2j\mu D_3}{Q_y Q_z} & \frac{-2j\mu W}{Q_x Q_y Q_z} \\
\frac{-2j\epsilon W}{Q_z Q_x} & \frac{2j\epsilon D_2}{Q_x Q_y} & \frac{2j\mu\epsilon^2 W_y}{Q_x Q_y Q_z} & \frac{A_1 + B_3}{Q_x Q_y} & \frac{2\mu\epsilon W_x W_y}{Q_x Q_y Q_z} & \frac{2\mu\epsilon W_z W_x}{Q_x Q_y Q_z} \\
\frac{2j\mu\epsilon^2 W_z}{Q_z Q_x} & \frac{-2j\epsilon W}{Q_x Q_y Q_z} & \frac{2j\epsilon D_3}{Q_y Q_z} & \frac{2\mu\epsilon W_x W_y}{Q_x Q_y Q_z} & \frac{Q_y Q_z}{A_2 + B_1} & \frac{Q_z Q_x}{2\mu\epsilon W_y W_z} \\
\frac{2j\epsilon D_1}{Q_z Q_x} & \frac{2j\mu\epsilon^2 W_x}{Q_y Q_x} & \frac{-2j\epsilon W}{Q_x Q_y Q_z} & \frac{2\mu\epsilon W_z W_x}{Q_x Q_y} & \frac{2\mu\epsilon W_y W_z}{Q_x Q_y Q_z} & \frac{A_3 + B_2}{Q_x Q_y Q_z} \\
\frac{Q_x Q_y Q_z}{Q_x Q_y} & \frac{Q_x Q_y}{Q_x Q_y} & \frac{Q_x Q_y}{Q_x Q_y} & \frac{Q_x Q_y}{Q_x Q_y} & \frac{Q_y Q_z}{Q_y Q_z} & \frac{Q_x Q_y Q_z}{Q_x Q_y Q_z}
\end{bmatrix} \quad (5.11)$$

The eigenvalues of the  $\Lambda$  can be found as:

$$\lambda_1 = \lambda_2 = 1$$

$$\lambda_3 = \lambda_4 = \frac{\sqrt{R^2 - S^2} + jS}{R} \quad (5.12)$$

$$\lambda_5 = \lambda_6 = \lambda_3^* = \frac{\sqrt{R^2 - S^2} - jS}{R}$$

where

$$R = (\mu\epsilon + W_x^2)(\mu\epsilon + W_y^2)(\mu\epsilon + W_z^2)$$

$$S = \sqrt{4\mu\epsilon(\mu\epsilon W_x^2 + \mu\epsilon W_y^2 + \mu\epsilon W_z^2 + W_x^2 W_y^2 + W_y^2 W_z^2 + W_z^2 W_x^2)(\mu^3 \epsilon^3 + W_x^2 W_y^2 W_z^2)}$$

Similarly to section 3.2, it can be shown that all the eigenvalues have the magnitude of one. Based on the Fourier spectral analysis theory [22], the proposed fourth order ADI-FDTD scheme is unconditionally stable regardless of time step.

Numerical dispersion of the high order ADI-FDTD algorithm can also be obtained by assuming:

$$F_{\alpha} |_{i+\frac{1}{2},j,k}^n = F_{\alpha}^n e^{j\omega n \Delta t} e^{-j(k_x i \Delta x + k_y j \Delta y + k_z k \Delta z)} \quad (5.13)$$

By substitution equation (5.13) into equation (5.9), we have:

$$(e^{j\omega \Delta t} \mathbf{I} - \mathbf{A})\mathbf{F} = 0 \quad (5.14)$$

where  $\mathbf{I}$  is a 6 by 6 identity matrix.

For the nontrivial solution of (5.14), we have

$$\det(e^{j\omega \Delta t} \mathbf{I} - \mathbf{A}) = 0 \quad (5.15)$$

It lead to the following dispersion relation:

$$\omega = 0 \quad (5.16)$$

and

$$\begin{aligned} \sin^2(\omega \Delta t) &= \frac{S^2}{R^2} \\ &= \frac{4\mu\epsilon(\mu\epsilon W_x^2 + \mu\epsilon W_y^2 + \mu\epsilon W_z^2 + W_x^2 W_y^2 + W_y^2 W_z^2 + W_z^2 W_x^2)(\mu^3 \epsilon^3 + W_x^2 W_y^2 W_z^2)}{(\mu\epsilon + W_x^2)^2 (\mu\epsilon + W_y^2)^2 (\mu\epsilon + W_z^2)^2} \end{aligned} \quad (5.17)$$

Again, the solution  $\omega = 0$  represents stationary solutions that correspond to the electrostatic and magnetostatic solutions. It represents the non-propagating solutions in the ADI-FDTD mesh. The nontrivial solution (5.17) corresponds to the propagating solution of the fourth order ADI-FDTD mesh. It describes the dispersion relationship among the numerical wave numbers in the  $x$ ,  $y$ , and  $z$  directions, the wave angular frequency, the grid size and time step.



#### 5.4 Comparisons between the fourth order ADI-FDTD and the second order ADI-FDTD

Figure 5.1 and Figure 5.2 show the numerical phase velocity versus the wave propagation angles for the second and fourth order ADI-FDTD in the spherical coordinate system, respectively. The error caused by numerical dispersion of fourth order scheme is much smaller than that of second order scheme. The maximum error with fourth-order is 0.1% while the maximum error with second-order is 0.5%. Figure 5.3 shows that even when the spatial increment is doubled, the dispersion error is comparable with that of the second order scheme with dense grid. Consequently, the memory requirement can be reduce eight times for three-dimensional problem while maintaining the same dispersion level.

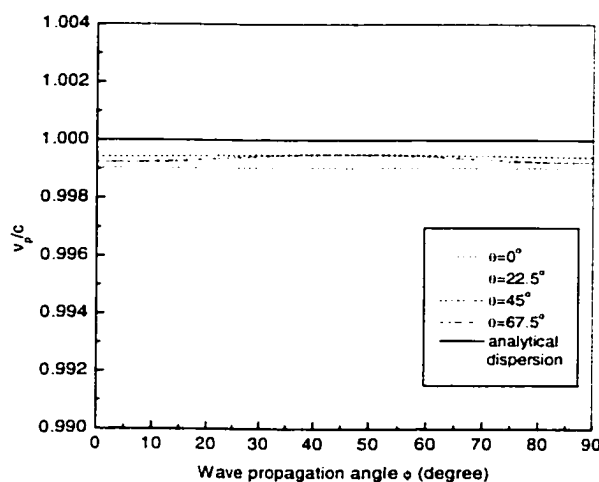


Figure 5.1 Numerical phase velocity versus wave propagation angle in the fourth order ADI-FDTD grid with  $\delta = \lambda / 20$  and  $\Delta t = \delta / c / 3$

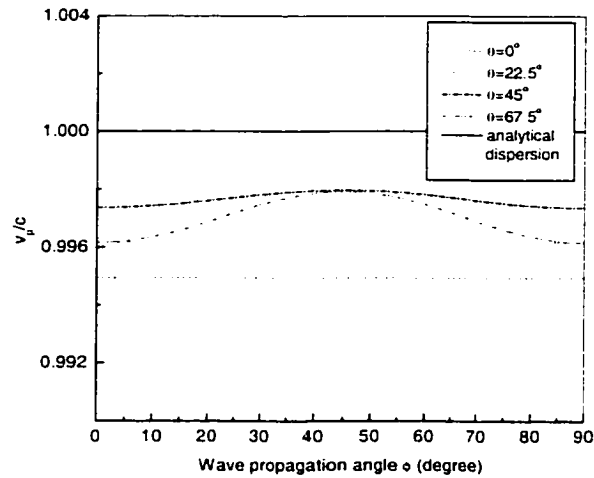


Figure 5.2 Numerical phase velocity versus wave propagation angle in the second order ADI-FDTD grid with  $\delta = \lambda/20$  and  $\Delta t = \delta/c/3$

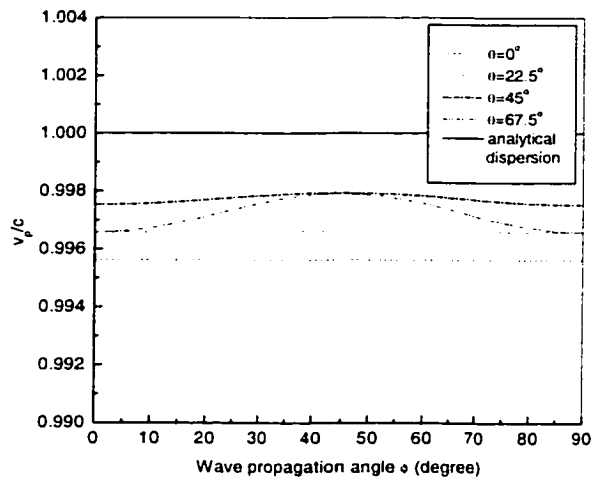


Figure 5.3 Numerical phase velocity versus wave propagation angle in the fourth order ADI-FDTD grid with  $\delta = \lambda/10$  and  $\Delta t = \delta/c/3$

Figure 5.4 shows the dispersion errors of the fourth-order ADI-FDTD in comparison with the second order ADI-FDTD. Again, A grid resolution  $\delta = \lambda/20$  was chosen. It can be seen that the numerical dispersion is reduced significantly

at small time step. For large time step, the advantage of high order ADI-FDTD will decrease because the time step becomes a dominant factor of numerical dispersion.

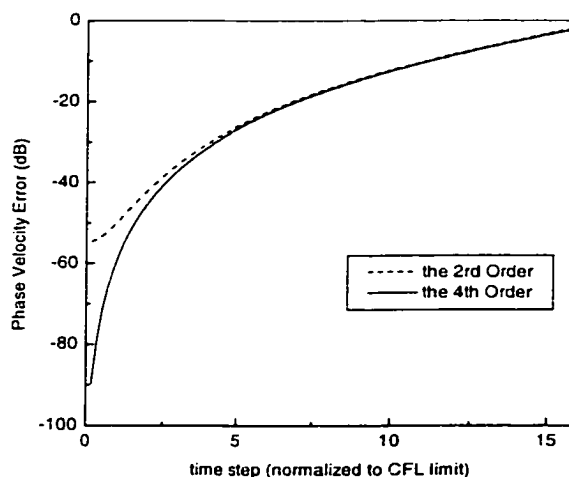


Figure 5.4 The numerical phase velocity error versus time step for the fourth order and the second order scheme.

## 5.5 Discussions and Conclusions

Based on the second-order ADI-FDTD scheme, an improved ADI-FDTD scheme with fourth-order accuracy in spatial domain has been developed. The high order ADI-FDTD scheme also has unconditional stability which has been proved theoretically in this chapter. Compared with the second order ADI-FDTD, the fourth order ADI-FDTD scheme shows better dispersion, isotropy and can be used to model electromagnetic wave propagation on a coarse grid, leading to a saving of memory as high as eight times.

## **Chapter 6 Conclusion and Suggestions for Future Directions**

### **6.1 Summary**

Time-domain numerical computation techniques in electromagnetics are intensively studied nowadays and are of great interest to designers of RF and microwave circuits and researchers in related fields. In particular, there is increased interest in transient EM field analysis that has its roots in two main events: 1) the advent of digital signal processing and transmission technology operating with wide band high-frequency signals; and 2) the increased capability of state-of-the-art computers with capability of handling heavy CPU time and memory requirements. The main purpose of this thesis is to study existing time-domain methods, their advantages and disadvantages, their applicability to a variety of problems, and to develop new approaches which would further increase computational efficiency.

Background knowledge relevant to this thesis is reviewed in Chapter 1 and Chapter 2. Both frequency domain and time domain computational electromagnetic methods were described. State of art time domain techniques such as PSTD and MRTD were also introduced. In chapter 2, the fundamental of FDTD was illustrated. The basics of ADI technique which is an efficient approach for solving parabolic partial differential equations was reviewed. A modified ADI technique has been developed to derive the unconditionally stable ADI-FDTD scheme. Numerical simulation results for conventional FDTD and ADI-FDTD are presented. Comparison shows that ADI-FDTD can use big time step beyond CFL limits with tolerable error. The analytical proof of unconditional stability of ADI-FDTD is presented in Chapter 3, and further validated with the numerical experiments. With total removal of the CFL condition in ADI-FDTD, a logical continuation of this research leads to numerical dispersion analysis which is

described in Chapter 4. After dispersion relation has been derived, the effects of propagation direction and large time step on the numerical dispersion was investigated. Furthermore, a unique characteristic of ADI-FDTD was found that *the dispersion errors of the fine mesh inside the small sub-structures will always be smaller than that of the coarse mesh if the time step is taken to be the same for both meshes*. Consequently, in a multigridding technique with the ADI-FDTD, the same time step may be used for both fine and coarse meshes as long as the dispersion errors with the coarse mesh are acceptable for accuracy. To further reduce the numerical dispersion, a high order approach has been proposed in Chapter 5. Dispersion analysis shows that a grid eight times coarser than that of second-order ADI-FDTD can be used while same level of accuracy can be maintained.

In conclusion, while the techniques such as MRTD and PSTD opened a way for reduction in computation memory, the proposed ADI-FDTD presented a way to reduce the number of iterations which leads to less CPU time. The work of this thesis has been published [99,130-131] and has led a new direction in the continuing effort of the electromagnetic modeling community towards improving computational efficiency of the FDTD algorithms.

## **6.2 Future Directions**

ADI-FDTD has been developed and investigated on different aspects such as stability and numerical dispersion. It offers a wide range of possibility for further investigation.

### **6.2.1 Absorbing boundary condition (ABC)**

Like the conventional FDTD, the ADI-FDTD is solved in every grid point of the solution domain. As a result, if a problem domain is an open domain, the domain must be truncated with the absorbing boundary condition. Several approximate

ABCs schemes [79,121-124] has been developed for FDTD scheme. Among them, Mur ABC [121] and PML [79] are used widely due to the simplicity and efficiency. To implement the Mur ABC and PML into the ADI-FDTD is one of the future works.

### **6.2.2            *Application of nonlinear materials***

In the case of high power microwave, nuclear explosion, or laser engineering, the pulses are likely to have very high intensity so that the material nonlinearity plays an important role in energy and signal transmission. Recent research has been reported on the use of the FDTD approach to model the pulse dynamics of nonlinear material [108]-[109]. The application of the proposed ADI-FDTD formulation to these problems is a challenge for the future.

### **6.2.3            *Combination of MRTD and ADI-FDTD for high accuracy***

One possibility of having a more advanced ADI-FDTD model with smaller errors is to incorporate the MRTD principle into the proposed ADI-FDTD scheme. By doing so, it is expected that the time step can be increased to a much larger value while the solution errors remain small because of the high accuracy of the MRTD model. In addition, since the MRTD allows the number of the grid points much smaller than that for the conventional FDTD, the combined saving in time with the proposed ADI-FDTD method and in the grid size with the MRTD could be very significant. Thus, incorporation of both techniques could well result in an efficient FDTD algorithm that can handle electrically large electromagnetic structures effectively in the near future.

### **6.2.4            *Temporal High-order ADI-FDTD schemes***

Increasing the order of accuracy is an option to mitigate the effect of numerical dispersion errors. This can be done in either spatial or temporal domain or both.

In chapter 5, a high order ADI-FDTD in spatial domain has been developed to illustrate its advantage over the standard ADI-FDTD in terms of numerical dispersion. The high order ADI-FDTD in temporal domain could be another research area. Further more, high order in both temporal and spatial domain may be investigated.

In conclusion, the proposed ADI-FDTD has laid a foundation for a new direction in FDTD type of modeling. Although the basic theory and preliminary numerical results have been presented in this thesis, much work still needs to be done in the terms of its extensive application and advanced models.

## References

- [1] R. F. Harrington, *Field Computation by Moment Methods*, Macmillan, 1968.
- [2] E. K. Miller, "A Selective Survey of Computational Electromagnetics," *IEEE Trans. Antennas and Propagation*, vol. 36, No. 9, pp. 1281-1305,
- [3] H. Nakano, S. R. Kerner, and N. G. Alexopoulos, "The Moment Method Solution for Printed Wire Antennas of Arbitrary Configuration," *IEEE Trans. Antennas and Propagation*, vol. 36, pp. 1667-1673, Dec. 1988.
- [4] R. F. Harrington and J. R. Mautz, "Characteristic Modes for Aperture Problems," *IEEE Trans. Microwave Theory and Techniques*, vol. 33, pp. 500-505, June 1985.
- [5] T. Itoh, Ed., *Numerical Techniques for Microwave and Millimeter-Wave Passive Structures*, Wiley, New York.
- [6] A. Khalil, A. B. Yakovlev, and M. B. Steer, "Efficient Method-of-Moments Formulation for the Modeling of Planar Conductive Layers in a Shielded Guided-Wave Structure," *IEEE Trans. Microwave Theory and Techniques*, vol. 47, no. 9, pp. 1730-1736, Sept. 1999.
- [7] C. K. Anandan, P. Debernardi, R. Orta, R. Tascone, and D. Trinchero, "Problem-Matched Basis Functions for Moment Method Analysis – An Application to Reflection Gratings," *IEEE Trans. Antennas and Propagation*, vol. 48, no. 1, pp. 35-40, Jan. 2000.
- [8] J. Moore and R. Pizer, Eds., *Moment Methods in Electromagnetics*, Research Studies Press Ltd, Letchworth, England, 1984.
- [9] R. Mittra, *Numerical and Asymptotic Techniques in Electromagnetics*, Springer-Verlag, 1975.
- [10] G. Manara, M. Bandinelli, and A. Monorchio, "Electromagnetic penetration and coupling to wires through apertures of arbitrary shape," *IEEE Trans. Electromagnetic Compatibility*, vol. 40, no. 4, pp. 391-396, Nov. 1998.
- [11] W. Chen and H. Chuang, "Numerical Computation of Human Interaction with Arbitrarily Oriented Superquadric Loop Antennas in Personal Communications," *IEEE Trans. Antennas and Propagation*, vol. 48, no. 6, pp. 821-828, Jun. 1998.



- [12] J. L. Volakis, A. Chatterjee, and L. C. Kempel, *Finite Element Method for Electromagnetics*, IEEE Inc, 1998.
- [13] J. B. Davies, "Finite Element Analysis of Waveguides and Cavities – a Review," *IEEE Trans. Magnetics*, vol. 29, no. 2, Mar. 1993.
- [14] B. M. A. Rahman, F. A. Fernandez, and J. B. Davies, "Review of Finite Element Methods for Microwave and Optical Waveguides," in *Proc. IEEE*, vol. 79. No. 10. Oct 1991.
- [15] G. Mur, "The finite-element modeling of three-dimensional electromagnetic fields using edge and nodal elements", *IEEE Trans. Antennas and Propagation*, vol. 41, pp.948-953, 1993.
- [16] J. M. and J. L. Volakis, "A finite element-boundary integral formulation for scattering by three-dimensional cavity-backed apertures," *IEEE Trans. Antennas and Propagation*, vol. 39, pp.97-104, 1991.
- [17] Z. J. Cendes and P. Silverster, "Numerical solution of dielectric loaded waveguide: I – Finite element analysis," *IEEE Trans. Microwave Theory and Techniques*, pp. 1124-1131, 1970.
- [18] H. Whitney, *Geometric Integration Theory*, Princeton University. Press, NJ, 1957.
- [19] J. C. Nedelec, Mixed finite elements in R3, *Numerical Math.*, 35, pp. 315-341, 1980.
- [20] G. Mur and AT. Dde Hoop, "A Finite element method for computing three-dimensional electromagnetic fields in inhomogeneous media. *IEEE Trans. Magnetics*, 21, pp. 2188-2191, Nov. 1985.
- [21] M. L. Barton and Z. J. Cendes, "New vector finite elements for three-dimensional magnetic field computation," *J. Appl. Phys*, 61(8), pp.3919-3921, Apr. 1987.
- [22] G. D. Smith, *Numerical Solution of Partial Differential Equations*, Oxford, Oxford University Press, 1978.
- [23] G. E. Forsythe and W. R. Wasow, *Finite Difference Methods for Partial Differential Equations*, New York, Wiley, 1960.
- [24] P. F. Ryff, P. P. Biringer, P. E. Burke, "Calculation Methods for Current Distribution in Single Turn Coils of Arbitrary Cross Section," *IEEE Trans. on PAS*, 89(2), 228-232, 1967.

- [25] M. S. Sarma, "Potential Functions in Electromagnetic Field problems," *IEEE Trans. on Mag.*, 6(3), 513-518, 1970
- [26] A. R. Mitchell, D. F. Griffiths, *The Finite Difference Method in Partial Difference Equations*, Wiley, 1980.
- [27] E. Schweig, W. B. Brdidge, "Computer Analysis of Dielectric Waveguides, A Finite Difference Method," *IEEE Trans. Microwave Theory and Techniques*, 32(5), 531-541, 1984.
- [28] T. Itoh and R. Mittra, "Spectral-domain approach for calculating the dispersion characteristics of microstrip lines," *IEEE Trans. Microwave Theory and Techniques*, vol. 21, no. 7, pp. 496-499, July 1973.
- [29] J. L. Tsalamengas "Rapidly Converging Spectral-Domain Analysis of Shield Layered Finlines," *IEEE Trans. Microwave Theory and Techniques*, vol. 47, no. 6, pp. 805-810, June 1999.
- [30] M. F. Iskander and T. S. Lind, "Electromagnetic coupling of coplanar waveguides and microstrip lines to highly lossy dielectric media," *IEEE Trans. Microwave Theory and Techniques*, vol. 37, no. 12, pp. 1910-1917, Dec. 1989.
- [31] Y. Chen and B. Beker, "Spectral-Domain Analysis of Open and Shielded Slotlines Printed on Various Anisotropic Substrates," *IEEE Trans. Microwave Theory and Techniques*, vol. 41, no. 11, pp. 1872-1877, Nov. 1993.
- [32] T. Itoh, *Numerical Techniques for Microwave and Millimeter-wave Passive Structures*, New York, Wiley, 1989.
- [33] 1. V. N. Feddeeva, "An approximated method of lines applied to certain boundary value problems," *Tr. Mat. Inst. im V. A. Steklova Akad. Nauk SSSR*, 28, pp 73-103, 1949.
- [34] 2. U. Schulz and R. Pregla, "A new technique for the analysis of plane waveguides and its application to microstrips with tuning septums," *Radio Sci.*, vol 16, pp. 1173-1178, 1981.
- [35] 3. S. Worm and R. Pregla, "Hybrid-Mode Analysis of Arbitrarily Shaped Planar Microwave Structures by the Method of Lines," *IEEE Trans. Microwave Theory and Techniques*, vol. 32, no. 2, pp. 191-196, Feb. 1995.

- [36] 4. A. P. Papachristoforos, "Method of lines for the calculation of excess capacitance for a cylindrical via in multilayer packaging," *IEE Proc. Microw. Antennas Propag.*, vol 146, no. 4, pp. 285-290, August 1999.
- [37] 5. D. Argollo, H. Abdalla Jr., and A. Soares, "Method of Lines Applied to Broadside Suspended Stripline Coupler Design," *IEEE Trans. Magnetics*, vol. 31, no. 3, pp. 1634-1636, May 1995.
- [38] J. R. Miletta, R. J. Chase, B. B. Luu, J. W. Williams, and V. J. Viverito, "Modeling of Army Research Laboratory EMP simulators," *IEEE Trans. Nuclear Science*, vol. 40, no. 6, pp. 1967-1976, Dec. 1993.
- [39] O. P. Gandhi and C. M. Furse, "Currents induced in the human body for exposure to ultrawideband electromagnetic pulses," *IEEE Trans. Electromagnetic Compatibility*, vol. 39, no. 2, pp. 174-180, May 1997.
- [40] K. S. Yee, "Numerical solution of initial boundary value problems involving Maxwell's equations in isotropic media," *IEEE Trans. Antennas and Propagation*, vol. 14, no. 3, pp. 302-307, May 1966.
- [41] K. L. Shlager and J. B. Scheider, "A Selective Survey of the Finite-Difference Time Domain Literature," *IEEE Antennas Propagation Mag.*, vol. 37, pp. 39-57, 1995.
- [42] P.B. Johns and R.L. Beurle, "Numerical Solution of Two-Dimensional Scattering Problems Using a Transmission Line Matrix," *Proc. IEEE*, vol. 118, Pt. H, pp. 1203-1208, 1971.
- [43] A. C. Cangellaris, C. Lin and K. K. Mei, "Point-Matched Time Domain Finite Element Methods for Electromagnetic Radiation and scattering," *IEEE Trans. on Antennas and Propagation*, vol. 35, No. 10, Oct. 1987.
- [44] S. Nam, H. Ling, and T. Itoh, "Characterization of Uniform Microstrip Line and Its Discontinuities Using the Time Domain Method of Lines," *IEEE Trans. Microwave Theory and Techniques*, vol. 37, pp. 2051-2057, 1989.
- [45] T. W. Veruttipong, "Time Domain Version of the Uniform GTD," *IEEE Trans. Antennas and Propagation*, vol. 38, pp. 1757-1764, 1990.
- [46] Allen Taflove, *Computational Electrodynamics: The Finite-Difference Time-Domain Method*, Artech House, 1995.
- [47] A. Taflove and M. E. Brodwin, "Numerical solution of steady-state electromagnetic scattering problems using the time-dependent Maxwell's

- equation," *IEEE Trans. Microwave Theory and Techniques*, vol. 23, pp. 623-630, Aug. 1975.
- [48] P. B. Johns, "The solution of inhomogeneous waveguide problems using a transmission-line matrix," *IEEE Trans. Microwave Theory and Techniques*, vol. 22, pp. 209-215, Mar. 1974.
- [49] S. Akhtarzad, and P. B. Johns, "Numerical solution of lossy waveguides: TLM computer program," *Electron. Lett.*, vol. 10, no. 15, pp. 309-311, July, 1974.
- [50] S. Akhtarzad, and P. B. Johns, "Solution of 6-component electromagnetic fields in three space dimensions and time by the T. L. M. method," *Electron. Lett.*, vol. 10, no.25/26, pp. 535-537, Dec. 1974.
- [51] Z. Chen, M. M. Ney, and W.J.R. Hofer, "A New Finite-Difference Time Domain Formulation and Its Equivalence with the TLM Symmetrical Condensed Node," *IEEE MTT-S Tran.*, vol. 39, pp.2160-2169, 1991.
- [52] J. Nelsen and W. Hofer, " A complete dispersion analysis of the condensed node TLM mesh," *IEEE Trans. Magnetics*, vol. 27, pp. 3982-3985, Sept. 1991.
- [53] P. Berini and K. Wu, "A Comprehensive Study of Numerical Anisotropy and Dispersion in 3-D TLM Meshes," *IEEE Trans. Microwave Theory and Techniques*, vol. 43, no. 5, pp. 1173-1181, May 1995.
- [54] M. Krumpholz and P. Russer, "On the dispersion in TLM and FDTD," *IEEE Trans. Microwave Theory and Techniques*, vol. 42, pp. 1275-1279, July. 1994.
- [55] F.J. German, G.K.Gothard, L.S. Riggs, and P. M. Goggans, "The Calculation of Radar Cross-Section (RCS) Using the TLM method," *Int. J. Numerical Modeling*, vol. 2, pp. 267-278, 1989.
- [56] M. A. Kolbehdari, M. Srinivasan, M. Nakhla, Q. Zhang, R. Achar, "Simultaneous Time and Frequency Domain Solutions of EM problems Using Finite Element and CFH Techniques," *IEEE Trans. Microwave Theory and Techniques*, vol. 44, no.9, Sept. 1996.
- [57] J. F. Lee, R. Lee, and A. Cangellaris, "Time-Domain Finite-Element Methods," *IEEE Trans. Antennas and Propagation*, vol. 45, no. 3, pp. 430-442, Mar. 1997.

- [58] S. Gedney and U. Navasariwala, "An Unconditionally Stable Finite Element Time Domain Solution of the Vector Wave Equation," *IEEE Microwave Guided Wave Lett.*, vol. 5, pp. 332-334, October 1995.
- [59] M. F. Wong, O. Picon, and V. F. Hanna, "A Finite Element Method Based on Whitney forms to Solve Maxwell equations in the time domain," *IEEE Trans. Magnetics*, vol. 31, no. 5, pp. 1618-1621, May 1995.
- [60] S Chang, R. Coccioli, Y. Qian, and T. Itoh, "A global finite-element time-domain analysis of active nonlinear microwave circuits," *IEEE Trans. Microwave Theory and Techniques*, vol. 47, no. 12, pp. 2410-2416, Dec. 1999.
- [61] T. Yamada and K. Tani, "Finite element time domain method using hexahedral elements," *IEEE Trans. on Magnetics*, vol. 33, no. 2, pp. 1476-1479, March 1997.
- [62] D. C. Dibben and R. Metaxas, "Time domain finite element analysis of multimode microwave applicators," *IEEE Trans. on Magnetics*, vol. 32, no. 3, pp. 942-945, May 1996.
- [63] M. Feliziani and F. Maradei, "Mixed finite-difference/Whitney-elements time domain (FD/WE-TD) method" *IEEE Trans. on Magnetics*, vol. 34, no. 5, pp. 3222-3227, Sept. 1998.
- [64] R. Wu, T. Itoh, "Hybrid finite-difference time-domain modeling of curved surfaces using tetrahedral edge elements," *IEEE Trans. Antennas and Propagation*, vol. 45, no. 8, pp. 1302-1309, Aug. 1997.
- [65] D. Koh, H. Lee, and T. Itoh, "A hybrid full-wave analysis of via-hole grounds using finite-difference and finite-element time-domain methods," *IEEE Trans. Microwave Theory and Techniques*, vol. 45, no. 12, pp. 2217-2223, Dec. 1997.
- [66] P. H. Aoyagi, J. F. Lee, and R. Mittra, "A Hybrid Yee algorithm/Scalarwave equation approach," *IEEE Trans. on Microwave Theory and Techniques*, vol. 41, no. 9, pp. 1593-1600, Sept. 1993.
- [67] M. Mrozowski, "A Hybrid PEE-FDTD algorithm for accelerated time domain analysis of electromagnetic wave in shielded structures," *IEEE Microwave Guided Wave Lett.*, vol. 4, no. 10, pp. 323-325, Oct. 1994.
- [68] M. Krumpholz and L. P. B. Katehi, "MRTD: New Time-Domain Schemes Based on Multiresolution Analysis," *IEEE Trans. on Microwave Theory and Techniques*, vol. 44, no. 4, pp. 555-571, Apr. 1996.

- [69] Q. H. Liu, "The Pseudospectral Time-Domain (PSTD) method: a new algorithm for solution of Maxwell's equations," *IEEE Antennas and Propagation Society International Symposium*, vol. 1, pp. 122-125, 1997.
- [70] R. Holland, "Implicit three-dimensional finite differencing of Maxwell's equations," *IEEE Trans. Nuclear Science*, Vol. NS-31, No. 6, pp. 1322-1326, 1984.
- [71] P. M. Goorjian, "Finite Difference Time Domain Algorithm Development for Maxwell Equations for Computational Electromagnetism," *IEEE Antennas and Propagation Society International Symposium*, Vol. 1, pp. 878-881, 1990.
- [72] P. M. Goorjian, "Algorithm Development for Maxwell's Equations for Computational Electromagnetism," AIAA Paper 90-0251, American Institute of Aeronautics & Astronautics, 28<sup>th</sup> Aerospace Sciences Meeting, Reno, NV, January 8-11, 1990.
- [73] T. Namiki and K. Ito, "A new FDTD algorithm free from the CFL condition restraint for a 2D-TE wave", *Digest of 1999 IEEE Antennas and Propagation Symposium*, Jul. 1999, Orlando, pp.192-195.
- [74] W. F. Ames, *Numerical Methods for Partial Differential Equations*, Academic Press, New York, 1977.
- [75] Q. H. Liu, "The PSTD algorithm: A time-domain method requiring only two cells per wavelength," *Microwave and Optical Technology Letters*, vol. 15, no. 3, pp. 158-165, Mar. 1997.
- [76] Q. H. Liu, "An FDTD algorithm with perfectly matched layers for conductive media," *Microwave and Optical Technology Letters*, vol. 14, no. 2, pp. 134-137, Feb. 1997.
- [77] Q. H. Liu, "A Frequency-Dependent PSTD Algorithm for General Dispersive Media," *IEEE Microwave and Guided Wave Letters*, vol. 9, no. 2, pp. 51-53, Feb. 1999.
- [78] Q. H. Liu, "PML and PSTD Algorithm for Arbitrary Lossy Anisotropic Media," *IEEE Microwave and Guided Wave Letters*, vol. 9, no. 2, pp. 48-50, Feb. 1999.
- [79] J. P. Berenger, "A perfectly matched layer for the absorption of electromagnetic waves," *J. Computat. Phys.*, vol. 114, pp. 185-200, Oct. 1994.

- [80] Y. F. Leung and C. H. Chan, "Combining the FDTD and PSTD Method," *Microwave and Optical Technology Letters*, vol. 23, no. 4, pp. 249-254, Nov. 1999.
- [81] M. Werthen and I. Wolff, "A novel wavelet based time domain simulation approach," *IEEE Microwave Guided Wave Letters*, vol. 6, pp.438-440, Dec. 1996.
- [82] M. Fujii and W. J. R. Hoefer, "A Three-Dimensional Haar-Wavelet-Based Multiresolution Analysis Similar to the FDTD Method – Derivation and Application," *IEEE Trans. on Microwave Theory and Techniques*, vol. 46, no. 12, pp. 2463-2475, Dec. 1998.
- [83] K. Goverdhanam, L. P. B. Katehi, and A. Cangellaris, "Application of multiresolution based FDTD multigrid," in 1997 IEEE MTT-S Int. Microwave Symp. Dig., pp. 333-336.
- [84] R. Robertson, E. Tentzeris, M. Krumpholz, and L. P. B. Katechi, "Application of MRTD analysis to dielectric cavity structures," in *Proc. Microwave Theory Tech. Soc.*, 1996, pp. 1840-1843.
- [85] K. Sabetfakhri and L. P. B. Katehi, "Analysis of integrated millimeterwave and submillimeter-wave waveguides using orthonormal wavelet expansions," *IEEE Trans. Microwave Theory and Techniques*, vol. 42, no. 12, pp. 2412-2422, Dec. 1994.
- [86] E. Tentzeris, R. Robertson, L. P. B. Katehi, and "Application of MRTD to printed transmission lines," in 1996 IEEE MTT-S Int. Microwave Symp. Dig. Pp. 573-577.
- [87] R. Robertson, E. M. Tentzeris, and L. P. B. Katehi, "Modeling of Membrane Patch Antennas Using MRTD Analysis," 1997 IEEE, pp.126-129.
- [88] M. Krumpholz, H. G. Winful, and L. P. B. Katehi, "Nonlinear Time-Domain Modeling by Multiresolution Time Domain (MRTD)," *IEEE Trans. Microwave Theory and Techniques*, vol. 45, no. 3, pp. 385-393, Mar. 1997.
- [89] M. Krumpholz and P. Russer, "Two-dimensional FDTD and TLM," *Int. J. Num. Modeling*, vol 7, no. 2, pp. 141-153, Feb. 1993.
- [90] M. Krumpholz and C. Huber P. Russer, "A field theoretical comparison of FDTD and TLM," *IEEE Trans. Microwave Theory and Techniques*, vol. 43, no. 8, pp. 1935-1950, Sept. 1995.

- [91] B. Z. Steinberg and Y. Leviatan, "On the use wavelet expansions in the method of moments," *IEEE Trans. Antennas and Propagation*, vol. 41, no. 5, pp. 610-619, May 1993.
- [92] I. Daubechies, "Ten lectures on wavelets," SIAM Rev. Philadelphia, PA, 1992.
- [93] G. Battle, "A block spin construction of ondeletters," *Comm. Math. Phys.*, vol. 110, pp. 601-615, 1987.
- [94] P. G. Lemarie, "Ondelettes a localization exponentielle," *J. Math. Pures Appl.*, vol. 67, pp. 227-236, 1988.
- [95] K. L. Shlager and J. B. Schneider, "Analysis of the dispersion properties of the multiresolution time-domain method," in *Proc. IEEE AP-S*, vol. 4, 1997, pp. 2144-2147.
- [96] I. Hong, N. Yoon, and H. Park, "Numerical dispersive characteristics and stability condition of the multiresolution time-domain (MRTD) method",
- [97] E. M. Tentzeris, R. L. Robertson, and L. P. B. Katehi, "Stability and dispersion Analysis of Battle-Lemarie-Based MRTD Schemes," *IEEE Trans. on Microwave Theory and Techniques*, vol. 47, pp. 1004-1013, July 1999.
- [98] E. M. Tentzeris, R. L. Robertson, J. F. Harvey, and L. P. B. Katehi, "PML Absorbing Boundary Conditions for the Characterization of Open Microwave Circuit Components Using Multiresolution Time-Domain Techniques (MRTD)," *IEEE Trans. Ant. Props.*, vol. 47, no. 11, pp. 1709-1715, Nov. 1999.
- [99] F. Zheng, Z. Chen, and J. Zhang, "A finite-different time-domain method without the Courant stability condition", *IEEE Microwave and Guided Wave Letters*, vol. 9, no. 11, pp. 441-443, Nov. 1999.
- [100] X. Zhang and K. K. Mei, "Time domain finite difference approach for the calculation of the frequency-dependent characteristics of the microstrip discontinuities," *IEEE Trans. Microwave Theory and Techniques*, vol. 36, pp. 1775-1787, Dec. 1988.
- [101] Z. Bi, K. Wu, C. Wu, and J. Litva, "A dispersive boundary condition for microstrip component analysis using the FDTD method," *IEEE Trans. Microwave Theory and Techniques*, vol. 40, pp. 774-776, Aug. 1992.



- [102] J. A. Pereda, L. A. Viela, A. Vegas, and A. prieto, "A treatment of magnetized ferites using the FDTD method," *IEEE Microwave and Guided Wave Letters*, vol. 3, 1993, pp. 136-138.
- [103] V. A. Thomas, M. E. Jones, M . J. Picket-May, A. Taflove, and E. Harrigan, "The use of SPICE lumped circuits as sub-grid models for high-speed elctronic circuit design," *IEEE Microwave and Guided Wave Letters*, vol. 4, 1994, pp. 141-143.
- [104] D. M. Sheen, S. M. Ali, M. D. Abouzabra, and J. A. Kong, "Application of the three-dimensional finite-differene time-domain method to the analysis of planar microstrip circuits," *IEEE Trans. Microwave Theory and Techniques*, vol. 38, pp. 849-857, 1990.
- [105] P. Harms, J. Lee, and R. Mittra, "Characterizing the cylindrical via discontinuity," *IEEE Trans. Microwave Theory and Techniques*, vol. 41, no. 8, pp. 153-156, Aug. 1993.
- [106] L. W. Ko and R. Mittra, "Acombination of FD-TD and Prony's methods for analyzing microwave integrated circuits," *IEEE Trans. Microwave Theory and Techniques*, vol. 39, no. 8, pp. 2176-2181, 1991.
- [107] S. Gedney, and F. Lansing, "A generalized Yee algorithm for the analysis of three-dimensional microwave circuit devices with planar symmetry," *IEEE Trans. Microwave Theory and Techniques*, vol. 42, no. 8, pp. 1514-1523, Aug. 1994.
- [108] E. Sano and T. Shibta, "Fullwave analysis of picosecond photoconductive switches," *IEEE J. Quanttum Electronics*, vol. 26, 1990, pp. 372-377.
- [109] R. W. Ziolkowski and J. B. Judkins, "Full-wave vetcor Maxwell's equations modeling of self-focusing of ultra-short optical pulses in a nonlinear Kerr medium exhibiting a finite response time," *J. Optical Society of America B*, vol. 10, 1993, pp. 186-198.
- [110] R. M. Joseph and A. Taflove, "Spatial solition deflection mechanism indicated by FTD-TD Maxwell's equation modeling," *IEEE Photonics Technology Letters*, 1994, pp. 1251-1254.
- [111] N. M. Potheary and C. J. Railton, "Analysis of Cross-Talk on High-Speed Digital Circuits Using the Finite Difference Time-Domain Method," *International Journal of Numerical Modeling*, 1991.

- [112] M. Rittweger, M. Werthen, and I. Wolff, "FDTD Simulation for Microwave Packages and Interconnects," *Proceeding of Workshop WSFC: EM Modeling of Microwave Packages and Interconnects*, IEEE Microwave Theory and Techniques Society International Microwave Symposium Digest, May 1993.
- [113] M. J. Piket-May, A. Taflove, and J. Baron, "FD-TD modeling of digital signal propagation in 3-D circuits with passive and active loads," *IEEE Trans. Microwave Theory and Techniques*, vol. 42, no. 8, pp. 1514-1523, Aug. 1994.
- [114] W. D. Becker, P. H. Harms, and R. Mittra, "Time-Domain electromagnetic analysis of interconnects in a computer chip package," *IEEE Trans. Microwave Theory and Techniques*, vol. 40, no. 8, pp. 430-451, 1992.
- [115] A. Reineix and B. Jecko, "Analysis of microstrip patch antennas using finite difference time domain method," *IEEE Trans. Antennas and Propagation*, vol. 37, pp. 1361-1369, 1989.
- [116] J. G. Maloney, G. S. Smith, and W. R. Scoot, "Accurate computation of the radiation from simple antenna using the finite-difference time-domain method," *IEEE Trans. Antennas and Propagation*, vol. 38, pp. 1059-1068, 1990.
- [117] P. A. Tirkas, and C. A. Balanis, "Finite-difference time-domain method for antenna radiation," *IEEE Trans. Antennas and Propagation*, vol. 40, pp. 334-340, 1992.
- [118] D. M. Sullivan, O. P. Gandhi, and A. Taflove, "Use of the Finite-Difference Time-Domain Method in Calculating EM absorption human models," *IEEE Trans. Biomedical Engineering*, vol. 35, pp. 179-186, 1988.
- [119] M. J. Piket-May, A. Taflove, W. C. Lin, D. S. Katz, V. Sathiaselan, and B. B. Mittal, "Initial results for automated computational modeling of patient-specific electromagnetic hyperthermia," *IEEE Trans. Biomedical Engineering*, vol. 39, pp. 226-237, 1992.
- [120] M. Okonieski and M. A. Stuchly, "A study of handset antenna and human body interaction," *IEEE Trans. Microwave Theory and Techniques*, vol. 44, no. 8, pp. 1855-1864, 1994.
- [121] G. Mur, "Absorbing boundary conditions for the finite-difference approximation of the time-domain electromagnetic field equations," *IEEE Trans. Electromagnetic Compatibility*, vol. 23, pp. 377-382, 1981.

- [122] K. K. Mei and J. Fang, "Superabsorption – a method to improve absorbing boundary conditions," *IEEE Trans. Antennas and Propagation*, vol. 40, pp. 1001-1010, 1992.
- [123] Z. P. Liao, H. L. Wong, B. P. Yang, and Y. F. Yuan, "A transmitting boundary for transient wave analyses," *Scientia Sinica (series A)*, vol. XXVII, 1984, pp. 1063-1076.
- [124] D. S. Katz, E. T. Thiele, and A. Taflove, "Validation and Extension to Three Dimensions of the Berenger PML Absorbing Boundary Condition for FD-TD Meshes," *IEEE Microwave and Guided Wave Letters*, vol. 4, no. 8, Aug. 1994.
- [125] I. S. Kim and W. J. R. Hoefer, "Numerical dispersion characteristics and stability factor for the TD-FD method," *Electronic Letters*, vol. 27, pp. 485-487, Mar. 1990.
- [126] K. L. Shlager, J. G. Maloney, S. L. Ray, and A. F. Peterson, "Relative accuracy of several finite-difference time-domain methods in two and three dimensions," *IEEE Trans. Antennas and Propagation*, vol. 41, no. 12, pp.1732-1737, Dec. 1993.
- [127] P. G. Petropoulos, "Phase error control for fd-td methods of second and fourth order accuracy," *IEEE Trans. Antennas and Propagation*, vol. 42, pp.859-862, Jun. 1994.
- [128] J. A. Pereda, O. Garcia, A. Vegas, and A. Prieto, "Numerical Dispersion and Stability Analysis of the FDTD Technique in Lossy Dielectrics," *IEEE Microwave and Guided Wave Letters*, vol. 8, no. 7, Jul. 1998.
- [129] D. W. Peaceman and H. H. Rachford, "The Numerical Solution of Parabolic and Elliptic Differential Equations," *J. Soc. Indust. Appl. Math.*, vol. 42, no. 3, pp. 28-41, 1955.
- [130] F. Zheng, Z. Chen and J. Zhang, "Towards the Development of a three-dimensional Unconditionally Stable Finite-Difference Time-Domain Method", *IEEE Trans. on Microwave Theory and Techniques*, vol. 48, no. 9, pp. 1550-1558, Sept. 2000.
- [131] F. Zheng and Z. Chen, "Numerical Dispersion Analysis of the Unconditionally Stable 3D ADI-FDTD Method", Accepted for publication in *IEEE Trans. on Microwave Theory and Techniques*.

- [132] J. Fang, *TIME DOMAIN COMPUTATION FOR MAXWELL'S EQUATIONS*, Ph.D. dissertation, Univ. of California at Berkeley, Nov. 1989.
- [133] M. F. Hadi and M. Piket-May, "A Modified FDTD (2,4) Scheme for Modeling Electrically Large Structures with High-Phase Accuracy," *IEEE Trans. Antennas and Propagation*, vol. 45, no. 2, Feb. 1997.
- [134] K. Lan, Y. Liu, and W. Lin, "A Higher Order (2,3) Scheme for Reducing Dispersion in FDTD Algorithm," *IEEE Trans. Electromagnetic Compatibility*, vol. 41, no. 2, pp. 160-165, May 1999.
- [135] J. B. Cole, "A High Accuracy FDTD Algorithm to Solve Microwave Propagation and Scattering Problems on a Coarse Grid," *IEEE Trans. Microwave Theory and Techniques*, vol. 43, no. 9, Sept. 1995.